Leak Before Break Evaluation of the Main Loop Piping of a CE Reactor Coolant System

Combustion Engineering, Inc.
1000 Prospect Hill Road
Windsor, CT 06095

Revision 1

November 1983

Table of Contents

ABSTRACT

The studies conducted by CE over the past decade related to the demonstration of leak-before-break in the main loop piping of a CE PWR are summarized. Recent analyses which address the safety margins available in meeting the leak-before-break criterion are also presented. The results clearly demonstrate that the margin against instability for detectable leaking cracks is substantial in terms of margin on material properties, loadings, and crack size required for instability for both normal operation and seismic conditions.

All the requirements necessary for the demonstration that a leak-before-break condition exists in the main loop piping of a CE PWR are shown to be satisfied with considerable margin.

1. INTRODUCTION

Nuclear power plants are designed to withstand very large mechanical loadings that are intended to envelop conservatively a wide range of hypothetical accident conditions. These loadings are typically associated with a hypothetical initiating event that is judged to be more severe than any realistic event. The primary coolant system main loop pipe break is one of these initiating events that forms the design basis for many systems and components of a pressurized water reactor (PWR).

The present criteria, which define the location, type and size of pipe breaks are based on the assumption that a sudden complete circumferential severance (guillotine break) of a pipe can occur Ref. (1). Advances in the field of fracture mechanics and elastic-plastic stress analysis during the past decade have provided the capability to more realistically assess the way that cracks would grow in piping systems. Application of these analytical methods to the main loop piping in the CE PWR has demonstrated that a leak before break condition exists and that a complete circumferential severance of a main loop pipe cannot occur.

The analyses that have been performed in support of the leak-before-break demonstration are described in this report. These analyses form the basis for the position that the existing criteria could be revised to not require the consideration of the guillotine break, and still satisfy the requirement of enveloping conservatively all possible accident conditions. Analyses are also presented which address the leak before break condition of axial slots in piping elbows. These analyses demonstrate that a large margin exists for leak-before-break.

This analysis emphasizes circumferential pipe cracks because the circumferential severance currently hypothesized is the most severe type of pipe break and results in the requirement for pipe whip restraints.

Many CE published reports are reviewed and summarized in order to bring all important CE work on the leak-before-break issue together in one report. Frequently, sections of these reports are restated "verbatim" with permission of the authors of the original studies.

2. LEAK-BEFORE-BREAK CRITERION

In order to demonstrate that a leak-before-break condition exists for a particular piping system, three conditions must be met. The first condition is that any initial flaws must tend to propagate through the pipe wall rather than in the circumferential or axial direction. This characteristic of the flaw growth is dependent on the loading and environmental conditions to which the piping is exposed. The second condition is that through wall cracks must open sufficiently to allow detection by normal leakage monitoring under normal full power loading conditions. The nature of the crack opening is dependent on the piping stiffness, the normal operation loadings and the material properties of the pipe.

The third condition is that cracks of detectable length must remain stable even under severe loading. The most severe loading is considered here to be the Safe-Shutdown Earthquake or SSE seismic loading. Crack stability is dependent on the toughness or crack resistance of the material, and the manner in which the cracked pipe is able to distribute or shed loads as crack extension occurs.

Leak-before-break can be demonstrated if the three conditions identified above are satisfied with sufficient margin to assure that unforeseen variations in loadings or material properties cannot cause one of the conditions to not be satisfied.

Analyses that have been performed by CE over the past decade addressing these three conditions are summarized in sections 3, 4, and 5. In section 6, more recent analyses aimed toward quantifying the safety margins in meeting the three conditions.

3. THROUGH WALL CRACK GROWTH

The first step in the leak-before-break evaluation is the determination of the manner in which a crack could grow through the pipe wall and cause a violation of pressure boundary integrity. Crack growth is caused by cyclic loading on an existing crack. In order to evaluate crack growth, the loading conditions and the initial crack size must be established.

a. Crack Size and Loadings

The anticipated loading conditions for CE PWR primary piping are shown in Table 1. These loading conditions are well understood and contain no severe thermal or dynamic conditions. These anticipated conditions are employed in the ASME code fatigue analysis for the piping. There is the possibility that a more severe loading, e.g. thermal transient, may occur during an emergency or faulted type of event, but the scarcity of such events precludes the need for consideration of such loadings in a fatigue or fatigue crack growth analysis.

The main loop piping has no valves which might open or shut, it experiences no rapid thermal transients during normal operation and it is not subject to significant flow stratification during normal operation. Clearly, since these statements cannot be made about piping in general, the conclusions drawn concerning leak before break apply only to the main loop piping.

The CE main loop pipes are fabricated and inspected in accordance with NB 2532 and NB 5000 of the ASME Section III Code which requires volumetric examination of 100% of the base metal and weld joints and allows indications no longer than three inches nor deeper than 10% of the pipe wall thickness. Therefore, only small cracks could exist in the piping before service. In order to conservatively evaluate crack growth and extension, a variety of crack sizes much larger than those expected to exist are considered in the subsequent analyses.

b. Crack Growth Analysis

Crack Growth analyses have been performed based on the methods of linear elastic fracture mechanics, Ref. (3). Recent analyses have employed the methods of the ASME Code Section XI as those fracture mechanics procedures have developed Ref. (4).

Section XI of the ASME Code, Ref. (5) defines a fatigue crack growth rate law of the form:

$$\frac{da}{dN} = C'(\Delta K_I)^n \qquad (1)$$

where n is the slope of the log (da/dN) vs. log (K_I) curve, and C' is a scaling constant. This material property curve has been determined experimentally, and the material constants for carbon steel for fatigue crack growth in a water environment are as follows: C' = 3.795×10^{-10} and n = 3.726. The rate of crack growth (da/dN) is measured in inches per cycle from this relationship. This crack growth law is intended to be a conservative upper bound to the

experimental data, however, recent fatigue crack growth studies have produced data which lie above this curve. Figure 1 shows the da/dN vs. K_I curve which has been proposed as a revision to the Section XI curve and is seen to envelope all of the fatigue crack growth data. The results of this study include the upper bound to the crack growth rate curve as given in Figure 1.

For the purpose of determining the range of defect sizes which could grow to threaten the integrity of the system, semi-elliptical shaped inner surface flaws were hypothesized for various initial crack depths, a_o, and lengths, $2C_o$. A computer methodology was used to evaluate the stress intensity factor for a given flaw size and loading function and then compute the growth rate in both the through thickness and circumferential directions of the flaw under cyclic loading conditions.

The method of analysis is based on the Section XI, Appendix A flaw evaluation procedure. This method is applicable to flaws which have not fully penetrated the wall thickness. From this method for K_I determination, the ΔK_I level is calculated based on the crack size and loading conditions. Using a stepping procedure for the number of cycles of loading in a given time period, depth and length crack growth rates are calculated and the corresponding change in crack size is determined. This permits a determination of the time to produce first leak when an existing flaw would enlarge and subsequently "pop-through" the thickness of the pipe. This "pop-through" phenomenon is what is meant by a suddenly-appearing through-thickness crack. The circumferential length of the through-wall crack is important to the determination of crack stability.

For cracks which are calculated to grow to penetrate the wall thickness, the subsequent calculation of the stress intensity factor, K_I, was evaluated using the finite element method since the Section XI flaw evaluation procedure does not extend to through-wall cracks. The finite element analysis enabled the determination of K_I as a function of the circumferential crack length, 2C, and the applied load. This information was incorporated into the crack growth procedure. In this manner the fatigue crack growth study was continued for circumferential growth of through-wall cracks.

A wide range of initial flaw sizes and shapes were considered, and the resulting crack growth rates were calculated for the design basis loading transients and corresponding frequencies of occurrence given in Table 1. An example of the predicted growth behavior for a defect with an initial depth of 0.5 in. and an initial length of 39.0 in. is shown in Figure 2. Under the influence of the prescribed cyclic loading history such a flaw was calculated to become a leaking crack in 21 years of operation, which is less than the normal (40 year) plant life. The circumferential extension of the crack is only about one inch which is negligible compared to the initial crack length. It should be emphasized that the loading histories used in this analysis are conservative representations of the design transients and are intended to describe the upper limit of possible reactor operating

experience. If, after formation of a through-wall crack, the defect remains undetected and operation of the reactor continues, the calculated fatigue crack growth is also shown in this figure. It can be seen that the through wall crack would remain stable for many more years of service, increasing the likelihood of detection.

Figure 3 shows a similar plot of crack size vs. years of operation for an initial flaw with dimensions a_o = 1.0 in. and 2 C_o = 34.0 in. This initial flaw size also results in the formation of a large circumferential through-wall leaking crack in only 4 years of reactor operation. The circumferential extension of this crack is negligible. Subsequent extension of the leaking crack due to continued operation is also shown on Figure 3.

The results of the fatigue crack growth study for a .35 in. deep and 45.5 long initial flaw are presented in Figure 4. From this figure it is seen that the time required to cause a leaking crack would be 38 years. Again circumferential extension even of such a long (half circumference) crack is negligible.

In earlier CE work, Ref. (3), it was shown that cracks shorter than those considered above would require many more than the design basis number of cycles of loading to grow through the pipe wall. The startup-shutdown transient was found to be the greatest contributor to the usage factor for the main loop piping. A cyclic stress, conservatively enveloping this startup-shutdown stress was applied to hypothetical flaws one inch deep and from 8 to 18 inches long in the circumferential direction in both the 42-inch diameter hot leg and 30-inch diameter cold leg piping. Figure 5 shows that the number of start-up-shutdown cycles necessary to cause a one-inch deep crack to grow through the pipe wall and leak is an order of magnitude greater than the plant life.

In these cases it was observed that the circumferential crack extension was small. The analyses indicate that the transients that the pipe is anticipated to experience produce preferential crack growth in the through-wall direction of the pipe thereby causing a leak prior to significant circumferential extension. In Reference 3 the same conclusions about preferential through thickness crack growth were also demonstrated for cracks in the axial direction.

One other crack extension mechanism, stress corrosion cracking has the potential to cause crack growth more uniformly around the pipe circumference. The CE main loop piping environment, however, is not corrosive and no evidence of stress corrosion in this piping has ever been observed. This crack growth mechanism is not considered to be active in CE main loop piping.

4. CRACK LEAKAGE

The second step in the leak-before-break evaluation is the determination of the amount of leakage which will result from a given crack which has extended through the pipe wall. CE has performed a detailed study of crack opening areas at two locations in the main loop piping: the pump discharge leg terminal end at the reactor vessel inlet nozzle and the hot leg terminal end at the reactor vessel outlet nozzle, Ref. (6). These locations are selected because they are regions of relatively high stress and are locations where guillotine ruptures must be postulated according to the present pipe break criteria, Ref. (1).

The crack opening area was calculated for normal operating conditions since these are the most prevalent conditions during plant operating life, when leakage is to be detected. Since the leak rate is related to the amount of crack opening, a finite element analysis was performed to calculate crack opening areas as a function of crack length for various orientations around the pipe at these locations.

a. Crack Opening Area Analysis

The crack opening area was determined for several circumferential through-crack lengths oriented at the top, bottom, and sides of the discharge leg and hot leg terminal ends at the reactor vessel nozzles under normal operating conditions. Figure 6 shows the locations in the primary coolant system of the regions analyzed. By symmetry of geometry, material, and normal operating loading, the results for these two regions also apply to the other pipe terminal ends at the reactor vessel nozzles. Figures 7 and 8 show the geometry details used for the finite element modeling of the discharge leg and hot leg, respectively, and the coordinate systems in which the forces and moments are specified. Table 2 gives the combined forces and moments due to pressure, weight, and thermal expansion for steady state normal operating conditions. All crack opening area analyses were linear elastic using the material property values which are given in Table 2. Plasticity is conservatively ignored since plastic deformation would cause greater opening areas and more leakage. The MARC finite element program was used to perform all crack opening area analyses.

The extent of the detailed model of both structures was chosen so that nozzle and pipe/elbow end modeling would have a negligible effect on crack opening area. Figure 9 shows the finite element mesh for the 30 inch discharge leg terminal end with a crack. The 42 inch pipe mesh is not shown because it is very similar. Figure 10 shows the mesh refinement in the structure immediately surrounding the crack which was needed for accurate crack opening area determination and simulation of cracks of different length without the need for overall mesh regeneration.

For each terminal end finite element model, the total combined "in-system" loads of Table 2 were applied to produce equivalent beam displacements and rotations at the ends of the models. These calculated displacements and rotations were then applied to the crack

models because the displacement-controlled loading was judged to realistically represent the nature of the actual normal operating loading applied to the cracked structures. The boundary deformations of these structures, even under loadings like axial pressure, are substantially constrained by the resisting stiffness of the rest of the piping-component system.

For determining leakage rates from a narrow through-thickness crack in the pipe, it is necessary to determine the minimum opening area at any location through the wall because that section limits the flow from such a crack. For this reason, the crack opening area was calculated at the outside surface, inside surface, and midplane of the pipe wall. The midplane crack opening area was calculated directly from the shell midplane displacements. For the inside and outside surface areas the relative displacements due to the through thickness rotations were added to the midplane displacements. The opening area computed at the midplane of the pipe wall was compared to the crack opening area at the surfaces. For the hot leg the smallest area was always greater than 92 percent of the midplane value for all crack sizes and orientations evaluated. For the discharge leg the smallest area was always above 73 percent of the midplane value for all crack sizes at all orientations, except the bottom. At the bottom, the area was as little as 23 percent of the midplane value for the shortest cracks. These results illustrate that there are significant variations in the crack opening area at the inner and outer surfaces of the pipe, especially for the minimum crack opening area orientation.

Figure 11 shows the minimum pipe surface crack opening areas vs crack length at the various orientations around the discharge leg terminal end. The bending moment at the terminal end produces a greater opening area on the top of the pipe than on the bottom during normal operating conditions. Cracks at all pipe orientations open significantly indicating that the axial load, caused mostly by system pressure, predominates over the bending moments.

Figure 12 shows the minimum pipe surface crack opening areas vs crack length at the top and side of the hot leg terminal end. Cracks hypothesized in the bottom of this pipe do not grow or open because the region is in compression.

b. Leak Detection

There are two major facets to crack detection based on leakage in addition to the crack opening size. These are the leak detection sensitivity, and the flow rate correlation for leakage through a crack. A more detailed discussion of leakage rates is presented in Ref. (7).

For a PWR in the USA leak detection systems capable of detecting less than 1.0 gallon per minute (gpm) leakage from the primary system, with a Technical Specification upper limit of 10 gpm are employed per the guidance of Regulatory Guide 1.45 utilized, Ref. (8). Diverse measurement means are utilized, including water inventory monitoring, sump level and flow monitoring, and measurement of airborn radioactive particulates or gases.

The other major facet of crack detection based on leak rate, namely the flow rate correlation for leakage through a given crack size, can not be predicted precisely. Variables such as surface roughness of the side walls of the crack, the nonparallel relationship of the side walls due to the elongated crack shape, and possibly zig-zag tearing of the material during crack formation all introduce uncertainties in defining an exact flow rate correlation.

NUREG/CR-1319 Ref. (9), provides a treatment of leakage through small cracks considering various uncertainties in crack definition, including crack wall surface roughness, effective L/Dh ratio of the elongated crack shape, and the possibility that the crack may be longer at the inside of the pipe wall than at the outer surface of the pipe, resulting in a convergent opening. The results of Figure 4-13 of Reference (9) for typical PWR conditions at 2250 psi and 550°F for a high friction factor of .01 are replotted on Figure 13 in units of gpm per square inch of crack opening versus outer surface crack area, Ae. Also plotted in Figure 13 are flow predictions based on similar orifice flow with a discharge coefficient of 0.6, and also a flow prediction using a Henry-Fauske, Ref. (10), critical flow model.

The Henry-Fauske correlation was developed on the basis of subcooled flow through nozzles, and provides an upper bound for flow through an irregular crack opening. The orifice flow does not consider subcooled water effects, and the constant discharge coefficient does not consider the irregular crack shape. Even so, the orifice prediction falls in the range of the NUREG/CR-1319 predictions, providing a measure of comparison.

The NUREG/CR-1319 predictions show a slight increase in flow rate per unit of exit plane area with increasing area, and a large increase for decreasing Ae/Ao ratios. Since, for the purposes of identifying a through wall crack by means of leakage it would be conservative to underpredict the flow rate, the lowest value of all of these various predictions is recommended. The lowest flow rate prediction is about 885 gpm/sq. in. at .001 sq. in. This means that a crack which opens to slightly greater than .001 sq. in. will leak at least 1 gpm, and, therefore, will be within the range of detection by the normal leakage monioring systems for a PWR.

Using the relationship between leakage rate and crack area of 885 gpm per square inch, the leakage rate for all the crack cases of Figures 11 and 12 can be determined. These flow rates are shown in Figure 14.

Considering some margin for conservatism, through wall cracks resulting in leakage of 1 to 2 gpm will be detected during operation. This limit is also shown on Figure 14. It can be seen that relatively small cracks produce detectable leakage. For all locations except the bottom of both terminal ends, a 5-inch long crack would be detectable. For the bottom of the discharge leg terminal end a 10 inch (254 mm) long crack would be detectable. The crack length required for detectable leakage at the bottom of the pipe is greater than the other orientations because the normal operating loading is smaller in this region. This smaller loading is seen later when the stability of cracks of various orientations is considered.

The bottom of the hot leg terminal end is always in compression and is not considered a viable crack location.

5. Crack Stability Analyses

The third condition for leak before break is that cracks which are large enough to leak will remain stable during extreme loading conditions, thereby preventing a complete pipe severance. Sufficient margin on stability must be available to account for variations in actual leak detectability, material properties and loading events between the time of the beginning of leakage and plant shutdown for leak repair.

CE has performed fracture mechanics analysis on a variety of hypothetical crack sizes subject to a variety of loading conditions. Both normal operation loads and seismic loadings have been considered to determine the size of crack which will remain stable under various loading conditions.

a. Crack Stability Criteria

Two crack stability criteria have been used over the years to assess the likelihood of unstable crack extension in the main loop piping. These methods are the traditional linear elastic fracture mechanics which employs a K_{IC} criterion, and the Ductile Tearing or J-integral ductile fracture mechanics which employ a J_{IC} and Tearing Modulus criterion.

.1 Instability Principle

In linear elastic fracture mechanics, the stress intensity factor at the tip of a hypothetical crack, K_I, is computed as a function of loading and geometry. This factor represents essentially the crack opening force applied. This value is compared to the fracture toughness, K_{IC} which is the material resistance to fracture. If

$$K_I < K_{IC}$$

then the crack is stable and if

$$K_I \geq K_{IC}, \text{ then}$$

unstable crack extension occurs.

The ductile fracture mechanics methods have been developed more recently and, therefore have been used in various stages of that development in the analyses described here. The tearing modulus concept is an elastic plastic crack instability theory based on the J integral elastic plastic crack tip parameter and a J-resistance curve material property such as shown in Figure 15 Ref. (11). This figure shows the results of a series of tests indicating the amount of crack extension as a function of the value of J at the crack tip. The J value below which there is essentially no crack extension is called J_{IC}.

The slope of the line beyond J_{IC} giving the rate of increase of J required for subsequent crack extension, $\partial J/\partial a$, is used to assess the stability of the crack. Figure 16 is an idealization of the J-

resistance curve which illustrates the instability criterion. If the loading on the crack is such that the rate of change of J with crack extension $\partial J/\partial a$, applied is greater than the resistance $\partial J/\partial a$ material, then unstable crack extension will occur.

If $\partial J/\partial a$ applied is less than $\partial J/\partial a$ material then unstable crack extension will not occur even though J_{IC} is exceeded. The non-dimensional tearing modulus T, is defined as:

$$T = \frac{\partial J}{\partial a} \frac{E}{\sigma_o^2} \qquad (2)$$

where E is Young's modulus and σ_o is the yield stress of the material. Figure 17 shows how the point of instability can be found as the intersection of the loading curve in terms of J(T) and the J resistance material property curve. This figure illustrates how the structural behavior influences crack instability. If the J applied does not increase with crack extension more than the J-Resistance curve because of load redistribution or load shedding, i.e. $T_{applied}$ is small, then the crack will not become unstable. If however, the crack loading, J applied increases rapidly with crack extension i.e. $T_{applied}$ is large, instability will occur.

.2 Material Properties

The main loop piping for System 80 designs is constructed from SA516 Gr70 plate. The J-resistance curve for this material developed in reference (11), is shown in Figure 15.

The figure indicates that J_{IC} ranges from 600 in lb/in^2 at 300F to 400 in lb/in^2 at 550F. The slope of the J vs a curve, however, is essentially the same at both temperatures. From the figure, the slope, $\partial J/\partial a$, can be measured as a function of J.

Using the relationship for tearing modulus in equation (2), and the temperature dependent yield stress values σ_o = 34 ksi at 300F and σ_o = 30 ksi at 550F, the J vs Tmat instability curves are developed. These curves are shown in Figure 17.

Confirmation of the applicability of the J resistance curve of Figure 15 to the piping material used in actual plants can be attempted by comparison with actual material data. The material data obtained for each pipe section, however, is typically limited to Charpy tests so a Charpy/K_{IC}/J_{IC} correlation must be employed. Figure 18 shows the Charpy energy vs temperature data for Palo Verde Unit 1 SA516 Gr70 pipe material (in plate form). Figure 19 shows the Charpy energy for weld material for a SA516 Gr. 70 to SA533 B1 or 508 Class 2 welds, typical of the pipe to component safe end welds.

Using the Barsom-Rolfe-Novak correlation

$$K_{IC}^2 = 2E\,(CV_N)^{3/2} \qquad (3)$$

where CV_N is the Charpy energy,

and the plane strain relationship

$$J_{IC} = \frac{K_{IC}^2\,(1-\nu^2)}{E} \qquad (4)$$

where ν is Poisson's ratio, the resulting K_{IC} and J_{IC} vs temperature relationships are shown in Figure 20 and 21 for the base metal and weld material.

Figure 21 indicates that the J_{IC} value of 400 to 600 inlb/in.^{2} (of Figure 15) is reasonable for the actual pipe material at operating temperatures. The figure also indicates that the weld material has a significantly higher J_{IC} and use of the pipe material J_{IC} for stability evaluations will be very conservative for welds. For the cases of linear elasticity and small scale yield fracture mechanics the parameter J is related to K_I by

$$\begin{aligned} K_I &= \sqrt{J \cdot E/(1-\nu^2)} && \text{for plane strain} \\ K &= \sqrt{J \cdot E} && \text{for plane stress} \end{aligned} \qquad (5)$$

This relationship is frequently used with the finite element method for the calculation of K_I. It also permits a comparison of the two crack stability criteria. For example, from Figure 15, J_{IC} is found to be about 600 in-lb/in.^{2} for SA 516 Gr. 70. According to equation (3), assuming plane stress, and $E = 30 \times 10^6$ psi, $K_{IC} = 134$ ksi$\sqrt{\text{in.}}$ It is generally accepted that linear elastic fracture mechanics applies until K_{IC} approaches the upper shelf toughness which is in the 200 ksi$\sqrt{\text{in}}$ to 250 ksi$\sqrt{\text{in}}$ range. Using 225 ksi$\sqrt{\text{in}}$ as an average upper shelf toughness, the corresponding J would be 1690 in lb/in.^{2}. Figure 15 indicates that significant crack extension would result from application of a J value of this magnitude. The rate of increase of J, however, is required to assess crack instability.

b. Normal Operating Loads

Both short through wall and long through wall circumferential cracks have been analyzed for crack stability. Static analyses have been employed for small cracks to determine the margin against crack instability for cracks which may be just leaking during normal operation Ref. (6).

The stability of through-wall cracks in primary system piping is evaluated using the J-integral technique. The crack tip parameter, J, can be compared to the experimentally determined elastic-plastic toughness, J_{IC}, to evaluate the stability of a crack. For $J < J_{IC}$, no crack extension will occur, hence, the crack will remain stable.

The J-integral was evaluated in the finite element analysis using Park's method Ref. (12) which has been demonstrated to produce accurate results without the need for special crack tip elements. The J-integral value was calculated at both crack tips for normal operation loadings which include pressure, weight and thermal expansion forces, at various orientations around the circumference of the terminal end models discussed in Section 4a. From the calculated stress values, no significant plastic deformation would be expected at the crack tip under normal operating loads for crack lengths less than 25 inches or so. A plot of J vs crack length is shown in Figure 22 for through-wall cracks centered at the top and side of the hot leg terminal end and the top, outward side and bottom of the discharge leg terminal end. For all orientations, the calculated J-integral value increases as crack length increases. The J value for the hot leg follows the pattern associated with a dominant bending load. It reaches 224 in-lb/in^2 for a 22 inch crack at the top of the pipe. For the discharge leg the J values are much less than the J values for the top of the hot leg. The J value for a 17 1/2 inch crack at the top of the discharge leg is only 26 in-lb/in.^{2} The crack in the bottom of the discharge leg terminal end, which was seen to have the largest crack length for detectable leakage from Figure 14 has, by far, the lowest J value. This indicates that the bottom is not a critical region for crack stability or concern for violation of the leak-before-break criteria.

The computed J values for all cracks are well below the critical value of J_{IC} in Figure 15, thereby assuring that no crack extension due to normal operating loads will occur for these cracks.

A dynamic elastic plastic analysis was performed to evaluate the stability and opening area of long hypothetical circumferential cracks, in the 30-in. ID, cold leg pipe in Ref. (13). The pipe is assumed to be under normal operating pressure of 2250 psi and subject to the axial load caused by that pressure. A circumferential crack is assumed to suddenly appear with a length of half the circumference of the pipe. A schematic view of the pipe containing the circumferential crack is shown in Figure 23. Since two planes of symmetry exist, one quarter of the pipe can be modeled. The finite element model of one-quarter of the pipe is shown flattened out and not to scale in Figure 24. The boundary axially remote from the crack is permitted to move axially and rotate as a plane. The force on the boundary is the axial force caused by the pressure and no depressurization due to the crack opening is assumed.

The pipe material, SA516 Gr 70, was permitted to deform plastically in accordance with the stress strain curve of Figure 25. The crack opening area during the opening is shown in Figure 26. The maximum opening of 5.3 in.^{2} occurs at 3.0 milliseconds. This opening would result in over 5000 gpm leakage on the basis of the leak rate relationship discussed in Section 4.b.

The J-integral computed during the opening is shown in Figure 27. These values were computed by MARC and are the average of two near crack contours. The maximum J-integral value is 1250 in-lb/in.^{2} which is above the J_{IC} value of Figure 15. The tearing modulus

criterion is, therefore, required to indicate whether the crack is stable or unstable. From Figure 17, the T mat value at J=1250 in-lb/in is about 280.
The J applied of 1250 in lb/in.^{2} corresponds to a half circumference crack which has a half length, a, of 24 inches. Recent work (see Section 6.b) has indicated that $J_{applied}$ for this geometry can be approximated as a cubic function of crack length, ie,

$$J_{applied} = C_J a^3 \qquad (6)$$

and, therefore,

$$\partial J/\partial a_{\ applied} = 3C_J a^2 \qquad (7)$$

Substituting equation 6 into equation 7 leads to:

$$\partial J/\partial a_{\ applied} = 3J/a = 156 \text{ in lb/in.}^2/\text{in.}$$

and, therefore,

$$T_{applied} = \frac{\partial J}{\partial a}\frac{E}{\sigma_0^2} = \frac{(156)(29\times10^6)}{(30\times10^3)^2} = 5.0$$

Since $T_{applied} < T_{mat}$ this tearing modulus evaluation indicates that crack instability will not occur. It is concluded, therefore, that the circumferential crack halfway around the pipe will not be unstable if it suddenly appears during normal operating conditions.

c. Analysis of Crack Subject to Seismic Loads

In order to determine the largest crack which would remain stable under seismic loadings, a dynamic elastic plastic finite element analysis of a crack in the discharge leg terminal end was performed (Ref.14).

In the previous section it was demonstrated that a crack must exist more than halfway around the circumference of the pipe before instability (rapid crack growth) can occur due to normal operating loads.

As a first consideration for the seismic analysis, the same crack size will be evaluated for stability. Therefore, a one-half circumference stable crack is postulated to occur in the discharge leg terminal end, a region of particular concern to the integrity of the primary cooling system. The crack is presumed to exist at a point in the Safe Shutdown Earthquake (SSE) loading transient which would produce the most severe loading condition at the crack tip. A detailed elastic-plastic dynamic analysis was performed to determine the overall response of the pipe. The stress intensity factor, K_I, was computed as a function of time using the J-Integral technique. The calculated values for K_I are compared with experimental material toughness data to determine the inherent resistance of the material to further crack propagation. The maximum crack opening area is calculated in order to determine leak rates.

All computations were performed using the MARC general purpose nonlinear finite element program.

c.1 Main Loop Piping System Model

For the seismic analysis a model representing the entire primary system is employed.

A three dimensional shell model of the elbow section of the discharge leg pipe was constructed using doubly-curved thin shell elements to provide a detailed finite element description of this region. The shell element was chosen to model the pipe elbow and nozzle because through-thickness cracks can be modelled with relative ease, localized plasticity effects can be included, and the J-Integral technique can be utilized to calculate K_I at the crack tip.

Because the discharge leg is a single component in a more complex system, it is important to analyze the response of the pipe to seismic loads considering the interrelated effects due to the adjacent structural members. For this purpose, three-dimensional beam elements were used to model the reactor vessel and its vertical support columns, as well as the reactor coolant pump, its horizontal and vertical supports, and the snubber. Beam elements were also used for the remaining portions of the discharge leg pipe which were not modelled as shells. A superimposed view of the finite element model of the pipe and the other system structural components is presented in Figure 28.

Only one leg of the reactor coolant system was evaluated in this analysis. The criteria for analysis of uncoupled subsystems are discussed in Reference 15. The major components and their support structures are modelled so that the substructure model will respond as if it were part of the entire system. Seismic loading is applied as time history motion of the supports.

Boundary conditions were applied to the model at the points of attachment to the foundation. The behavior of the model was checked under static conditions, with and without the presence of a crack, to verify the overall response of the finite element model to externally applied loading.

A static analysis of the system containing a hypothetical one-half circumference crack was performed to determine the effects of internal operating pressure on the cracked structure. The crack was presumed to exist at the outside of the elbow halfway around the circumference of the pipe where crack opening effects are expected to be at a maximum. To be conservative, it was assumed that the presence of the crack does not produce a depressurization of the system which would tend to reduce the level of stress in the pipe.

The maximum static value of K_I at the crack tip was calculated to be 92 ksi $\sqrt{\text{in.}}$ This value of K_I due to a one-half circumferential crack in the discharge leg pipe under static operating pressure is well below the fracture toughness of carbon steel at 550°F operating

temperature, which has an upper shelf near 250 ksi $\sqrt{in.}$ Thus, the crack would be stable and would not tend to propagate further under pressure loading alone.

The crack opening area for static pressure loading was calculated to be 1.36 in^2. Figure 29 shows a magnified view of the crack opening displacements for a one-half circumferential crack under static operating pressure loading. In the dynamic analysis of Section 5.b, the maximum crack opening area under dynamic loading for a one-half circumference crack was determined to be 5.2 in^2. However, this value was based on the assumption of free (unrestrained) motion at both ends of the pipe. The end restraint provided by the reactor vessel and discharge pump significantly limits the amount of crack opening which can occur.

c.2 Seismic Loading Conditions

In the design of nuclear reactor components for seismic loading, excitations are usually applied in the form of support motion time histories rather than by externally applied forces. The deterministic earthquake response analysis of a structural system must consider these factors which contribute to the input conditions:

a. simple (rigid-body) translation of the base,
b. rigid base rotations,
c. relative motion of different support locations,
d. the effects of soil-structure interaction where the motion of the base does not directly follow the free-field motion.

For this analysis, all support motions were considered to be the same. This assumption is conservative based on the following method used for determining support time histories.

The in-structure response spectrum used to define the SSE loading conditions is shown in Figure 30.

The support acceleration time history was generated from the in-structure response spectra using a procedure for generating a seismic artificial time history with a compatible response spectra based on the Fourier transform method (Ref. 16,17). An advantage to using an artificial time history is that it can be generated with a short overall duration which maintains the identical design spectrum over the frequency range of interest. The only requirement is that the total duration must be significantly greater than the period of the lowest frequency. For this analysis, a total duration of 6 seconds was chosen for the seismic event, with a rise time of 1 second and a decay time of 2 seconds.

The resulting acceleration and velocity time histories for horizontal support motion are shown in Figure 31. In this Figure the maximum acceleration is 1.2 g from the artificially-generated time history, and the corresponding peak in velocity is 54 in/sec. Typical values for peak horizontal ground acceleration used in design basis earthquakes are on the order of 0.2 - 0.3 g (Ref. 15). It follows from this that the corresponding maximum velocity would be

approximately 12 in/sec. The seismic loading used in this analysis, therefore, represents a "very severe" earthquake.

The artificially-generated time history motion was applied to the support locations, in 3 directions, and the dynamic response of the discharge leg pipe was evaluated for these seismic loading conditions. The results of the analysis using the model of Figure 28, without a crack, were compared with the behavior of the coupled model during seismic loading (Ref. 15). The maximum values calculated for the support reaction forces and moments at the reactor vessel upper column support are in excellent agreement with the coupled model. This demonstrates the validity of the approach used in the seismic loading of the structure, and verifies the overall dynamic response of the structural model of Figure 28.

c.3 Elastic-Plastic Dynamic Analysis

The natural frequencies of the reactor coolant system were extracted by a modal analysis. It was determined that the first (lowest) natural frequency of the discharge leg pipe without a crack was 16-17 cycles per second. This is within the range of frequencies which would contribute to normal modes during seismic loading.

The static load state of the system with operating pressure was used as the initial state for the dynamic analysis. The pipe was considered to be uncracked at time t=0 and a circumferential crack was presumed to initiate at a critical point during the seismic event. A criterion for crack initiation would, for example, be maximum tensile strain at the terminal end of the reactor vessel inlet nozzle. Generally it can be argued that maximum strain is produced in a structure during a seismic event shortly after the peak acceleration. On this basis, a large time step of 0.1 seconds was chosen for the early portion of the dynamic analysis during the "buildup" phase of the earthquake.

Direct integration of the dynamic equations was performed using the Newmark-Beta method. Stability problems did not arise since a recycling method was used to ensure that dynamic equilibrium was satisfied at the end of each time step within a set tolerance. In addition, a small amount of stiffness damping was included with a damping factor of 1.0×10^{-5}. This damping factor imposes less than .05 percent damping on modes with frequencies lower than 100 Hz.

From the time history plots in Figure 31, it is apparent that the maximum positive seismic excitation occurs at a time of t=1 second. This corresponds to the most severe externally applied loading for a one-half circumference crack around the outside of the pipe elbow.

Prior to the time of most severe loading, a smaller time step of 0.01 seconds was introduced at time t=0.9 seconds while the pipe remained uncracked. The smaller time step was chosen to delineate the high frequency response of the pipe (16-17 Hz) which would also contribute to the crack opening.

Figure 32 shows a response curve of the velocity time history at the midpoint of the discharge leg pipe. "Smoothing" effects due to the large time steps can be seen for time $t < 0.9$ seconds, whereas, the higher frequency response is apparent for time $t > 0.9$ seconds when the smaller time steps were used.

A determination of the most critical time to release the crack during the seismic analysis was based on energy principles. On that basis, it was determined that the loadings would produce maximum crack opening for a suddenly appearing crack initiated at $t = 0.99$ seconds.

A second analysis was performed which included the introduction of a one-half circumference crack at time $t = 0.99$ seconds. The dynamic behavior of the pipe with the crack was traced with time steps of 0.01 seconds to determine the maximum crack opening. Local plasticity effects were taken into account at the crack tip region for stress levels exceeding the yield strength of the material. Work hardening effects were included for SA-516 Gr-70 carbon steel using the stress-strain curve shown in Figure 21 for this material. K_I values were calculated at each time step using the J-Integral technique for determination of the crack tip stress intensity factor. The analysis was continued for a sufficient number of time steps to determine the total extent of crack opening and the maximum stress intensity at the crack tip due to combined pressure and seismic loading.

For comparison with the generated seismic velocities, a plot of the velocity time history at the base of the reactor vessel support column is shown in Figure 33. The analysis was carried out to a total time of 1.19 seconds, well past the peak in the velocity curve.

A similar velocity time history at the midpoint of the discharge leg pipe is given in Figure 34. A noticeable difference in the velocity profile occurs at the point of crack opening. The change is apparent in both the magnitude and frequency of the natural periodic motion. A comparison with the uncracked velocity time history shown in Figure 28 indicates that the peak velocity is reduced due to the incidence of the crack. This indicates a reduction in the kinetic energy of the pipe resulting from a change in stiffness. In effect, energy in the pipe is reduced due to crack opening, and the response of the pipe with the crack is substantially different due to the change in stiffness of the system.

c.4 Resulting Crack Behavior

Crack opening effects are best described in terms of the stress intensity factor, K_I. A plot of K_I vs. time starting at the point of crack initiation is shown in Figure 35. The rapid release of energy following crack initiation is characterized by the sharp increase in K_I to a value of 107 ksi $\sqrt{\text{in}}$. The increase in K_I due to dynamic effects is approximately 16 percent above the static value of pressure loading alone. The response of the pipe following the opening of the crack causes fluctuations in the value of K_I about the average static value of 92 ksi $\sqrt{\text{in}}$. The contribution of the seismic loading to the crack opening is small in comparison to the pressure effects. This is due to the fact that the structural stiffness at the reactor vessel and pump ends of the discharge leg

pipe severely restricts the rotations and displacements which are a prerequisite to large crack opening effects. The support provided by the reactor vessel and the pump tends to hold the pipe in place so long as a portion of the pipe remains intact. This end constraint severely limits the effects of seismic loading on a crack in the discharge leg pipe. The calculated values for K_I remain well below the critical value for crack instability.

The maximum crack opening area for a one-half circumference crack under pressure and seismic loadings was calculated to be 1.65 $in.^2$. A 1.65 $in.^2$ crack opening can be compared with the maximum crack opening area of 5.42 $in.^2$ which would result from a one-half circumference crack in a pipe without the end constraint afforded by the reactor vessel and reactor coolant pump.

From this work it can be concluded that circumferential cracks must be larger than halfway around the circumference before the effects of both pressure and SSE could cause rapid crack extension.

d. Axial Slot in Elbow

In addition to circumferential or guillotine type breaks, axial cracks or slots are included in the list of design basis pipe breaks. Reference 1 shows that slots are to be hypothesized on the inside of two of the pump suction leg elbows.

In order to evaluate the "leak-before-break" concept and compute leakage areas in the pump suction elbow, a finite element model of one half of a 90° elbow was constructed using shell elements available in the MARC program. The shell model is augmented with a beam at the end to facilitate the application of boundary conditions and the moment loads on the elbow end. Appropriate boundary conditions are chosen on the lines of symmetry and ends. Details of a typical mesh in the surface coordinate system are shown in Figure 36. Figure 37 shows the mesh in a cartesian coordinate system.

A number of different crack lengths, 8, 12, 16 and 20 degrees, on the half elbow are chosen for leakage area and J_I calculations. The crack lengths correspond to approximately 8, 12, 16 and 20 inches crack length at the inside radius of the torus on the 90° elbow.

Operating pressure (2250 psi) and the maximum bending moment due to normal plus seismic loadings (1,000,000 in-lb) are applied to the cracked elbow. An elastic static analysis was then performed. The total crack opening area and J integral vs crack length are presented in Figure 38. The leakage area ranges from 0 to 0.7 square inches whereas J varies from 0 to 500 inlb/$in.^2$.

Using the value of 885 gpm/$in.^2$ of crack area, the 8 inch long crack would be clearly detectable with a leakage of about 60 gpm. A crack of length much less than 8 inches therefore would be detectable at a 10 gpm rate.

An elastic plastic analysis of the 20 inch long crack in the pump suction leg elbow was performed to assess the conservatism of the elastic analysis. The resulting crack opening area for the same

loading condition was 1.0 in.^{2} and the corresponding J_I was essentially unchanged. This result indicates that the elastic analysis for leak-before-break evaluation is conservative because the elastic analysis produces a lower leakage area but (for these loadings) essentially the same value of J_I.

The maximum value of the Tearing Modulus for the largest crack analyzed is:

$$T = \frac{\partial J}{\partial a} \cdot \frac{E}{\sigma^2}$$

$$= 50 \times \frac{29 \times 10^6}{(30 \times 10^3)^2} = 1.6$$

An evaluation of the contributions of the pressure and moment loadings shows that only the pressure loading contributes to the stress concentration and leakage areas. The end moment has negligible effect on these parameters because the moment predominantly produces only axial stress in the elbow which has no effect on crack opening.

6. MARGINS

In order to assess the safety margins for the leak-before-break condition in the main loop piping of System 80 plants, two dynamic analyses have been performed. The first analysis is intended to establish the margin of safety on the seismic load carrying capability of the pipe with a leaking crack. The second analysis is intended to establish the margin of safety on the leaking crack length relative to the critical crack length.

In addition to the dynamic analyses, two static analyses have been performed to verify and bound the margins of safety. The static effect of the maximum seismic moment on various cracks at the discharge leg terminal end is computed, and a tearing instability analysis is performed in order to illustrate the inherent stability of the main loop piping system.

a. Safety Margin on Seismic Load Carrying Capability

To assess the margin and seismic load carrying capability, an analysis was performed to determine the likelihood of extension of a crack which is just large enough to leak at a 10 gpm rate during normal operation. The SSE loading was applied and the ductile fracture J-resistance curve was conservatively considered to be degraded to 25% of nominal properties of J_{IC} and T_{mat}. These properties are shown in Figure 39. In Section 5a, it was shown that the weld toughness properties are significantly better than the base metal properties for the main loop piping. The arbitrary degredation of a factor of four, therefore, is not intended to represent weld material properties or to imply that less ductile properties actually might exist in service. The use of an additional safety factor of four was imposed to more clearly demonstrate the stability of the piping system.

The analysis procedure is essentially the same as that used for the seismic analysis in Section 5c. The finite element mesh in the crack region has been made to be consistent with the mesh used for the static crack opening calculations in Section 4a. The overall system model has been extended to include the steam generators in order to obtain more accurate system response. The finite element mesh is shown in Figure 40.

From the crack opening area calculation described in Section 4a, cracks of the same size in the top and outward side of the discharge leg terminal end are found to open essentially the same when subjected to normal operating loads. For a 10 gpm leakage, Figure 17 indicates that a crack length of 7.5 to 8 inches would be required. For the seismic loading analysis, therefore, the crack length is assumed to extend over a 30° arc since that results in a crack length on the inside diameter of the pipe of 7.85 inches.

The SSE loading was developed from the seismic response spectra by the fourier transform method for generating an artificial time history as described in Section 5c. The response spectra utilized is considered typical for System 80 plants and is shown in Figure 41 and the generated support displacement history is shown in Figure 42. A comparison of the spectrum with the enveloping spectrum of the analysis of section 5c (Figure 30) further shows the severity of the

envelope used previously. The several displacement cycles in Figure 42 have essentially the same form and magnitude. For this analysis, a displacement which envelopes each cycle is applied as a representative loading condition for all cycles during the seismic event. The representative seismic cycle loading is shown in Figure 42. Consideration is given to the number of cycles which the crack tip experiences in assessing crack stability.

The normal full power loadings are statically applied to the finite element model containing the 30° circumferential crack to simulate the initial condition for the dynamic analysis. The J integral value and crack opening area are found to be essentially the same as those given in section 4a, thereby confirming that modelling changes did not significantly effect the static results. The seismic support motions are then applied and the resulting J and crack opening area histories are shown in Figure 43 and 44.

The J integral value is not greatly affected by the seismic loadings, which is consistent with the results of the analysis of section 5c. Similarily, the crack opening area increase due to the seismic loads is very small. The J integral results when compared to the "degraded" value of J_{IC} (100 to 150 in lb/in.^{2} from Figure 39), show a considerable margin against instability.

b. Safety Margin on Crack Length

To assess the margin on crack length, the smallest length of crack which will be unstable when subjected to the SSE loading and evaluated using only 25% of the ductile crack resistance properties must be determined. For this analysis the loading conditions are applied in the same manner as in the analysis of Section 6a. The assumed crack size, however, is much larger. Previous analyses indicated that a crack must be more than halfway around the circumference in order to be unstable even during seismic loading. Those analyses, however, did not consider the significant property reduction employed in this analysis.

The ductile crack stability criterion states that a crack will be unstable if:

$$J \geq J_{IC} \text{ and}$$

$$\text{the tearing modulus } T = \frac{\partial J}{\partial a} \frac{E}{\sigma_o^2} > T_{mat.}$$

In order to determine T, more than one crack size must be evaluated so that the derivative term $\partial J/\partial a$ can be evaluated.

It is appropriate, therefore, to consider the cracks for evaluation to be a half circumference crack and a crack somewhat less than half circumference long. Evaluation of these cracks will enable a comparison with previous work and enable an interpolation or slight extrapolation to the length which will be unstable for the imposed loads and properties.

The crack opening area results for the normal loadings of section 4a

show that the opening is greater for cracks on the top and outward side of the elbow and less for the bottom and inward side. It is assumed, therefore, that the top and outward side are the crack locations to consider for the most conservative stability evaluation. The two long cracks which are evaluated are a half circumferential crack centered 30° toward the outside from the top and a one third circumferential crack also centered at 30° toward the outside from the top of the elbow. These assumed cracks are shown in Figure 45.

The normal operation loads are statically imposed on the finite element model containing the larger cracks. For the half circumferential crack, the J value is 374 in lb/in.^{2}, at the "a" end crack tip and 227 in lb/in.^{2} at the "b" end crack tip. The average

value is slightly higher than the value found in Section 5c. (The K_I average of 92 ksi $\sqrt{in}$ found in section 5c corresponds to a J value of 282 in lb/in.^{2}). This is reasonable because the skewed crack is expected to be slightly more severe than an outward side crack. The excellent agreement, however, confirms the new modelling and gives confidence in the consistency of the results. The J value for the one third circumference crack is 109 in lb/in.^{2} at the "a" end crack tip and 84 in lb/in.^{2} at the "b" end.

A plot of static normal operation load J vs half crack length is shown in Figure 46. For the larger crack sizes the J values fit a cubic curve in crack length very precisely. This cubic relationship enables a more precise calculation of $T_{applied}$. This cubic form was used in section 5b in order to obtain $T_{applied}$ from only one analysis. Also shown is the degraded J_{IC} which indicates that for cracks greater than 150° in circumference, $J_{applied} > J_{IC}$. The value of $T_{applied}$ however, for the "a" tip of the half circumference crack is only 1.5 which is much lower than the degraded value of Figure 39. An instability diagram using the degraded values of Figure 39 is shown in Figure 47. The applied loadings for the normal operation load for the 180° and 120° circumferential cracks in also shown. The margin between the loading values and the instability line show that instability will not occur for these cracks during normal operation even if the degraded properties are considered.

In order to compute J for normal operation plus seismic loads the seismic support displacements are applied in the same manner as in the previous section and the dynamic analysis procedes in the same way. The resulting J vs time curves for each of the crack tips is shown in Figure 48 for the 120° crack and in Figure 49 for the 180° crack. The increase in crack opening area caused by the seismic loading for both crack sizes is very small compared to the areas determined during normal operating conditions of 0.5 in.^{2} and 1.6 in.^{2} for the 120° circumferential and 180° circumferential cracks respectively.

The $J_{applied}$ and $T_{applied}$ values during the seismic loading are not changed significantly from the normal operation loading results. This is consistent with the results of section 5c where only a small increase in crack tip loading occurred for a much higher seismic loading. The $J_{applied}$ and $T_{applied}$ values, shown on the instability diagram of Figure 47 represent the seismic as well as the normal operating loading case. This analysis shows clearly, that very long cracks in the main loop piping will remain stable when subjected to normal operation and SSE loads even if the ductile crack resistance material properties are considered to be only a fourth of the nominal value.

These results satisfy, with considerable margin, the requirements for the demonstration of leak-before-break in the main loop piping.

c. Margin on Axial Slot in Elbow

The results of the analysis of the 20 inch long axial slot in the 90° pipe elbow described in Section 5d, are plotted on the instability diagram in Figure 50. The stability of this crack is evident from the curve, which reflects the very low value of $T_{applied}$.

d. Seismic Moments

The maximum bending moments computed by the traditional seismic analysis in the uncracked pipe at the discharge leg terminal end at the RV inlet nozzle are shown in Table 3. The maximum component, around the vertical axis, is 2, 140 in kips. The other components, about axes in the horizontal plane are less than half of the maximum moment. From Appendix A, it is seen that the seismic moments are much less than the normal operating moments.

In order to determine the effect of the crack on the magnitude of the applied moment, the finite element of model Figure 28 and 29 was used. A relative displacement between the pump and the reactor vessel which produced a moment mostly about the vertical axis at the crack location was imposed on the model and the crack length was increased. The crack was assumed to be located on the outside of the elbow where it would be opened by the bending moment. The decrease in the moment due to increasing the crack length is shown in Figure 51. From the figure, it can be seen that cracks shorter than 120° circumference cause less than a 10% reduction in bending moment. Longer cracks cause significantly more moment reduction. This moment reduction enhances the stability of the main loop piping system subject to seismic loads.

The J integral values for several crack lengths for the system relative motion which produces a moment of 2, 140 in-kips in the uncracked pipe are shown in Figure 52. These values are very small and are smaller than the occilations found in the dynamic analysis of Section 6a.

e. Tearing Instability Evaluation

In order to obtain a bounding check on the results of the seismic analyses of the main loop with cracked pipes, a stability analysis was performed. The analysis was performed according to the tearing instability procedure of NUREG CR3464 (Ref.18). This procedure conservatively presumes that the cracked section is loaded to be fully plastic.

The main step in the procedure is to determine the "residual elastic stiffness" of the piping system. A finite element model similar to the one in Figure 28 (except that the crack region was replaced by pipe elements) was employed. The pipe elements were disconnected in the rotational degrees of freedom to simulate a "ball and socket" joint. A unit moment of 1×10^6 in-lb about the vertical axis was applied on each side of the joint, as shown in Figure 53. The resulting rotations are also shown in the figure. Because this moment direction is the maximum during seismic loading, it is felt to be the proper direction for consideration of stability.

From Figure 53, the residual stiffness can be calculated as

$$K_\phi = \frac{M}{\phi} = \frac{1.0 \times 10^6}{2.256 \times 10^{-4}} \text{ in-lb}$$

$$= 0.443 \times 10^{10} \text{ in-lb}$$

Using the formula

$$T_{Appl} = \frac{2h^2 t E}{K_\phi}$$

where $h = R(\cos\theta + \sin\theta)$

and 2θ is the extent of the circumferential crack, t is pipe thickness and R is pipe radius,

the values of T appl are computed in Table 4. The maximum value in the Table, 13.5, is confined by the bounding equation

$$T_{Appl} = \frac{1.6\, E\, I}{2\, R\, K_\phi} = 13.5$$

where I is the pipe moment of inertia.

In Section 6b, it was seen that the T applied in the seismic analysis was on the order of 2. The valve computed above of 13.5 represents the fully plastic condition which is the upper bound of T applied. The T applied value for actual loadings is significantly lower.

Stability is assurred if T appl < T mat. From the figures 47 and 50, it is seen that T mat is much larger than the upper bound T applied, thereby assuring stability for any loading in addition to those explicitly considered in Section 6a and 6b.

7. CONCLUSIONS

In this report, a variety of crack sizes, loadings and material properties have been considered and analyzed in order to demonstrate that a leak-before-break condition exists in the main loop piping of a CE PWR. It was shown that cracks in this piping system would tend to grow through the pipe wall rather than circumferentially due to the fatigue loading conditions.

Conservative crack opening area calculations showed that a circumferential crack about 8 inches long in the top of side of the discharge leg terminal end would leak at a rate of 10 gpm but would have a high margin against instability even when subject to safe shutdown seismic loads. At the bottom of the terminal ends, a greater crack length is required for a leak rate of 10 gpm, but the loading in this region is so small that crack instability is not a concern. The margin against instability for detectably leaking cracks is demonstrated to be substantial in terms of margin on material propertes, on loadings, and on crack size required for instability.

An axial slot less than 8 inches in length was shown to leak more than 10 gpm. This size crack has a very high margin against instability since even

20 inch long cracks are clearly stable. The requirements for the demonstration of leak-before-break therefore are also satisfied for axial slot cracks in the piping elbows.

A tearing instability evaluation was also performed which demonstrated that the piping system is stable even when subject to a moment sufficient to cause a fully plastic pipe section. All these analyses clearly demonstrate that leak-before-break conditions are satisfied with considerable margin in the main loop piping of a CE PWR.

8. REFERENCES

1. "Design Basis Pipe Breaks for the Combustion Engineering Two Loop Reactor Coolant System," CENPD-168-A, Combustion Engineering, June 1977.

2. Reference Deleted

3. "Crack Size Considerations in Primary Piping," CENPD-78, Combustion Engineering, December 1973, also Appendix C of Reference 1.

4. Griesbach, T. J., "Dynamic Elastic Plastic Behavior of Circumferential Cracks in a Pipe Subjected to Seismic Loading Conditions", Presented at 1980 Pressure Vessels and Piping Technology Conference, San Francisco, 1980.

5. ASME Boiler and Pressure Vessel Code Section XI, Article A-4000, "Definition of Material Properties", New York, 1972.

6. Ayres, D. J., Griesbach, T. J., DeSaulniers, W. E., "An Evaluation of Leakage for Postulated Circumferential Cracks in PWR Primary System Piping", Paper F 7/4 6th SMiRT, Paris, France, 1981

7. Peck, D. A. "Determination of the Appropriate Stable Crack Size to be Used in A Rational Design Basis for Pipe Breaks", Paper 7/2, 6th SMiRT, Paris, France, 1981.

8. USNRC Regulatory Guide 1.45 "Reactor Coolant Pressure Boundary Leakage Detection Systems", May, 1973.

9. Mayfield, M. E., et al "Cold Leg Integrity Evaluation", NUREG/CR 1319, prepared by Battelle Columbus Laboratories for the US NRC, Washington D.C., February, 1980.

10. Henry, R. E., and Fauske, H. K., "The Two-Phase Critical Flow of One-Component Mixtures in Nozzles, Orifices and Short Tubes", Journal of Heat Transfer, Vol. 93, pp. 179-187, 1971.

11. Gudas, J. P., "Piping Material J_I-R Curve Characterization", presented at HSST Review Meeting, July 24, 1980, David Taylor Naval Ship R+D Center, Annapolis, MD.

12. Parks, D. M., "A Stiffness Derivative Finite Element Technique for Determination of Elastic Crack Tip Stress Integrity Factors," International Journal of Fracture, Vol. 10, No. 4, December, 1974.

13. Ayres, D. J., "Determination of the Largest Stable Suddenly Appearing Axial and Circumferential Through Cracks in Ductile Pressurized Pipe", Paper F 7/1, 4th International Conference on Structural Mechanics in Reactor Technology, San Francisco, August, 1977.

14. Griesbach, T. J., and Ayres, D. J., "Opening and Extension of Circumferential Cracks in a Pipe Subject to Dynamic Loads", Paper F 5/1, 5th International Conference on Structural Mechanics in Reactor Technology, Berlin (West), Germany, August, 1979; to be published in Nuclear Engineering and Design .

15. Gerdes, L. D., "Dynamic Structural Analysis of Uncoupled Subsystems", Paper K 6/18, 4th International Conference on Structural Mechanics in Reactor Technology, San Francisco, August, 1977.

16. Scanlon, R. H., and Sachs, K., "Earthquake Time Histories and Response Spectra", Journal of Engineering Mechanics Division, ASCE, Volume 100, August, 1974, pp. 635-655.

17. Scanlan, R. H., and Sachs, K., "Floor Response Spectra for Multi-Degree-of-Freedom Systems by Fourier Transform", Paper K 5/5, 3rd International Conference on Structural Mechanics in Reactor Technology, London, U.K., September, 1975.

18. Paris, P. C. and Tada, H., "The Application of Fracture Proof Design Methods Using Tearing Instability Theory to Nuclear Piping Postulating Circumferential Through Wall Cracks", NUREG/CR-3436 U.S.NRC, September 1983.

F45393

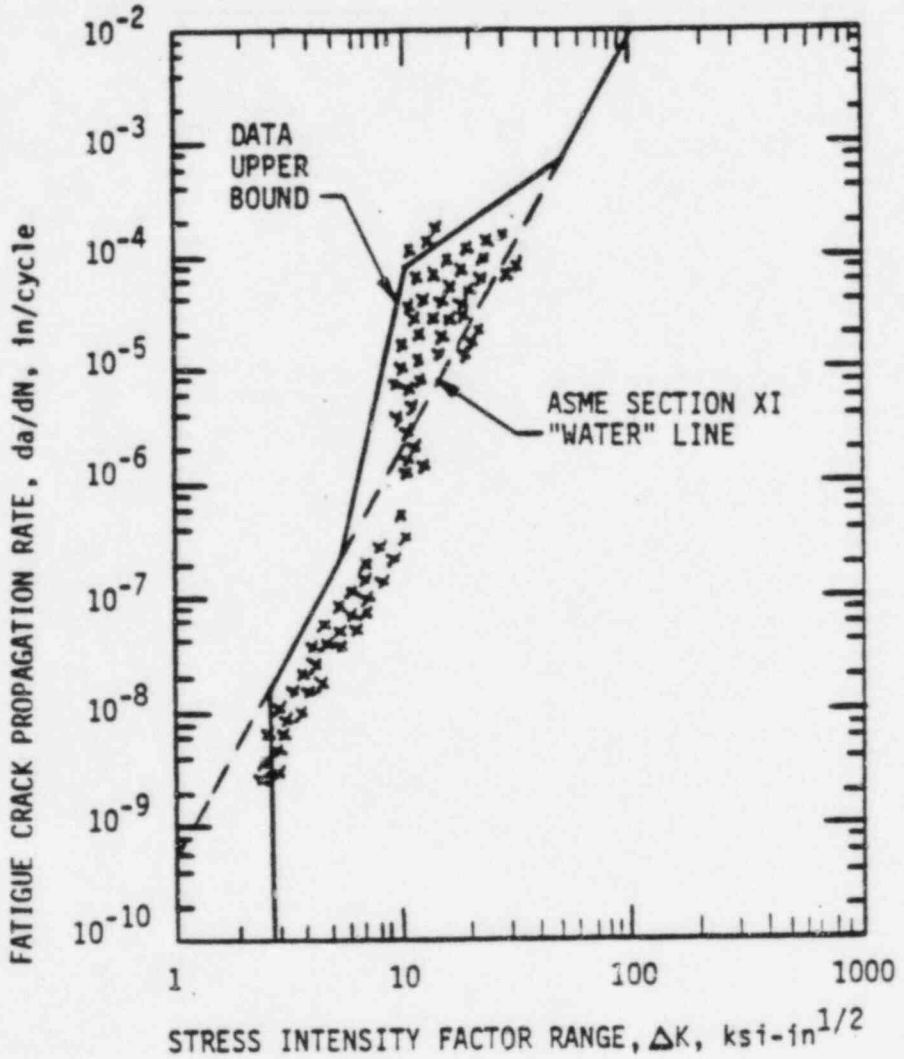

Fig. 1: FATIGUE CRACK GROWTH CURVE, da/dN vs. ΔK

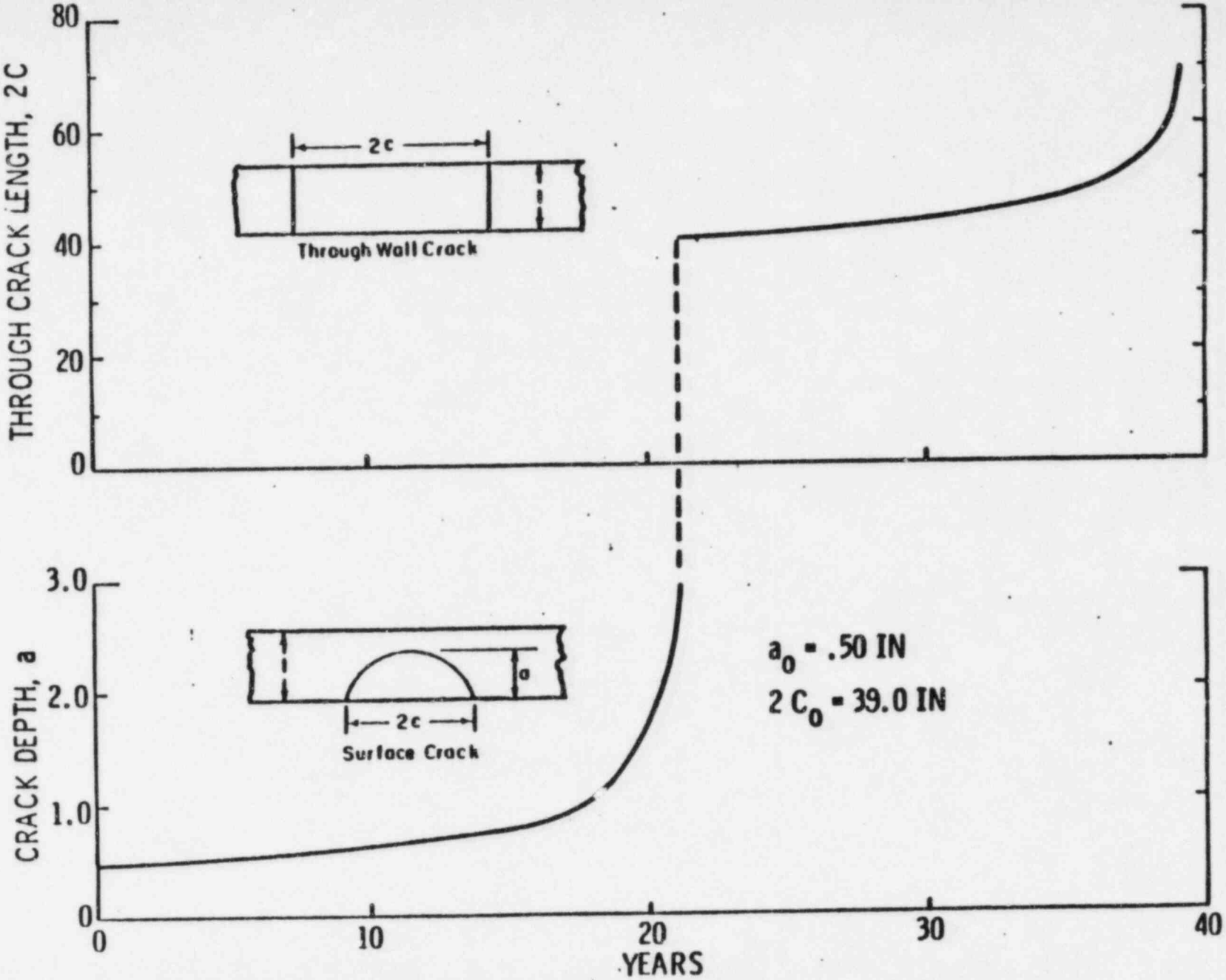

Fig. 2 FATIGUE CRACK GROWTH VS. YEARS OF OPERATION

a_0 = .50 in., 2 C_0 = 39.0 in.

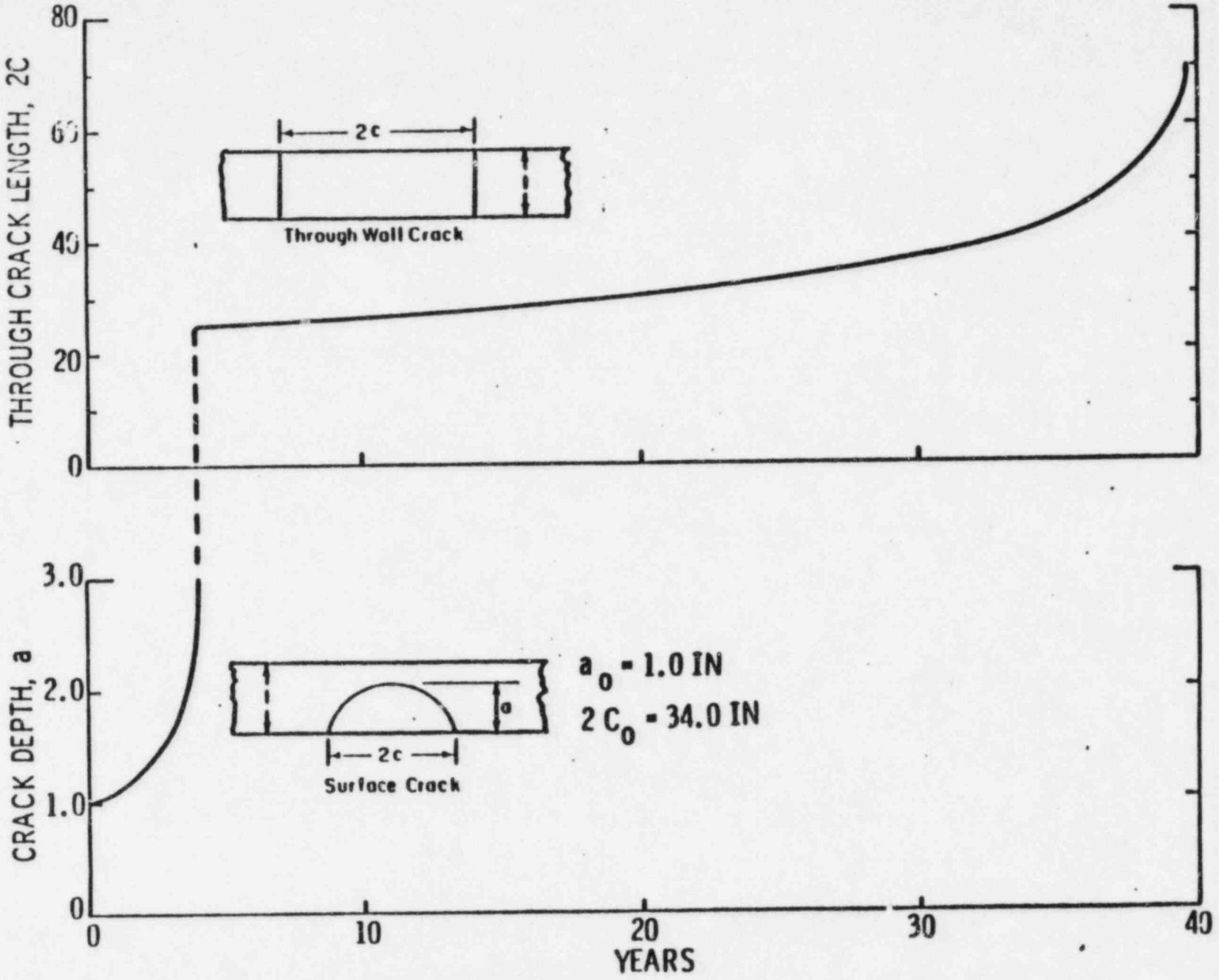

Fig. 3 FATGUE CRACK GROWTH VS. YEARS OF OPERATION
a_0=1.0 in., 2 C_0= 34.0 in.

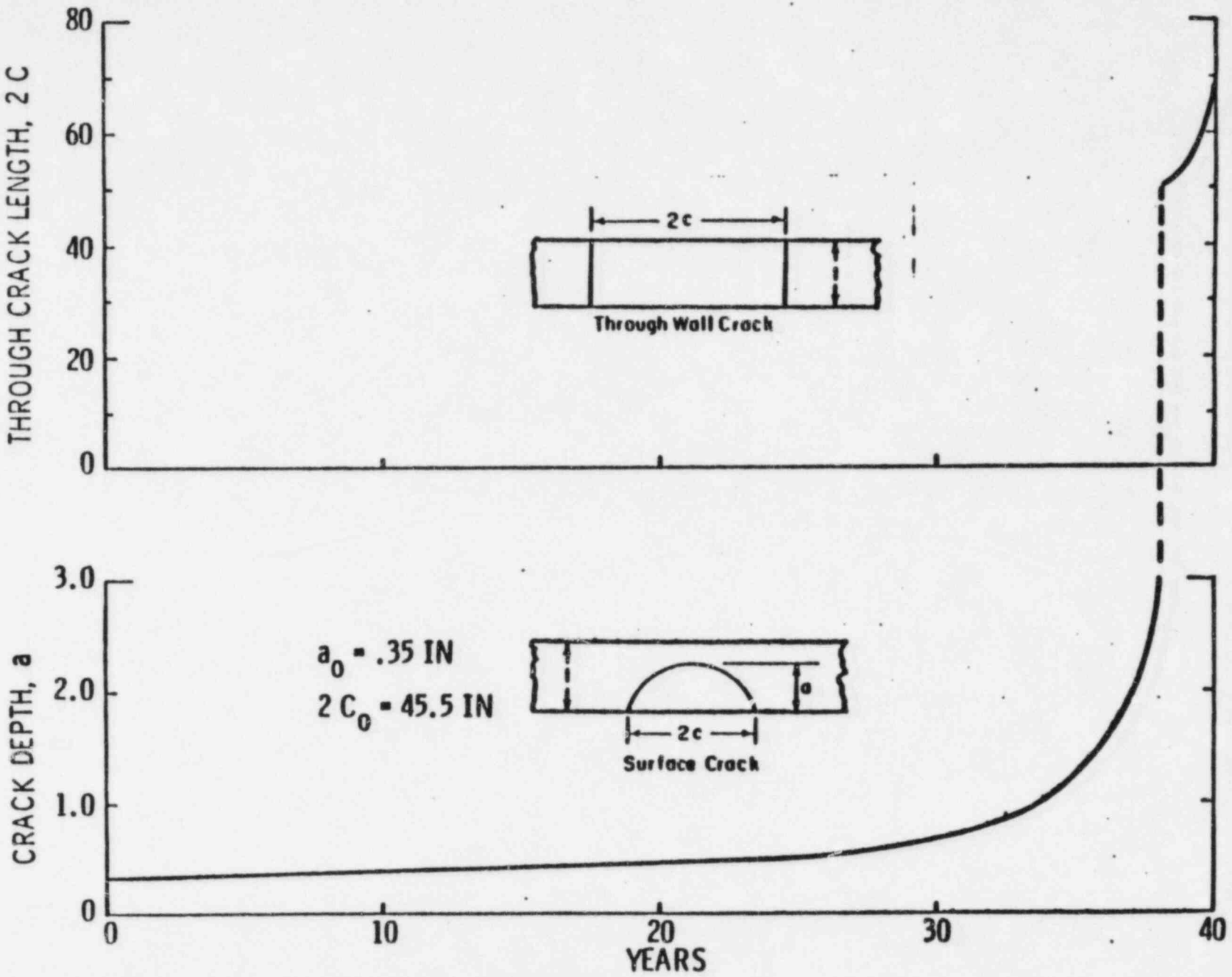

Fig. 4 FATIGUE CRACK GROWTH VS. YEARS OF OPERATION

a_0 = .35 in., 2 C_0 = 45.5 in.

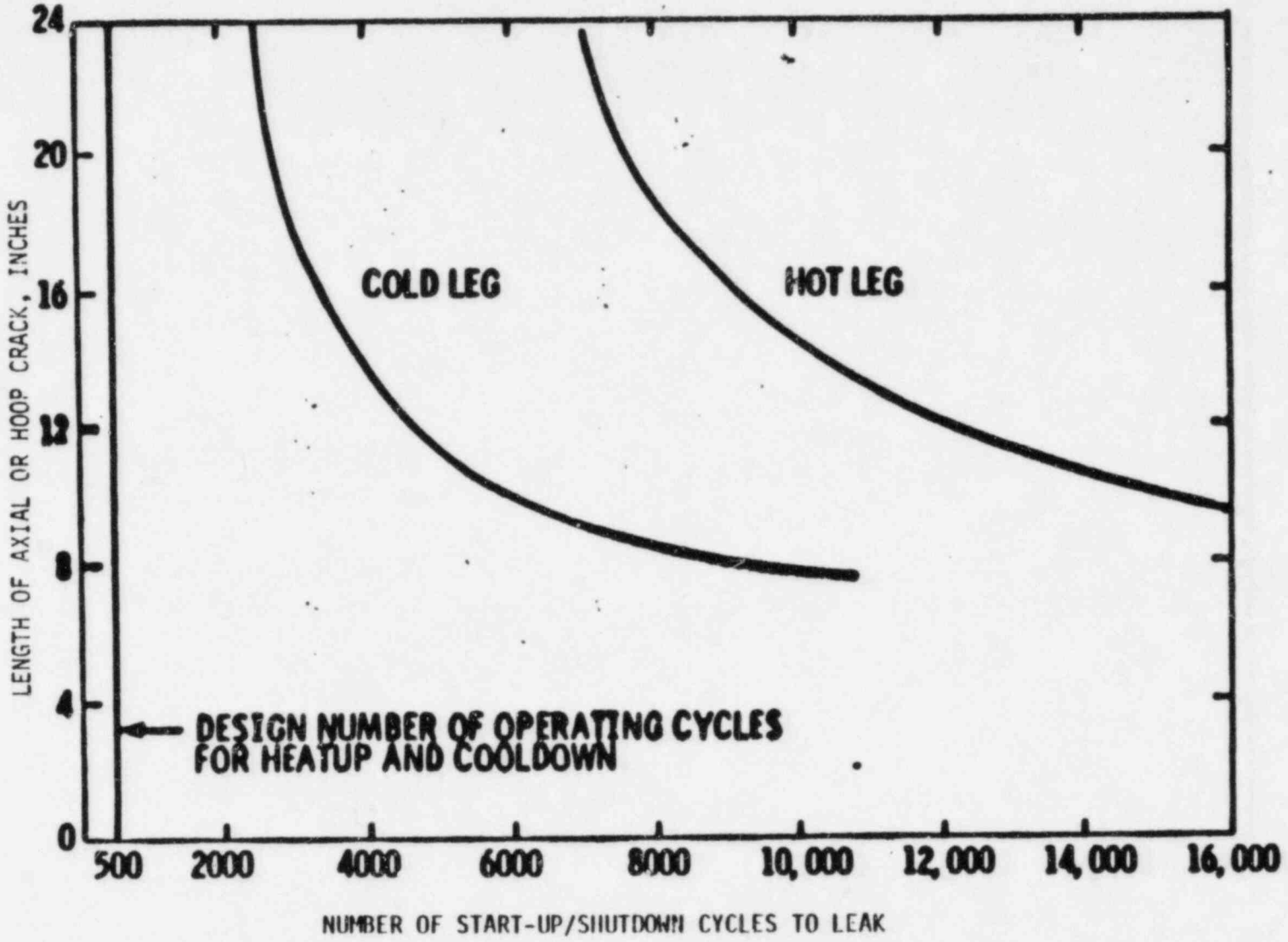

Fig. 5 NUMBER OF CYCLES AT 18 KSI TO CAUSE A CRACK ORIGIMALLY ONE INCH DEEP TO LEAK

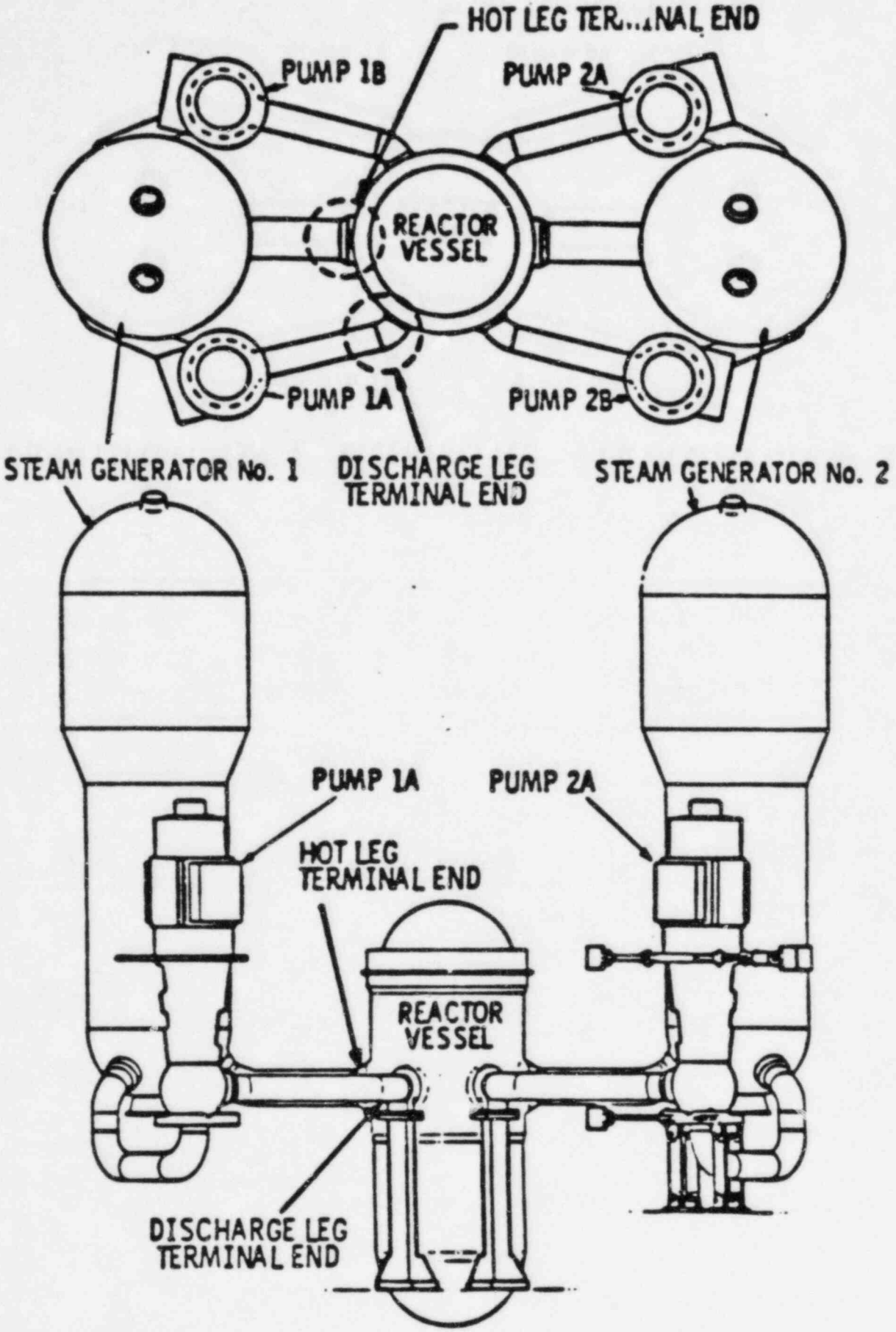

Fig. 6 NUCLEAR STEAM SUPPLY SYSTEM ARRANGEMENT SHOWING LOCATIONS IN THE PRIMARY COOLANT SYSTEM THAT WERE ANALYZED

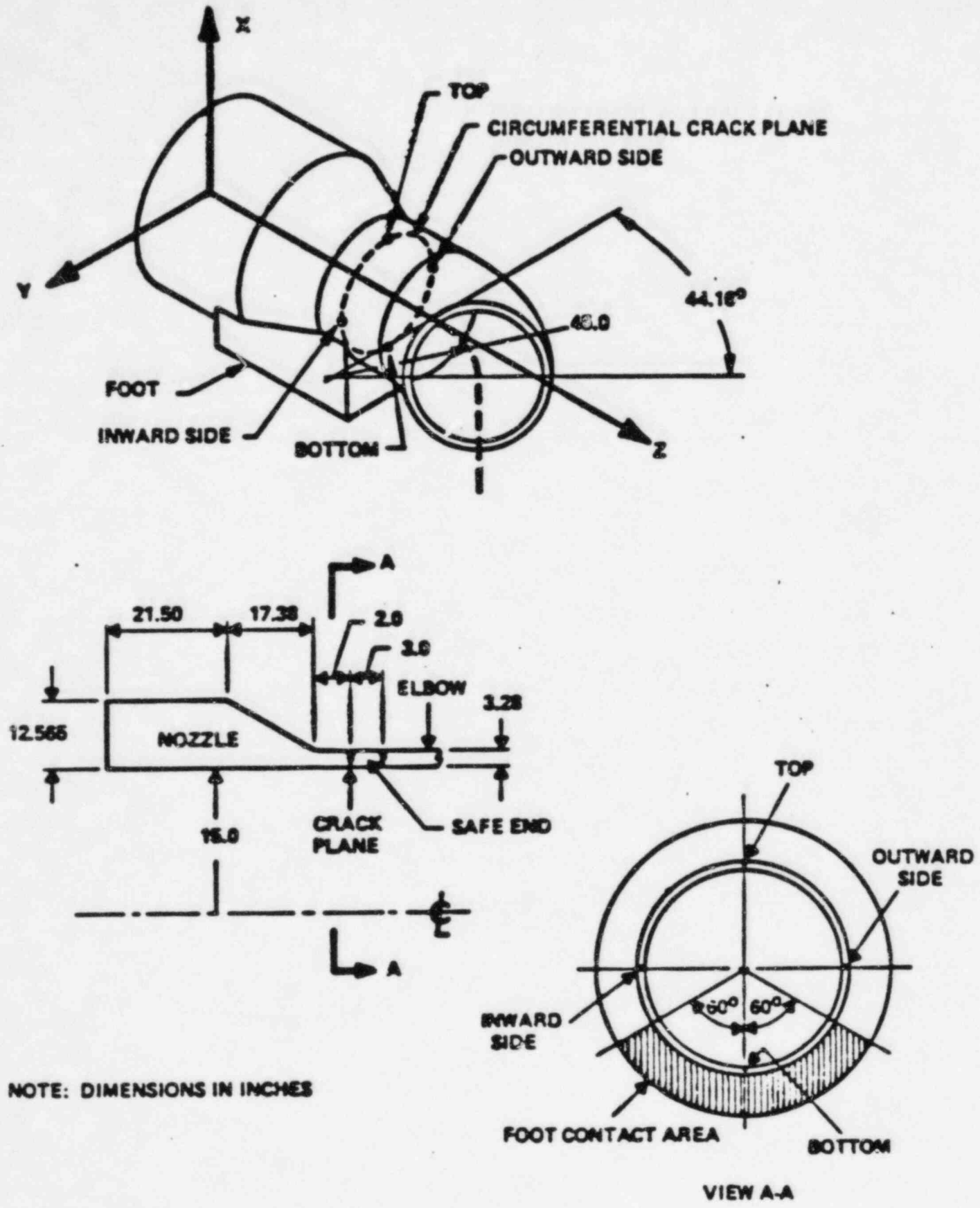

NOTE: DIMENSIONS IN INCHES

Fig. 7: DISCHARGE LEG TERMINAL END

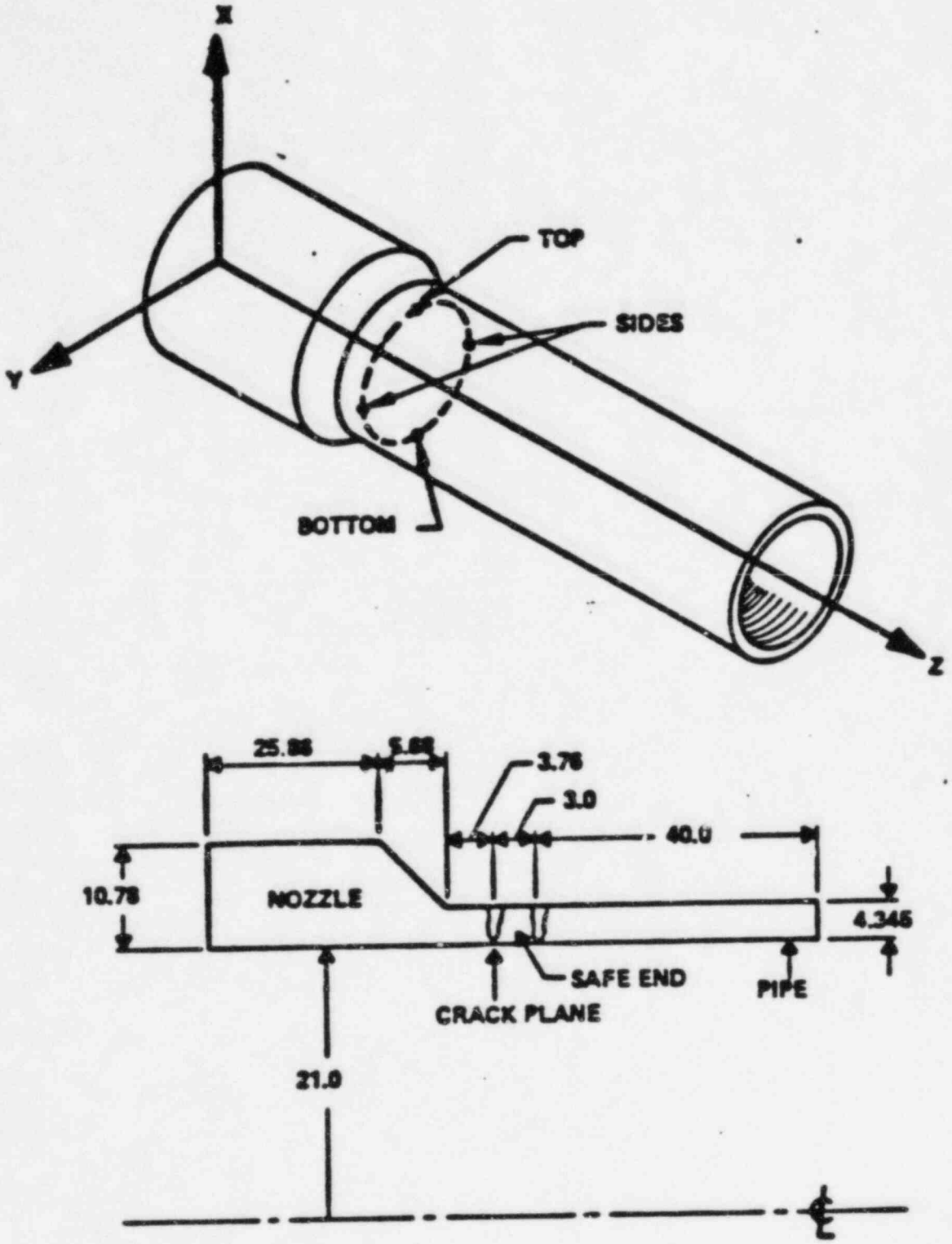

NOTE: DIMENSIONS IN INCHES

Fig. 8: HOT LEG TERMINAL END

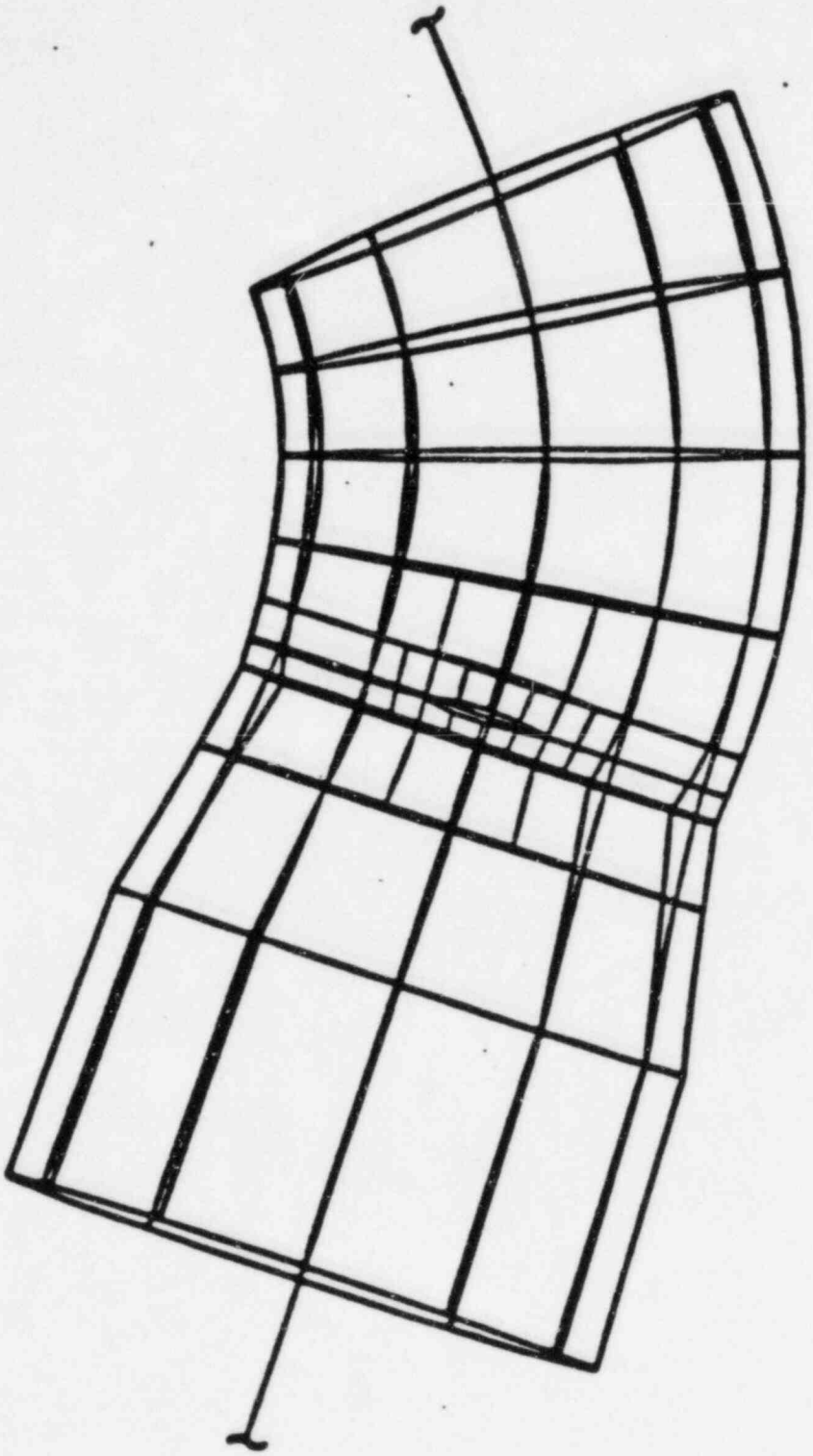

Fig. 9: FINITE ELEMENT MODEL AFTER DEFORMATION OF DISCHARGE LEG TERMINAL END WITH BOTTOM CRACK

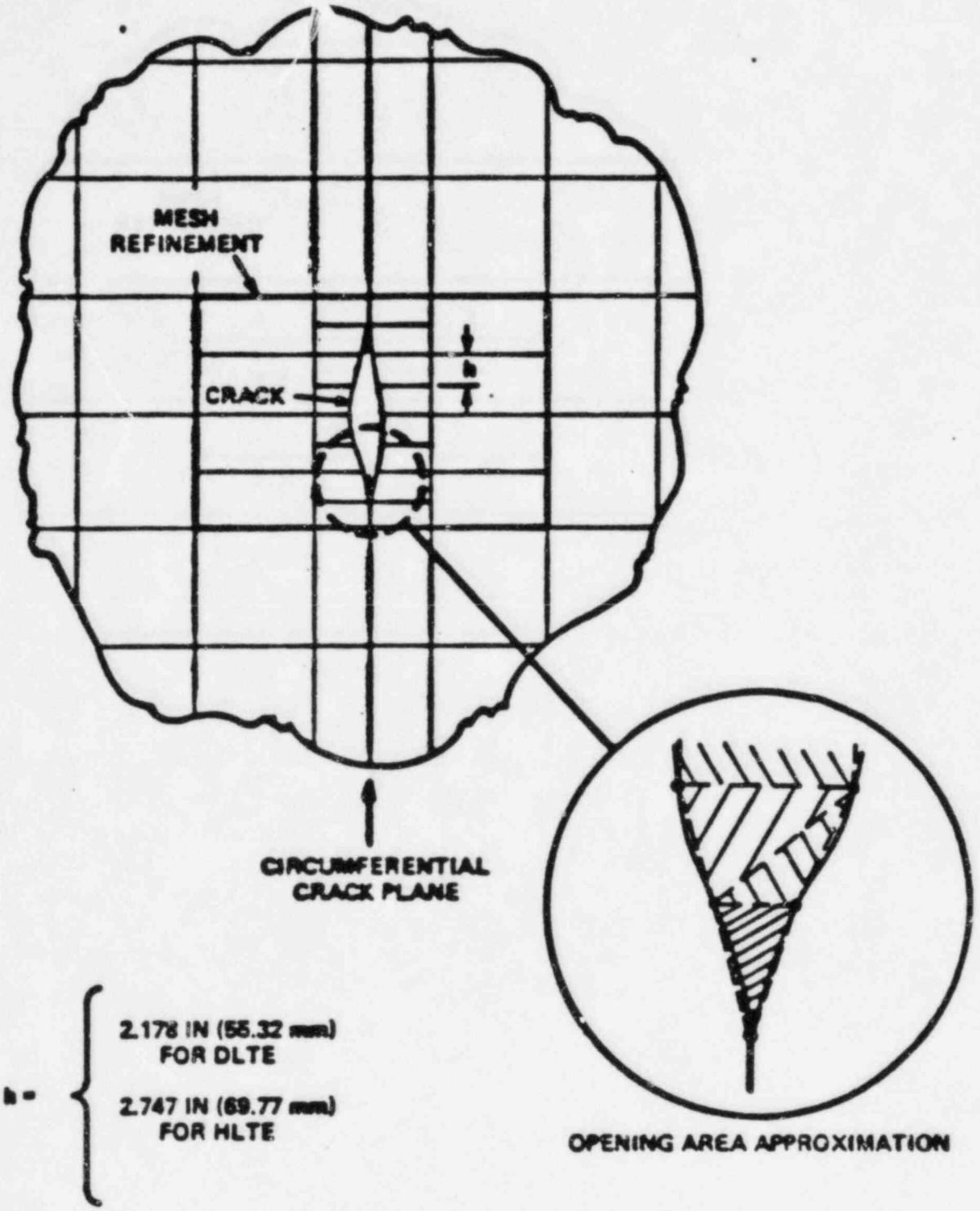

Fig. 10: MESH REFINEMENT FOR CRACK OPENING AREA MODELLING

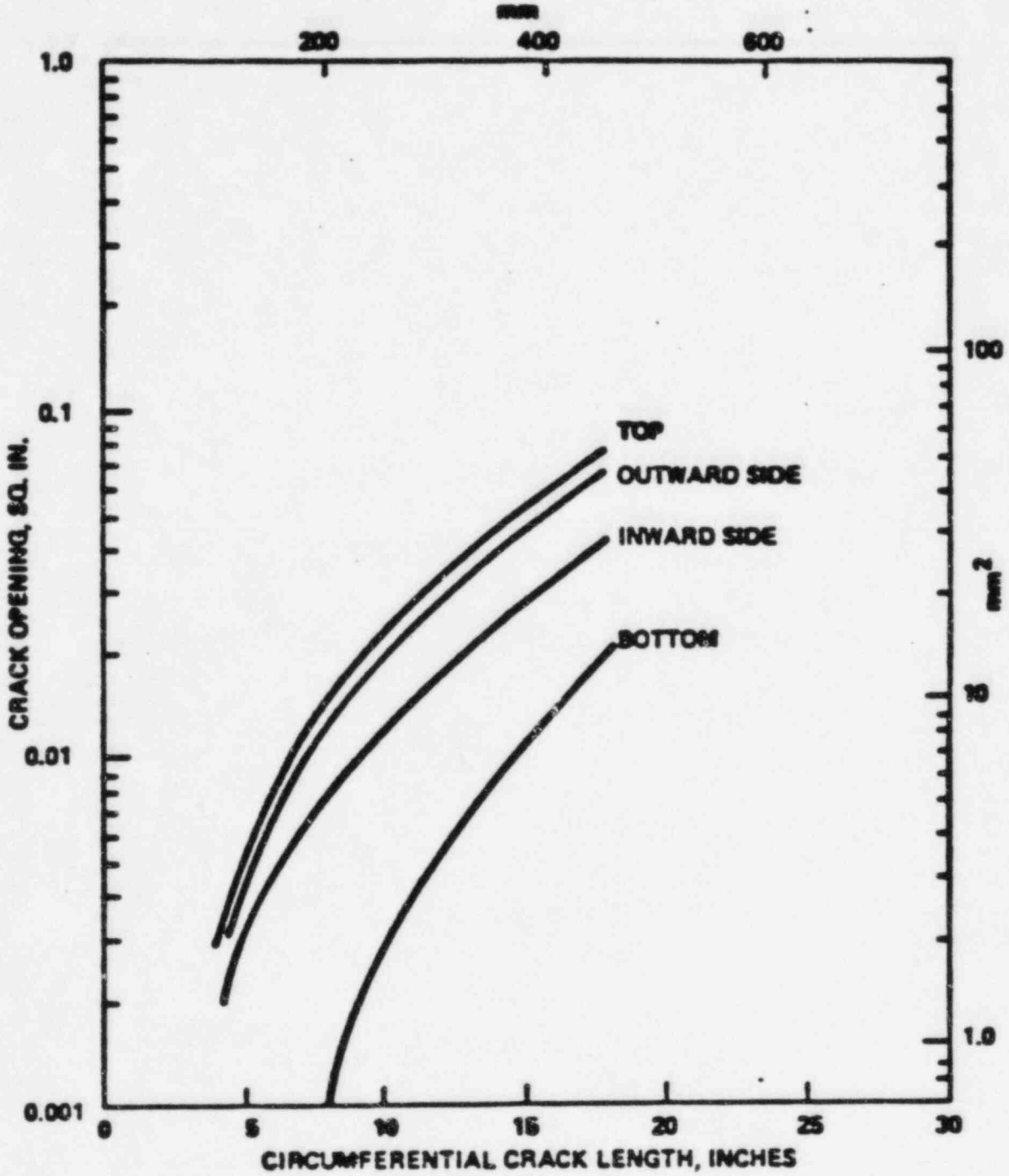

Fig. 11: CRACK OPENING AREA vs CRACK LENGTH FOR 30" DISCHARGE LEG TERMINAL END AT REACTOR VESSEL INLET NOZZLE WITH NORMAL OPERATING SYSTEM LOADS

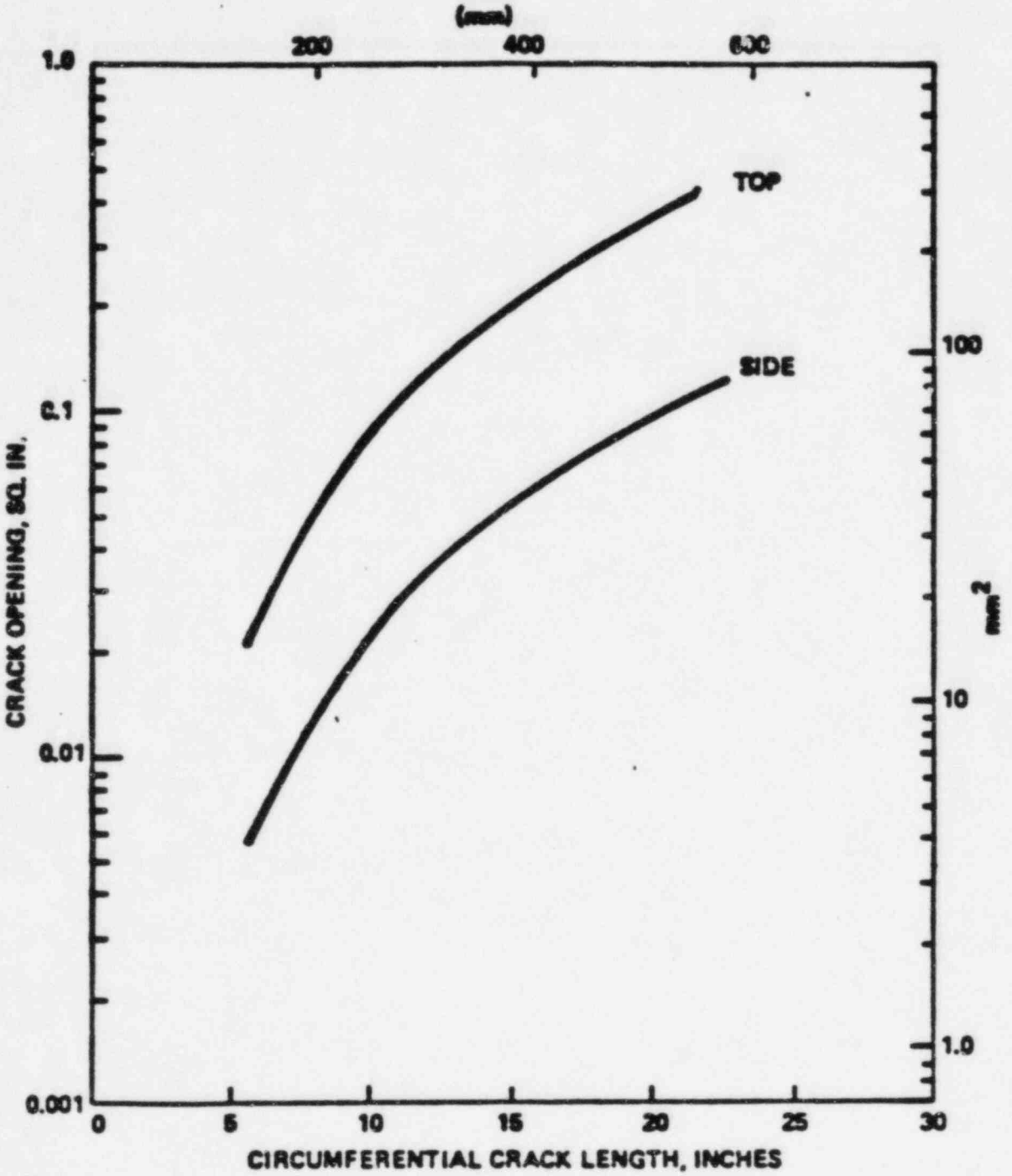

Fig. 12: CRACK OPENING AREA vs CRACK LENGTH FOR 42" HOT LEG TERMINAL END AT REACTOR VESSEL OUTLET NOZZLE WITH NORMAL OPERATING SYSTEM LOADS

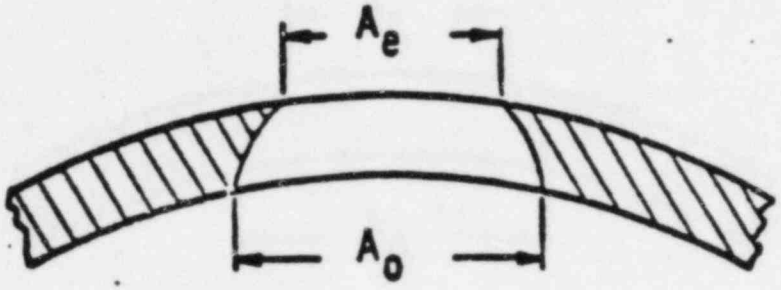

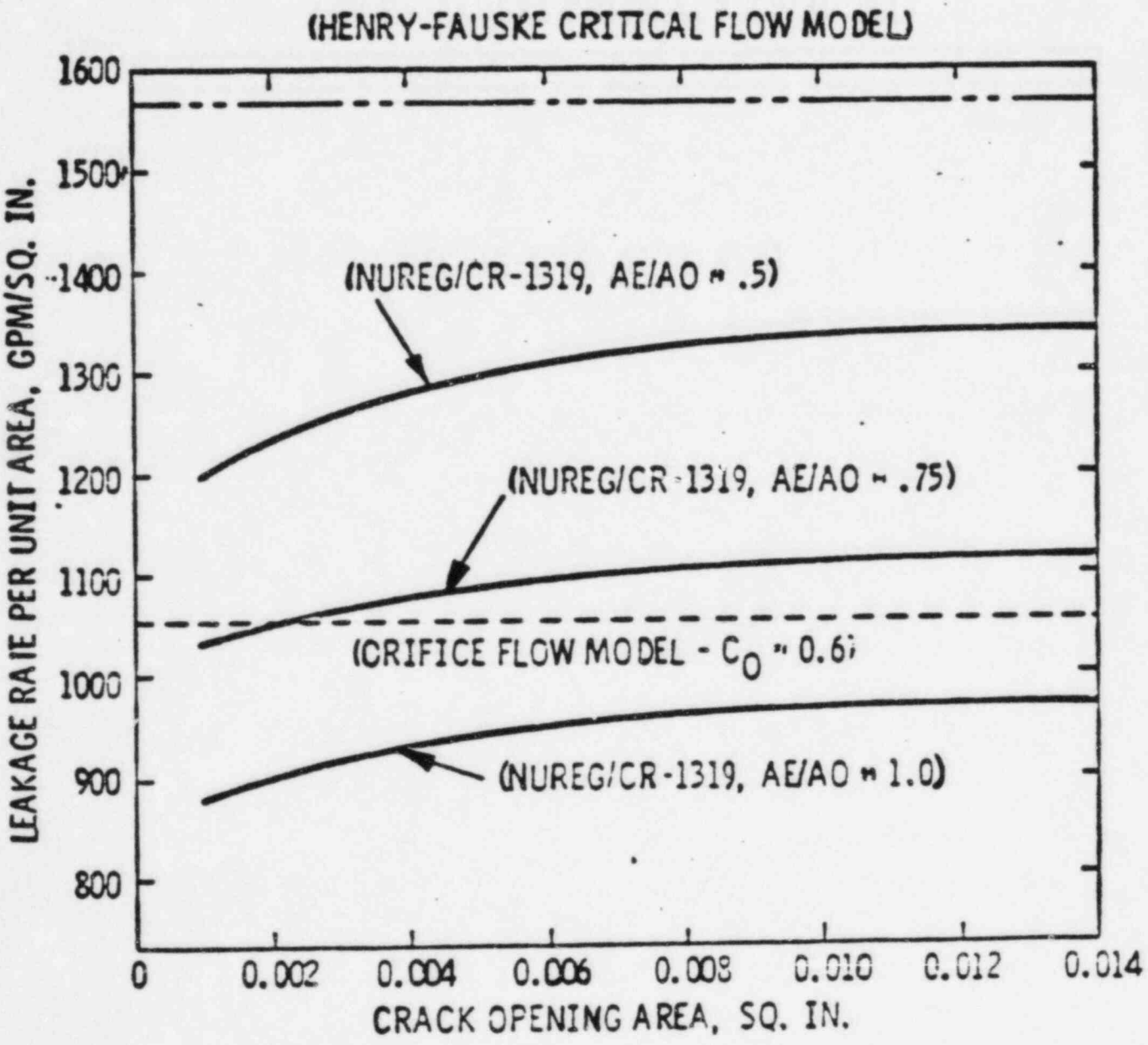

Fig. 13:

FLOW/CRACK AREA CORRELATIONS

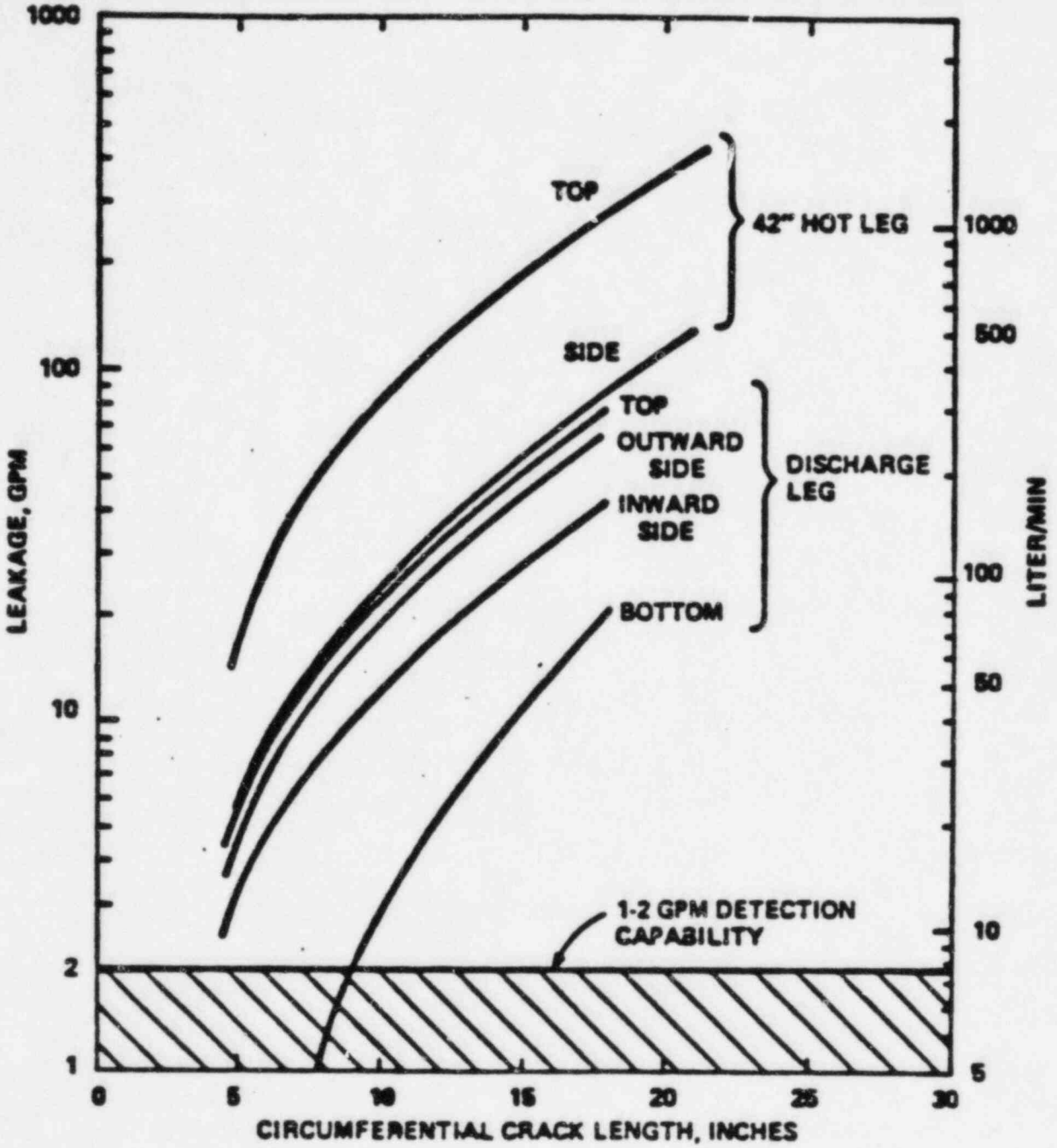

Fig. 14: LEAKAGE RATE vs CRACK LENGTH FOR 30" AND 42" PIPE TERMINAL ENDS AT REACTOR VESSEL NOZZLES WITH NORMAL OPERATING SYSTEM LOADS

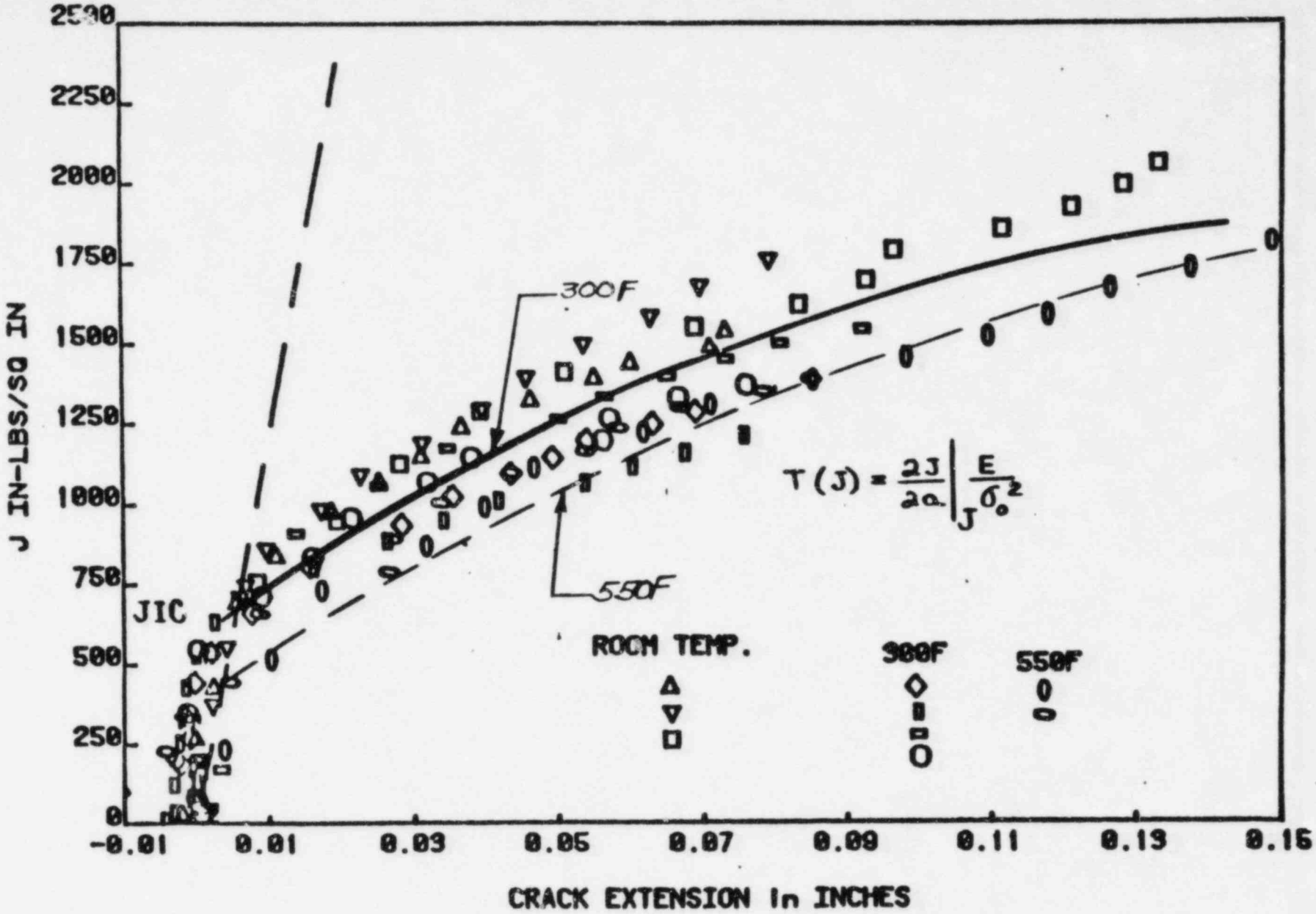

Fig. 15: J vs CRACK EXTENSION, A516 (20% SIDE GROOVES)

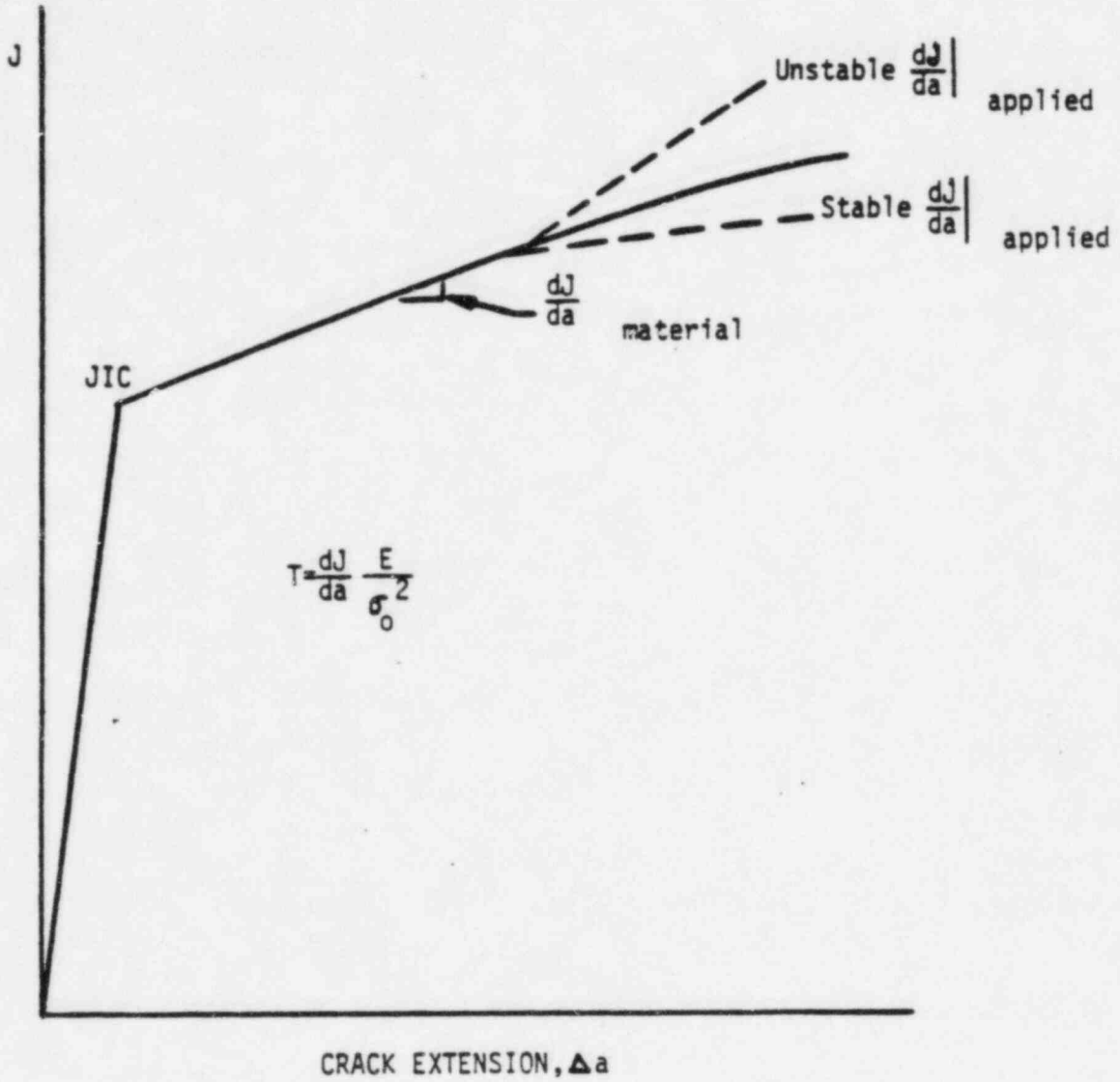

Fig. 16: PLASTIC INSTABILITY CRITERION

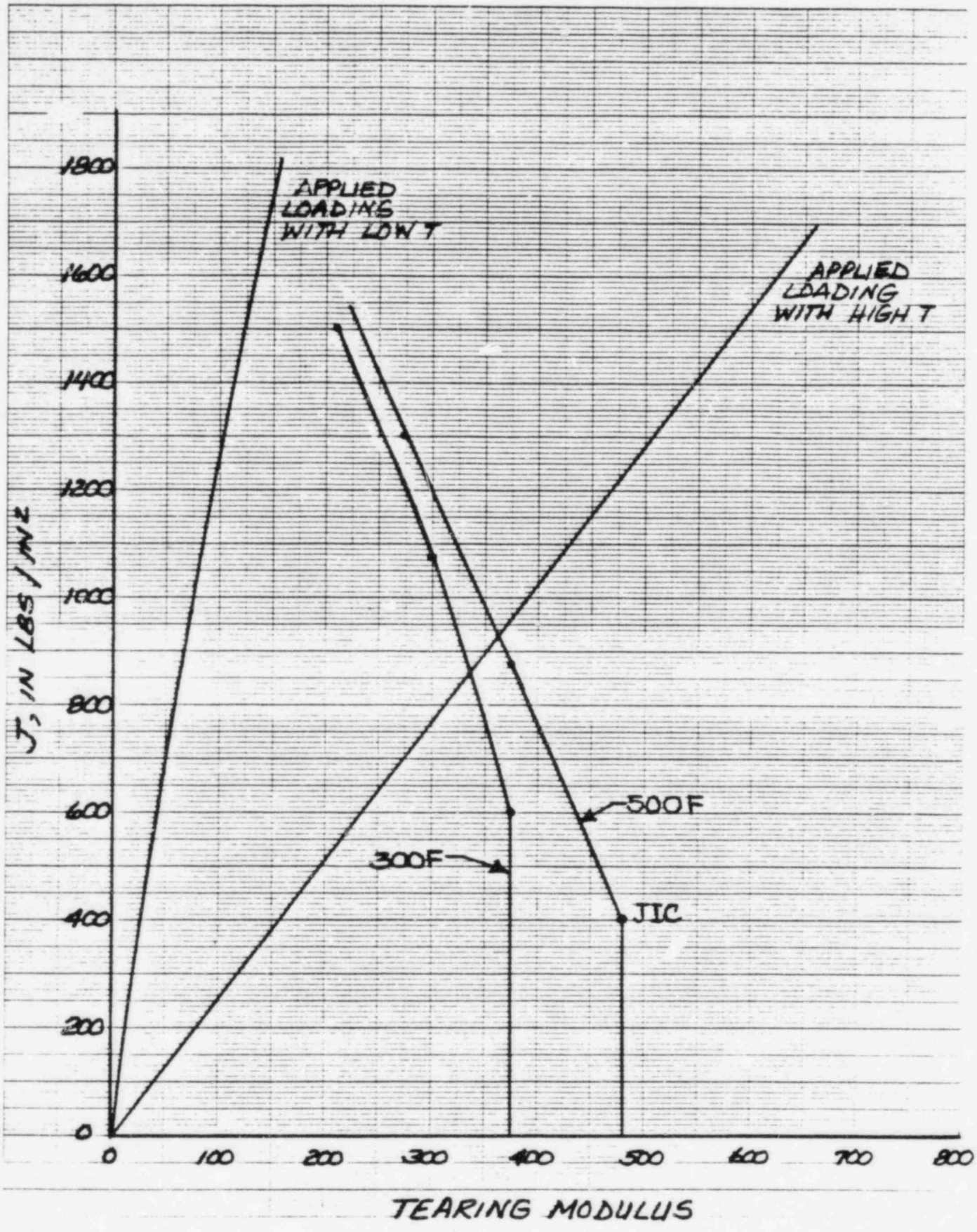

FIG. 17: INSTABILITY DIAGRAM ILLUSTRATING THE INTERACTIONS OF MATERIAL AND STRUCTURAL PARAMETERS

SA 516 GR. 70 PIPE (PLATE) MATERIAL FOR ARIZONA I

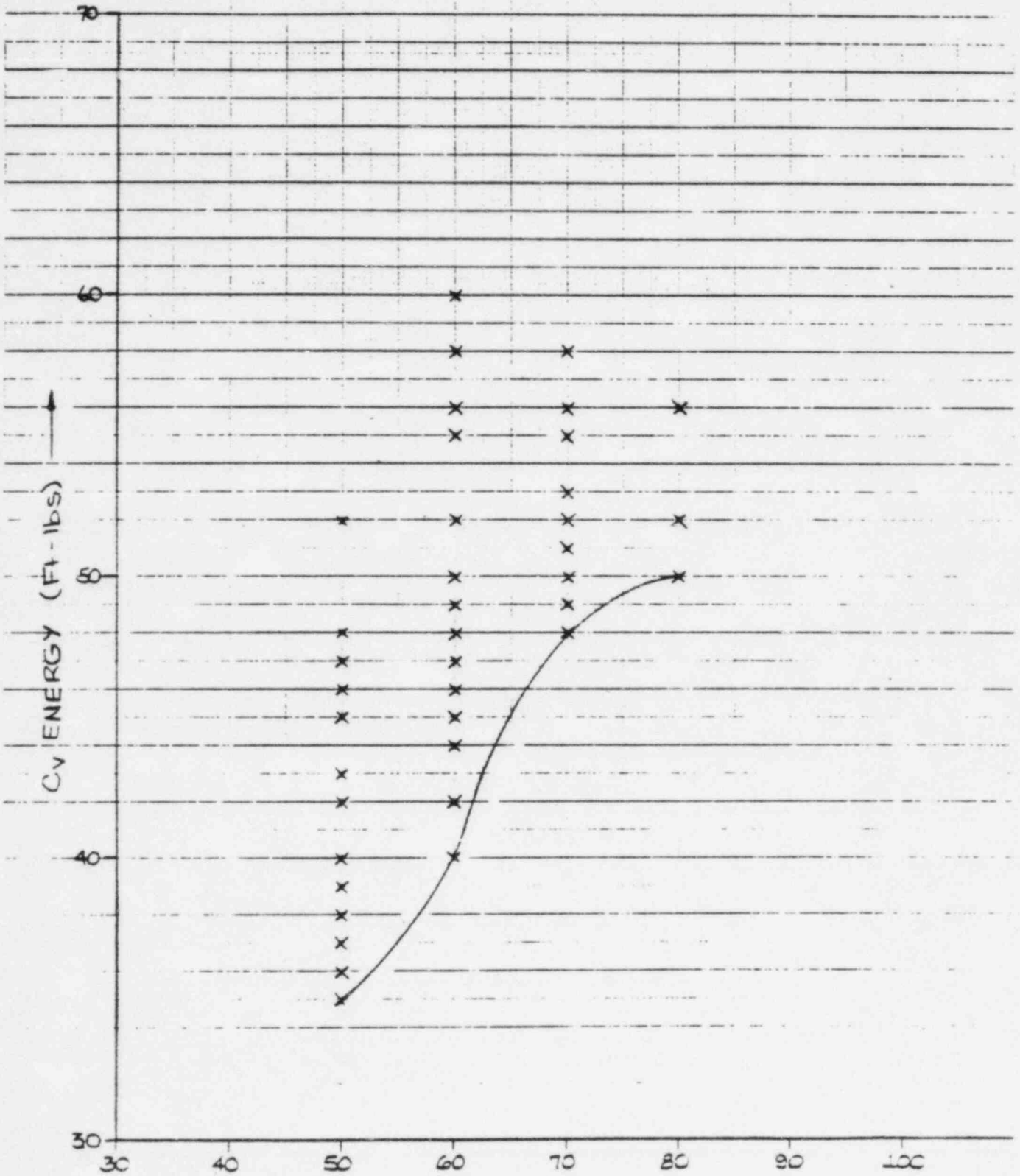

FIGURE 18

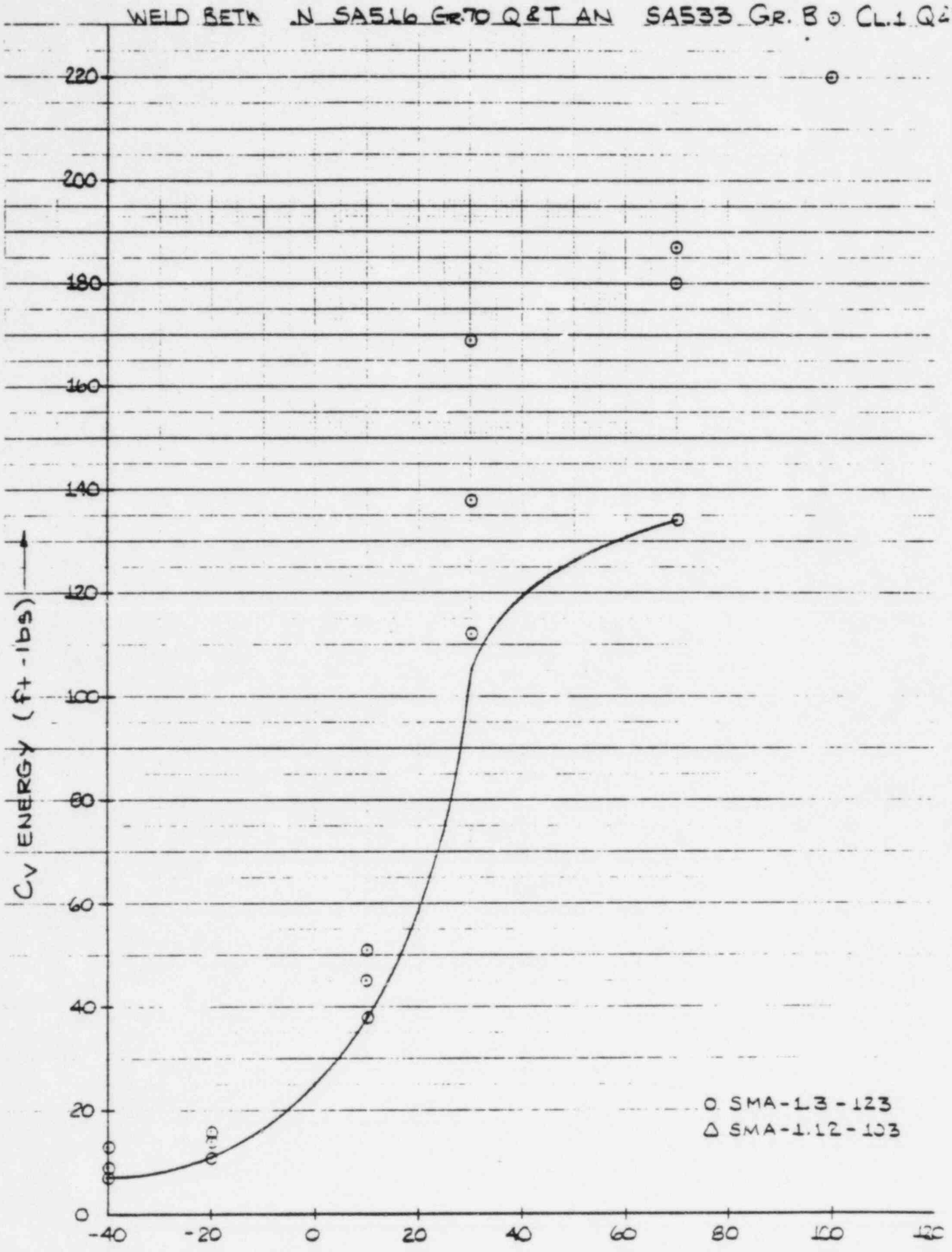

FIGURE 19

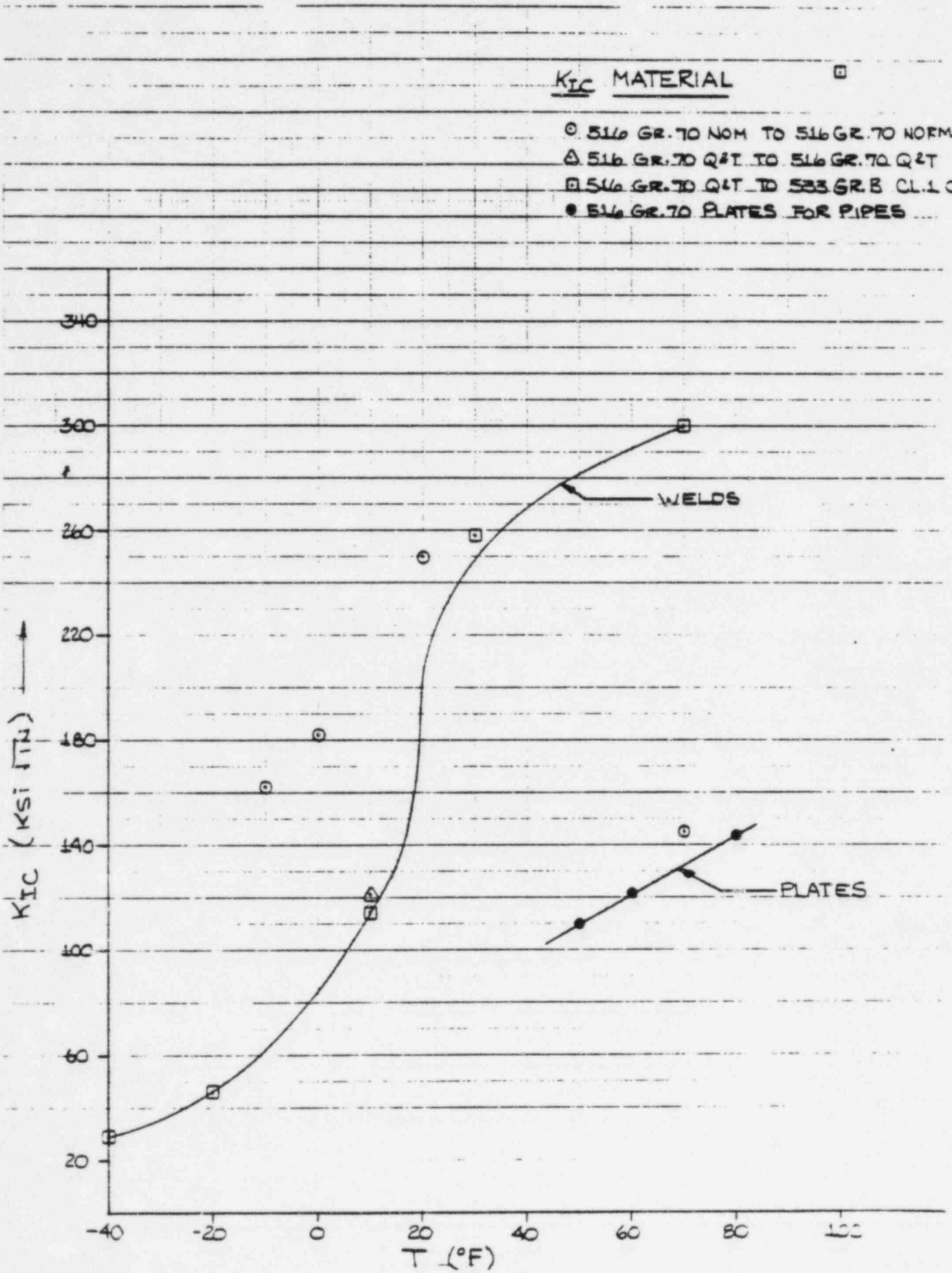

FIGURE 20

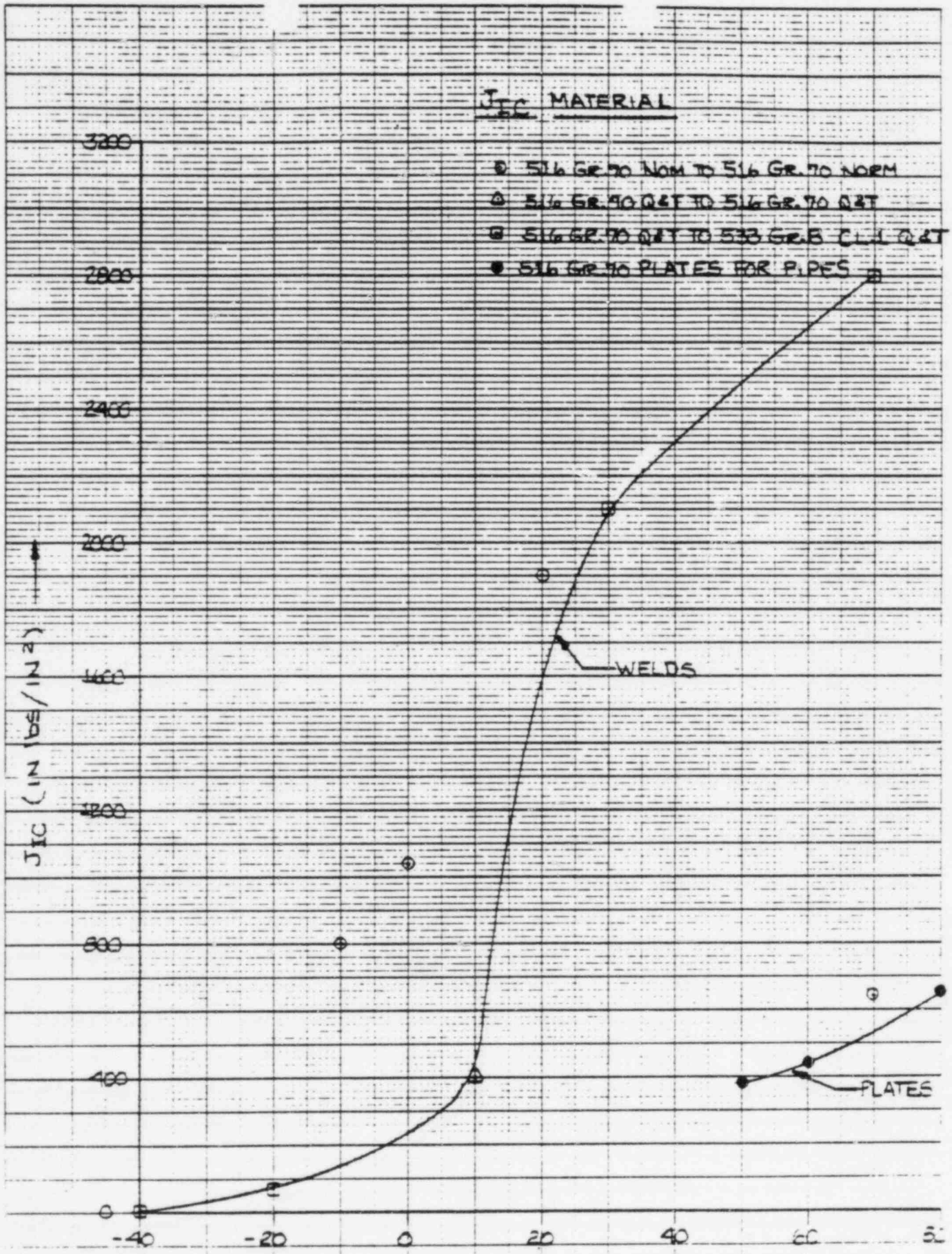

FIGURE 21

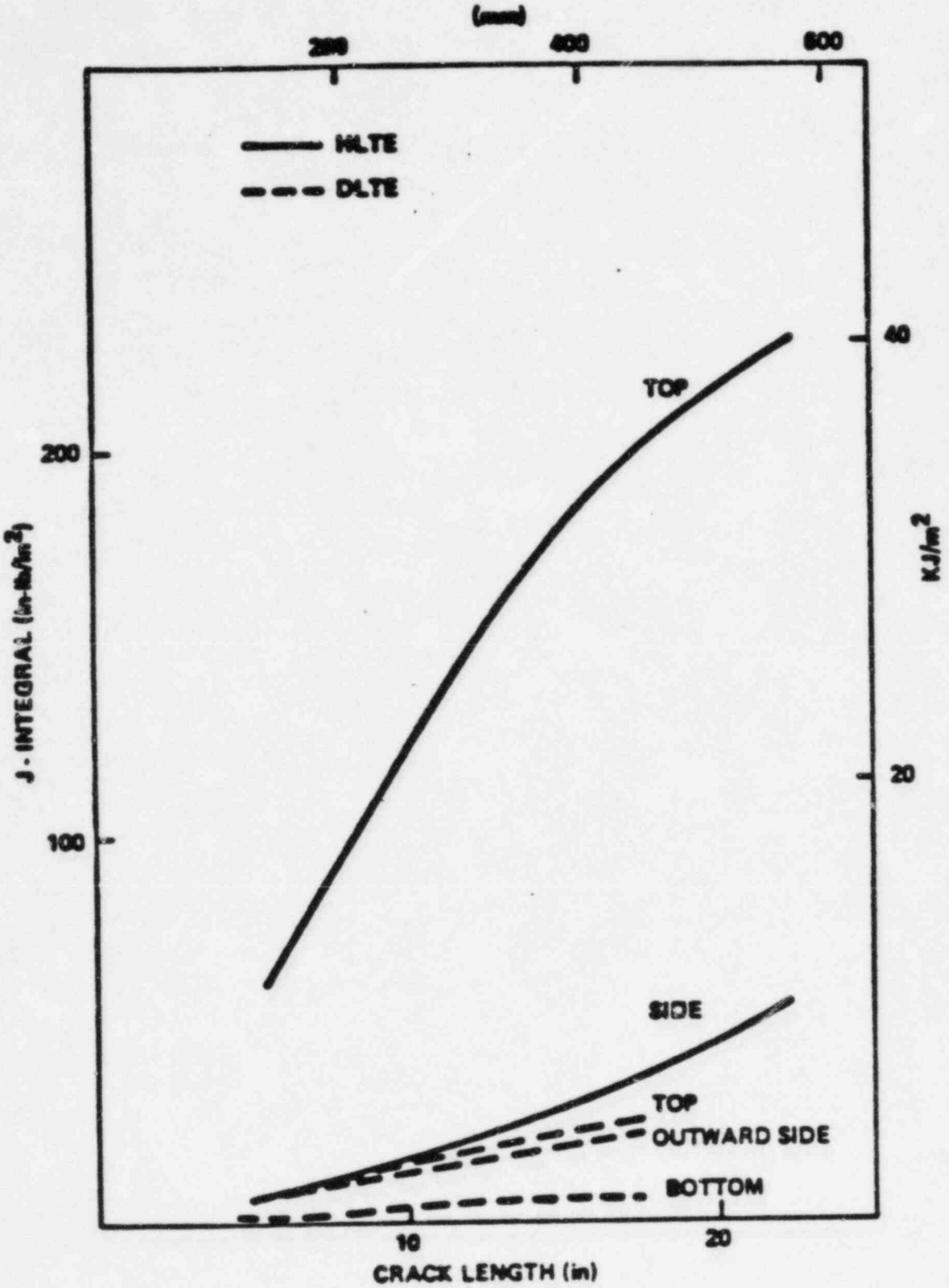

FIG 22 : MAXIMUM J - INTEGRAL VALUE

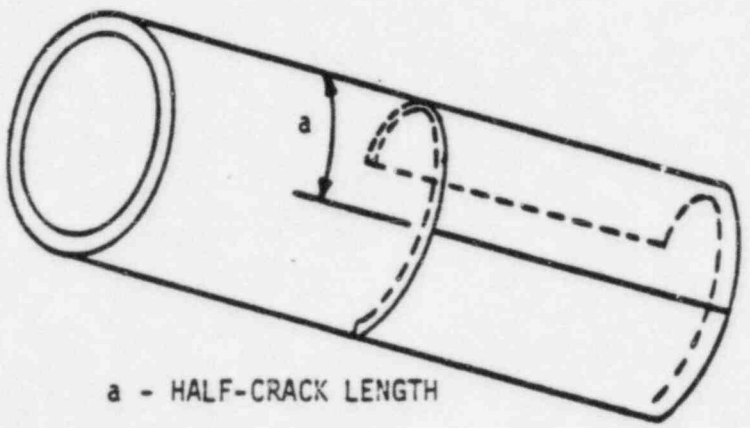

Fig. 23: GEOMETRY OF PIPE WITH HYPOTHETICAL HALF-CIRCUMFERENCE CRACK

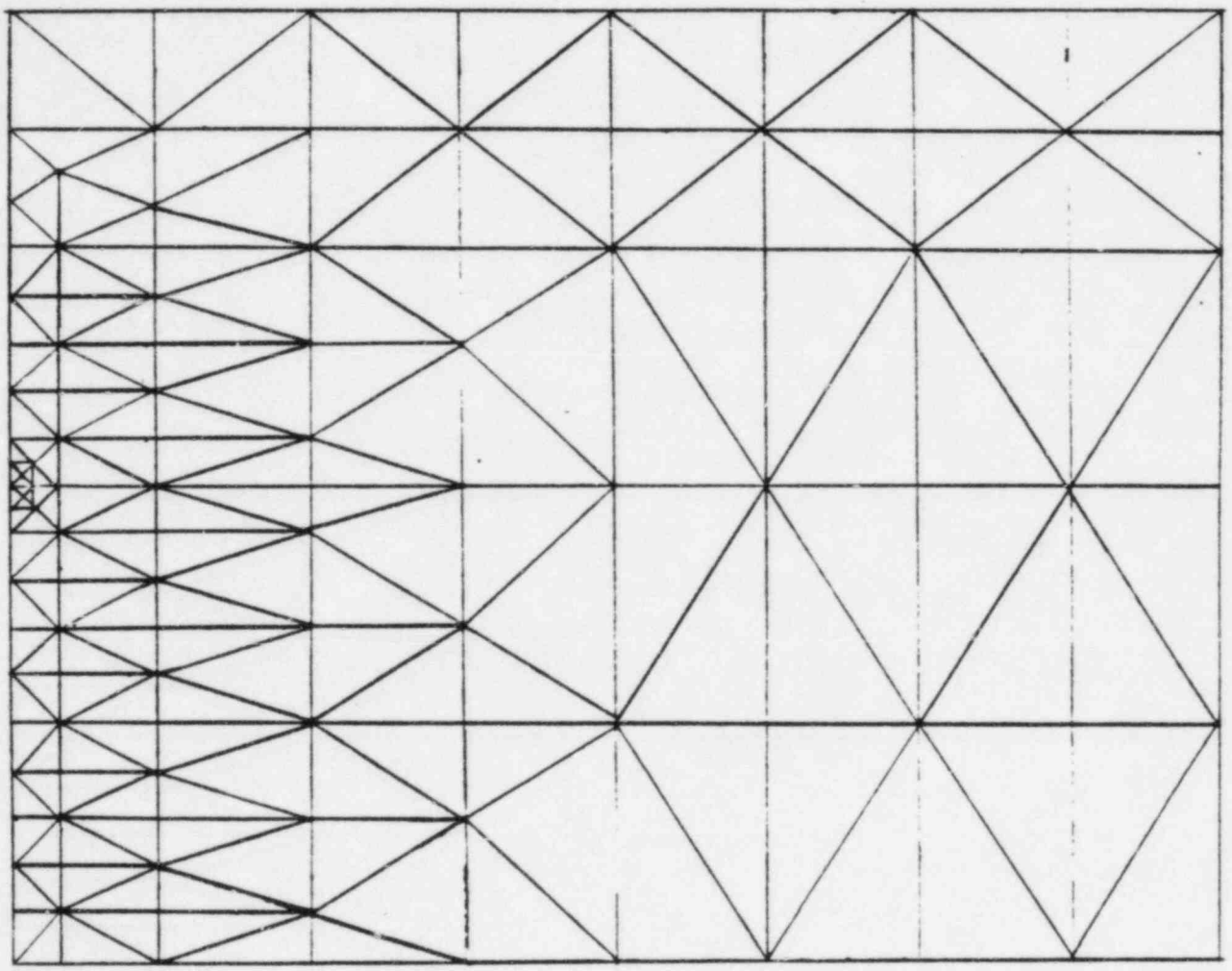

Fig. 24: SHELL MODEL FOR HALF-CIRCUMFERENCE CRACK IN PIPE

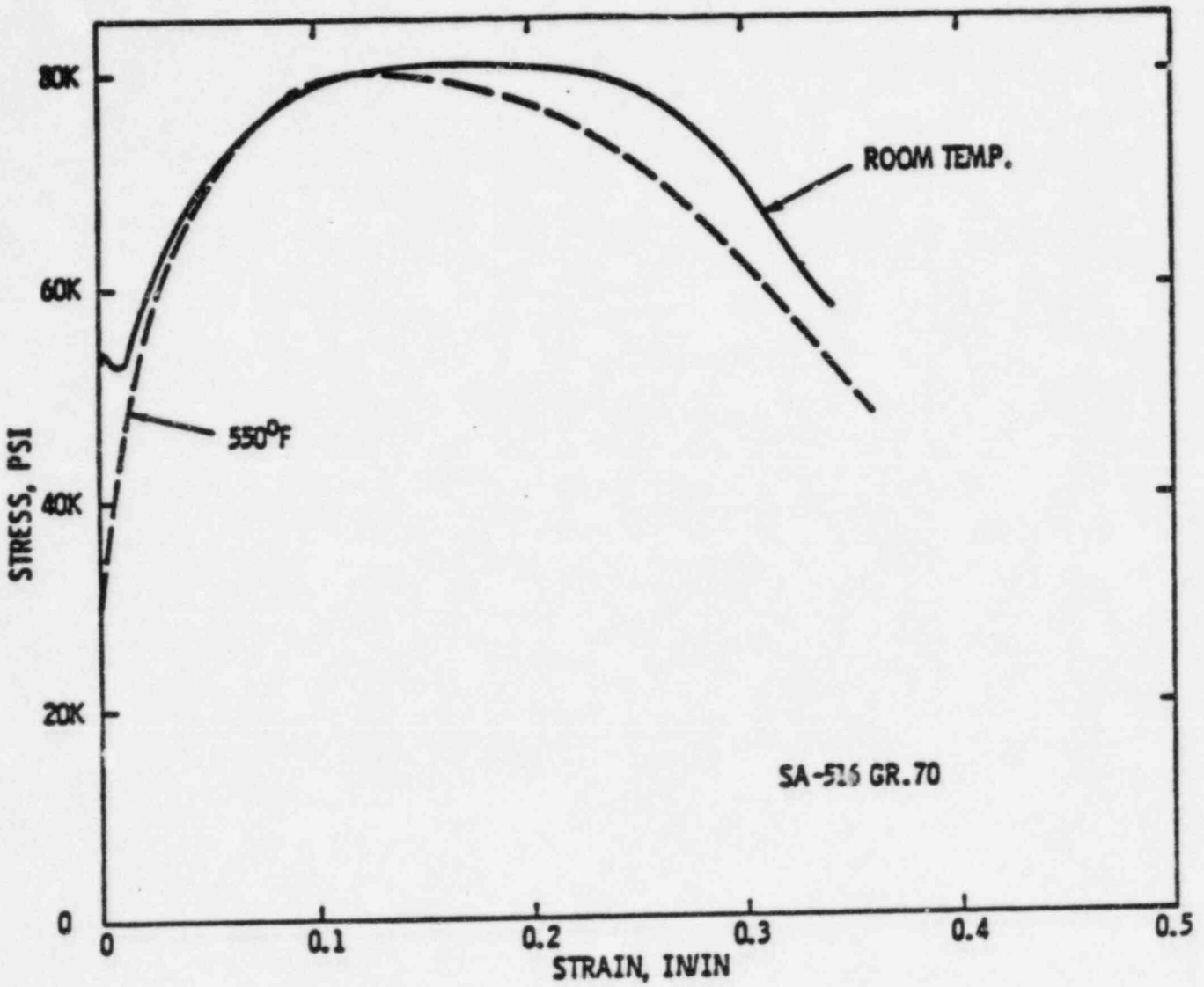

FIG. 25: STRESS-STRAIN CURVE

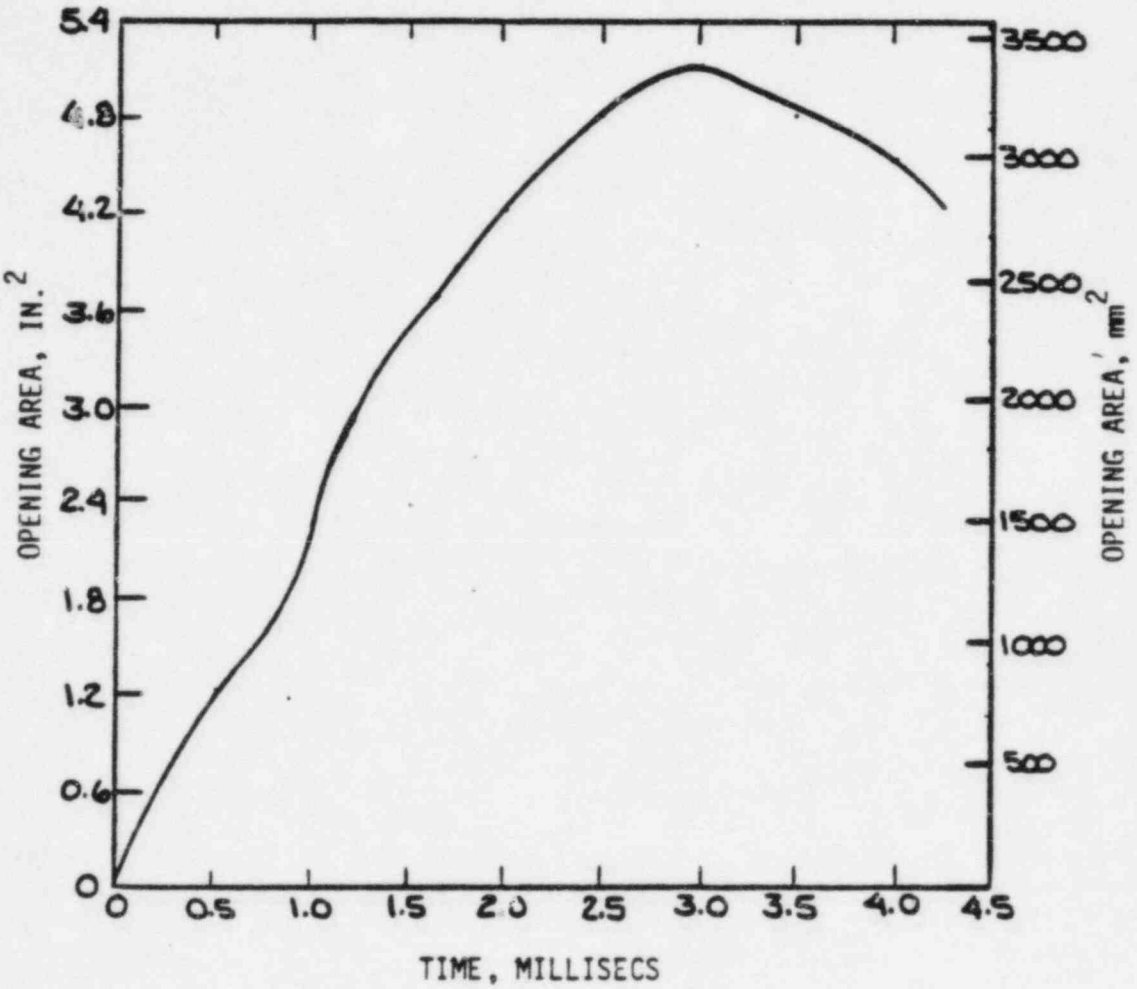

Fig. 26: OPENING AREA OF HALF-CIRCUMFERENCE CRACK VS. TIME

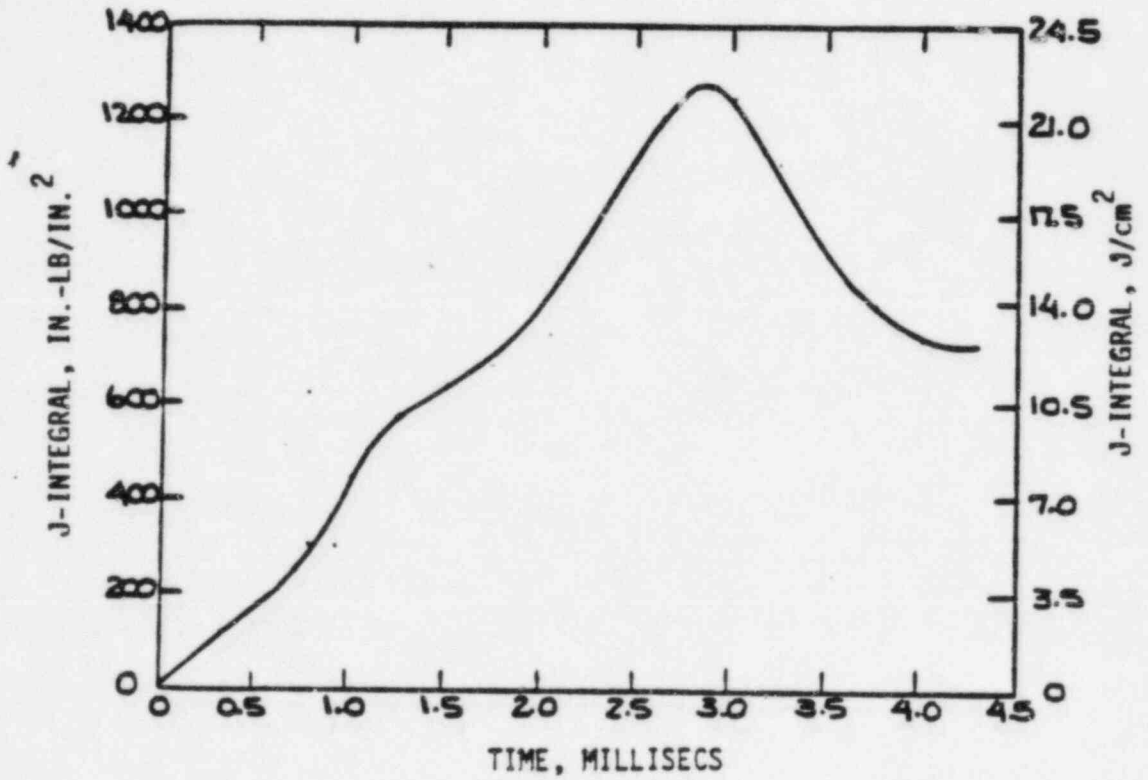

Fig. 27: J-INTEGRAL VS. TIME DURING OPENING OF HALF-CIRCUMFERENCE CRACK

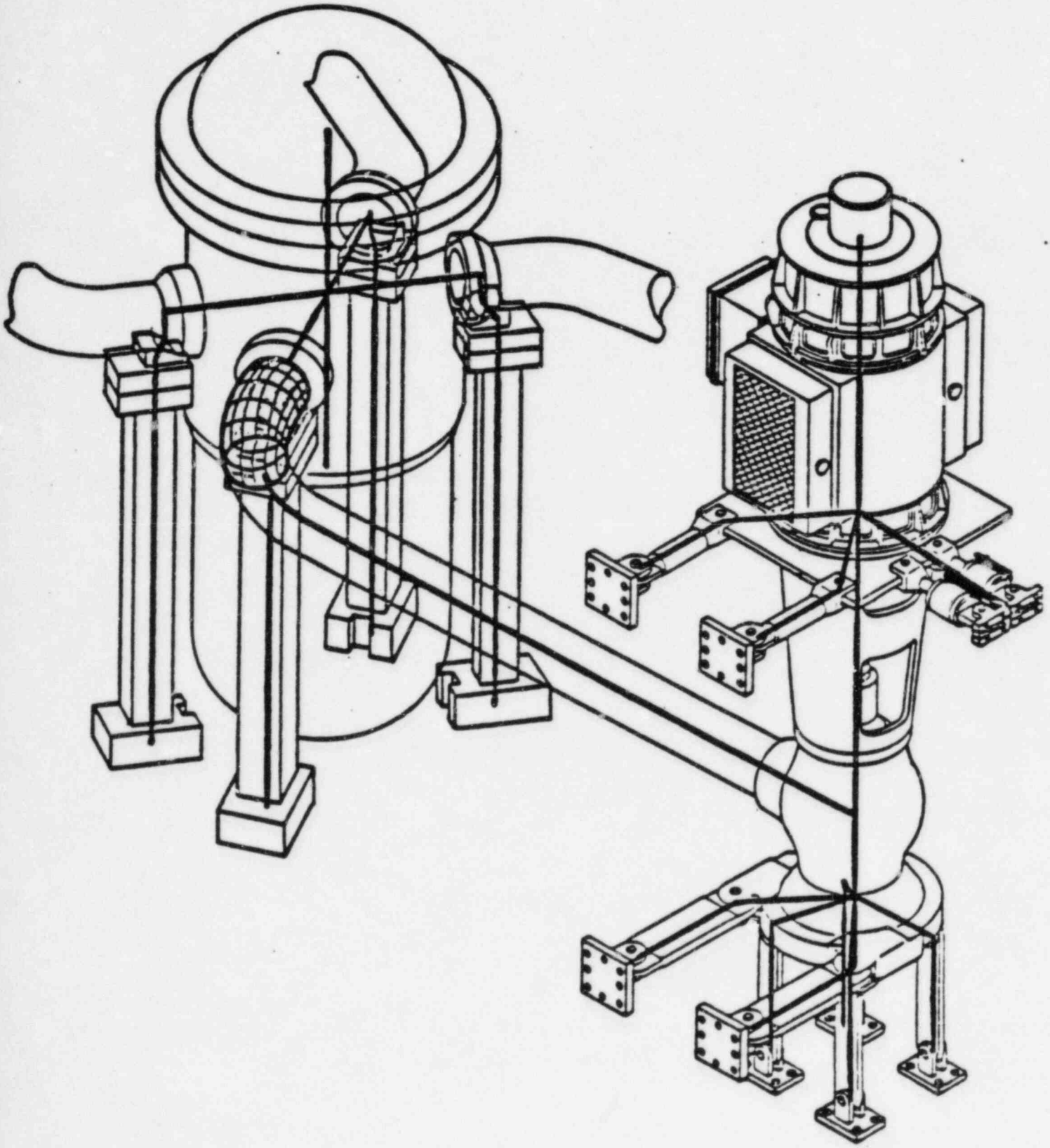

Fig. 28. FINITE ELEMENT MODEL FOR DYNAMIC ELASTIC PLASTIC SEISMIC ANALYSIS

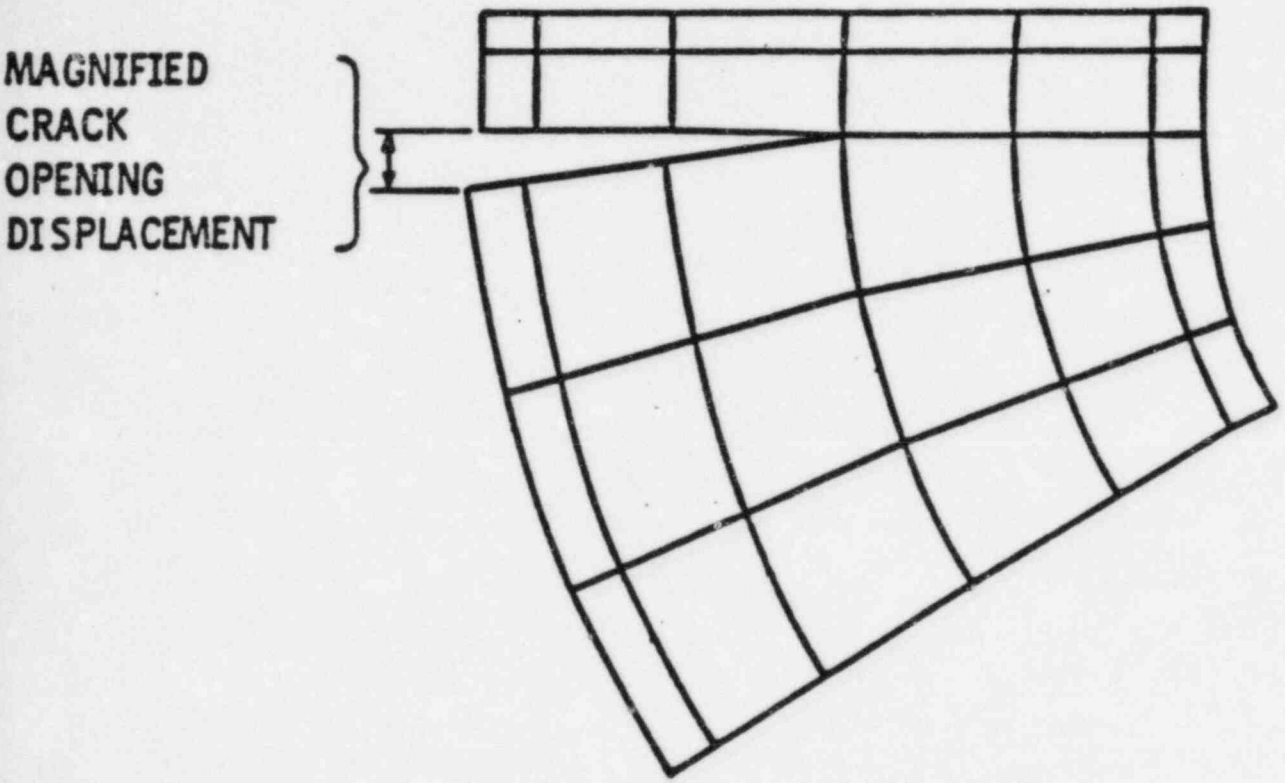

FIG. 29: TOP VIEW OF PIPE WITH CRACK

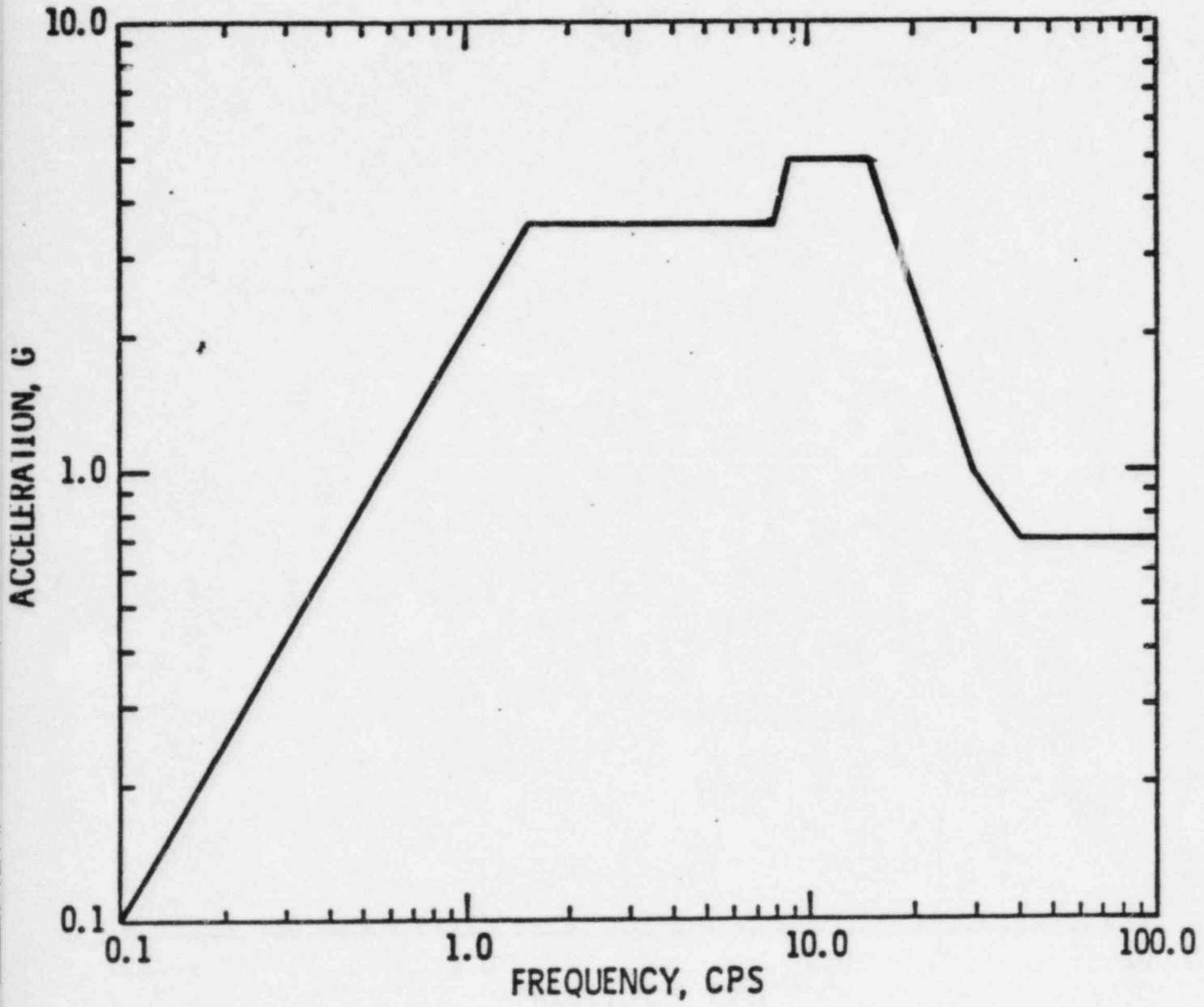

FIG. 30: SSE FREQUENCY RESPONSE SPECTRA

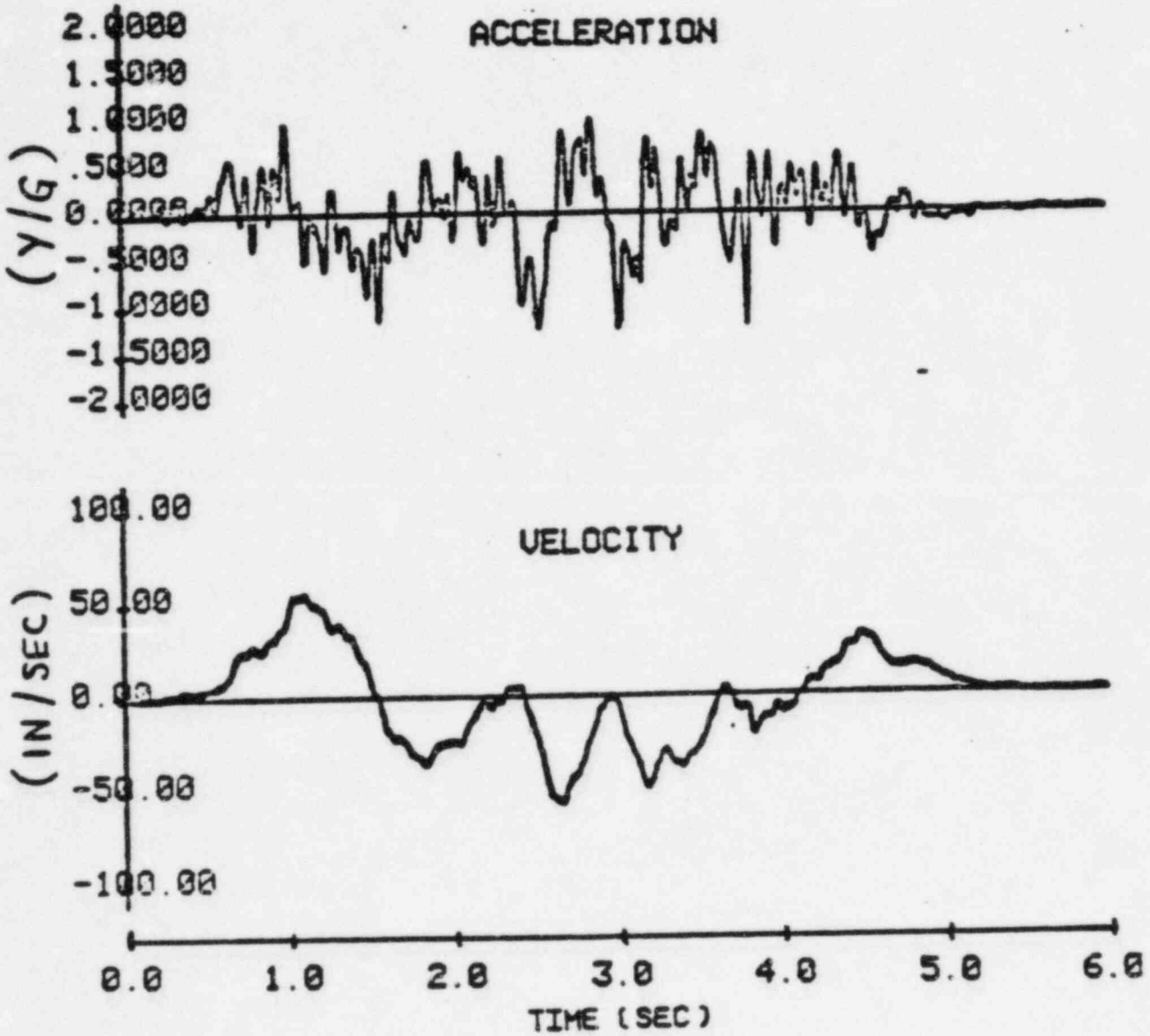

Fig. 31: TIME HISTORIES GENERATED FROM RESPONSE SPECTRA

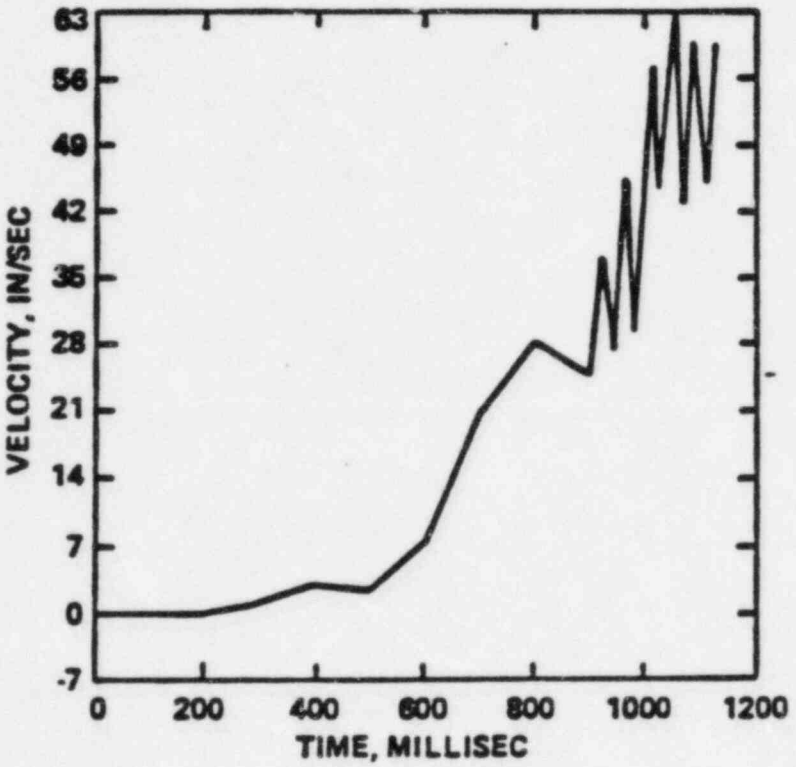

FIG. 32: VELOCITY IN PIPE vs TIME
(WITHOUT CRACK)

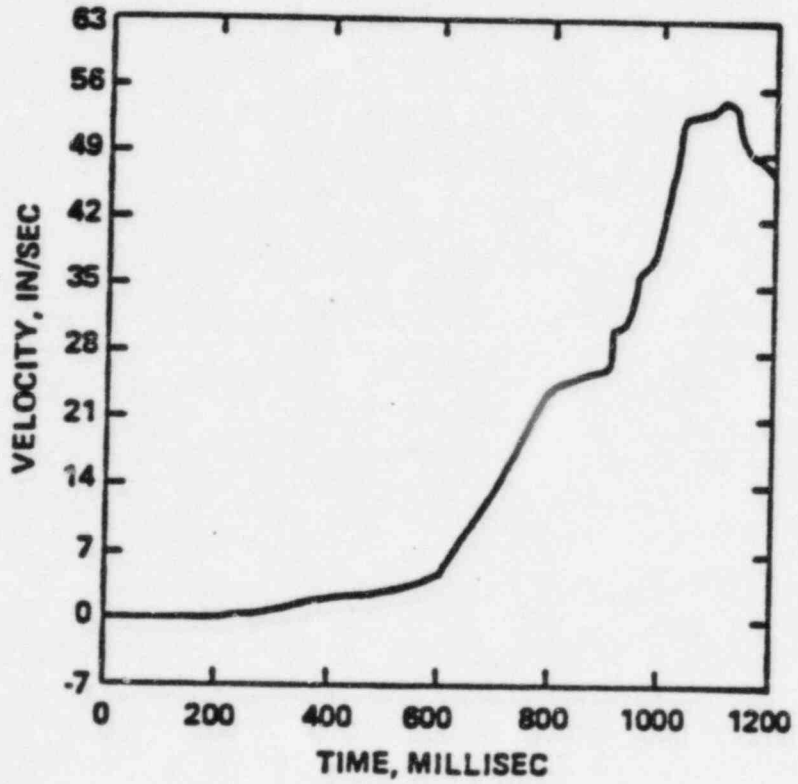

FIG. 33 : VELOCITY AT BASE vs TIME

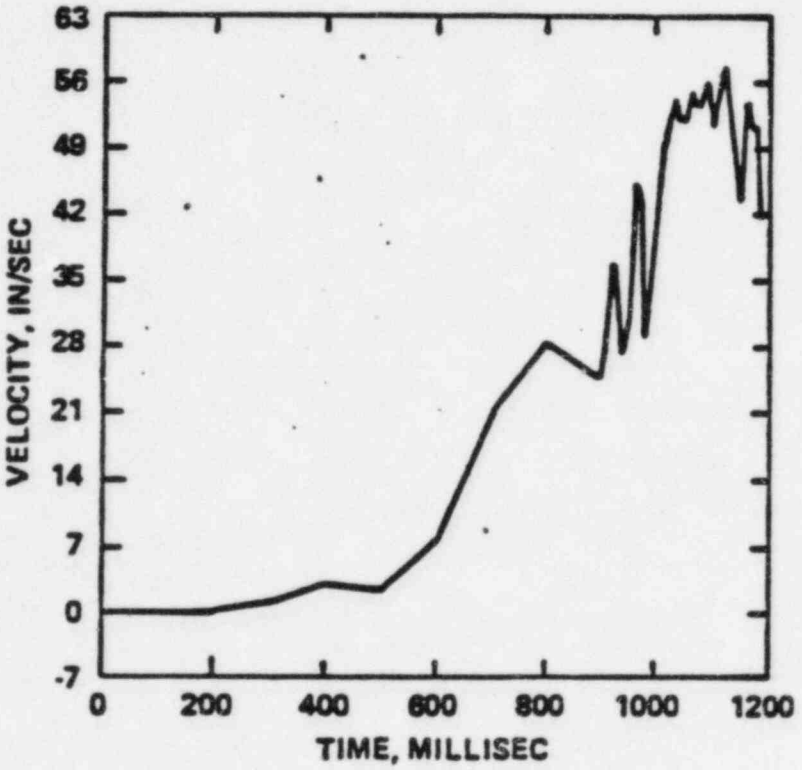

FIG.34: VELOCITY IN PIPE vs TIME
(1/2 CIRCUMFERENCE CRACK)

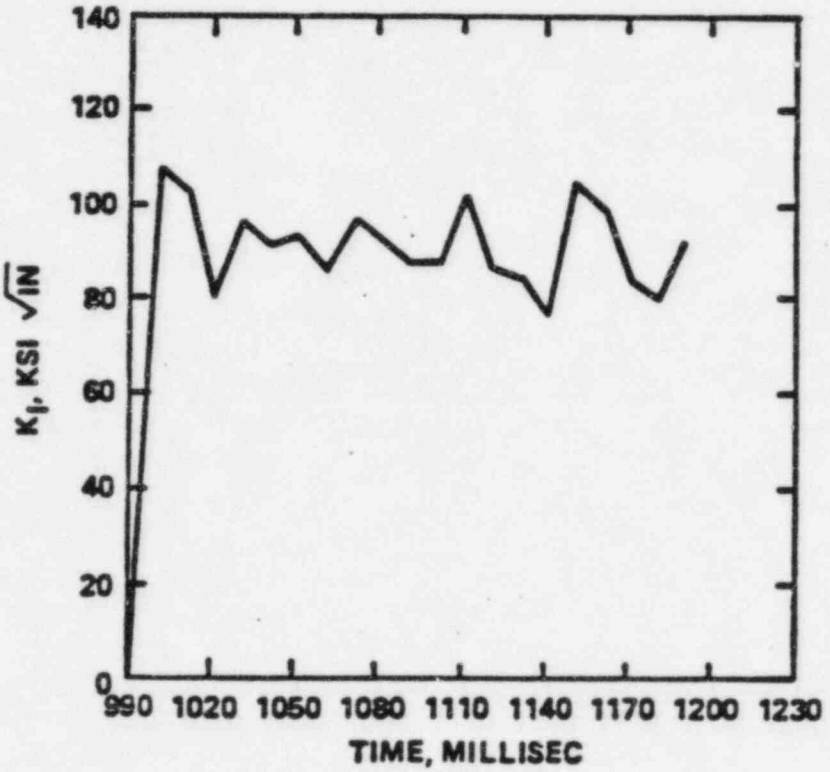

FIG. 3E: STRESS INTENSITY (K_I) vs TIME
(1/2 CIRCUMFERENCE CRACK)

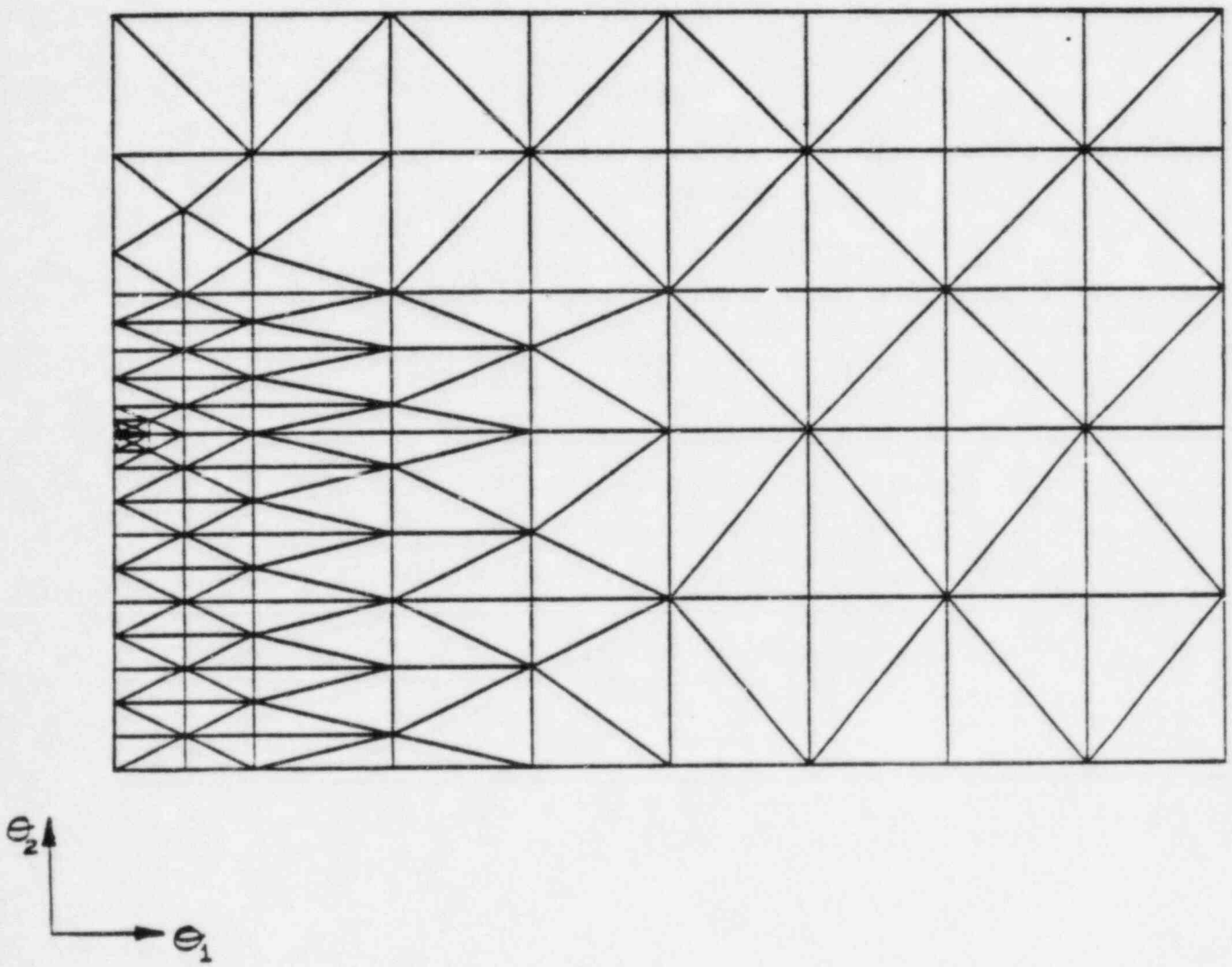

FIGURE 36: FINITE ELEMENT MESH IN SURFACE COORDINATE SYSTEM (20° CRACK IN 45° ELBOW)

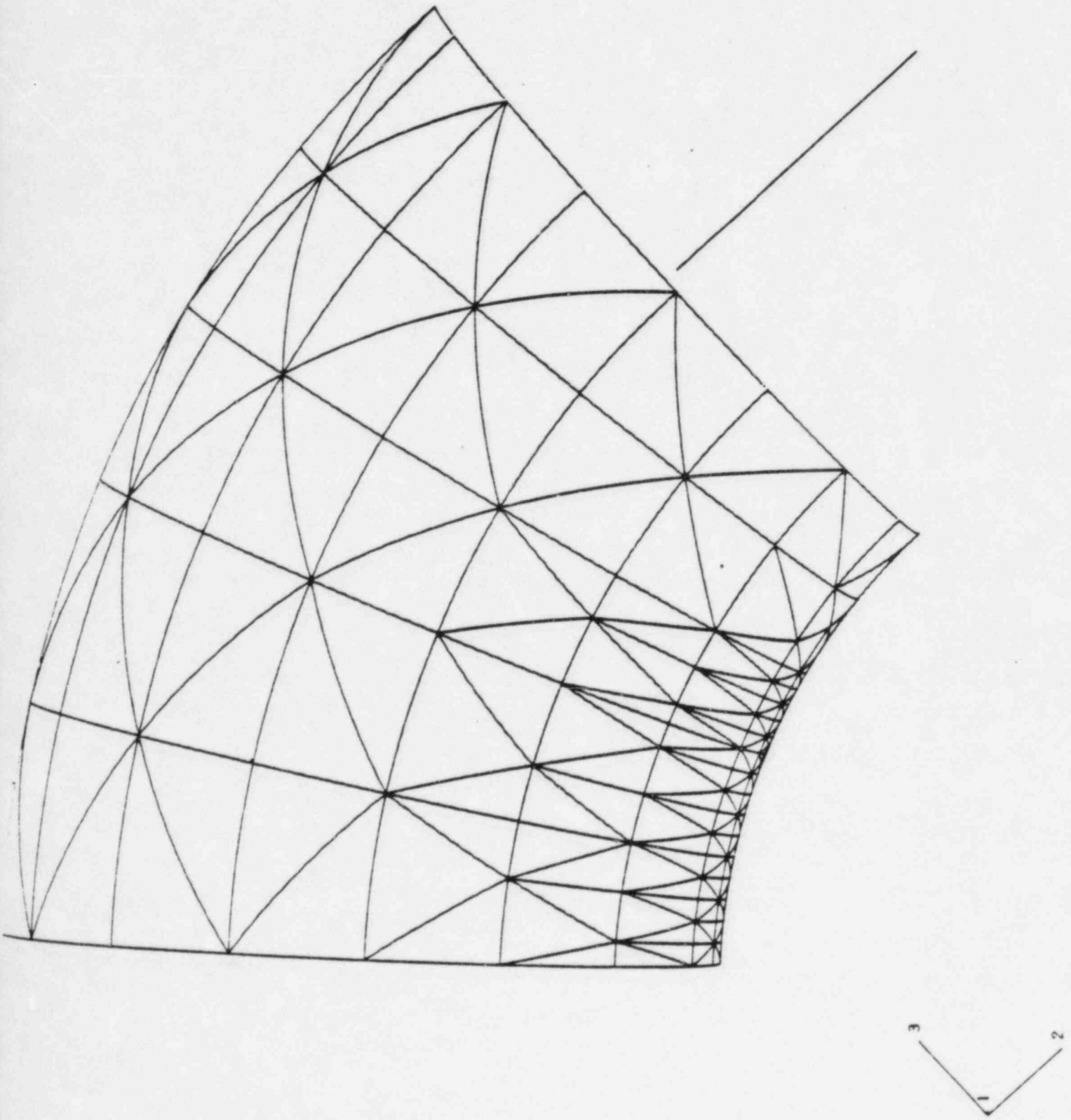

FIGURE 37 FINITE ELEMENT MESH IN X-Y-Z CARTESIAN COORDINATES (20° CRACK IN 45° ELBOW)

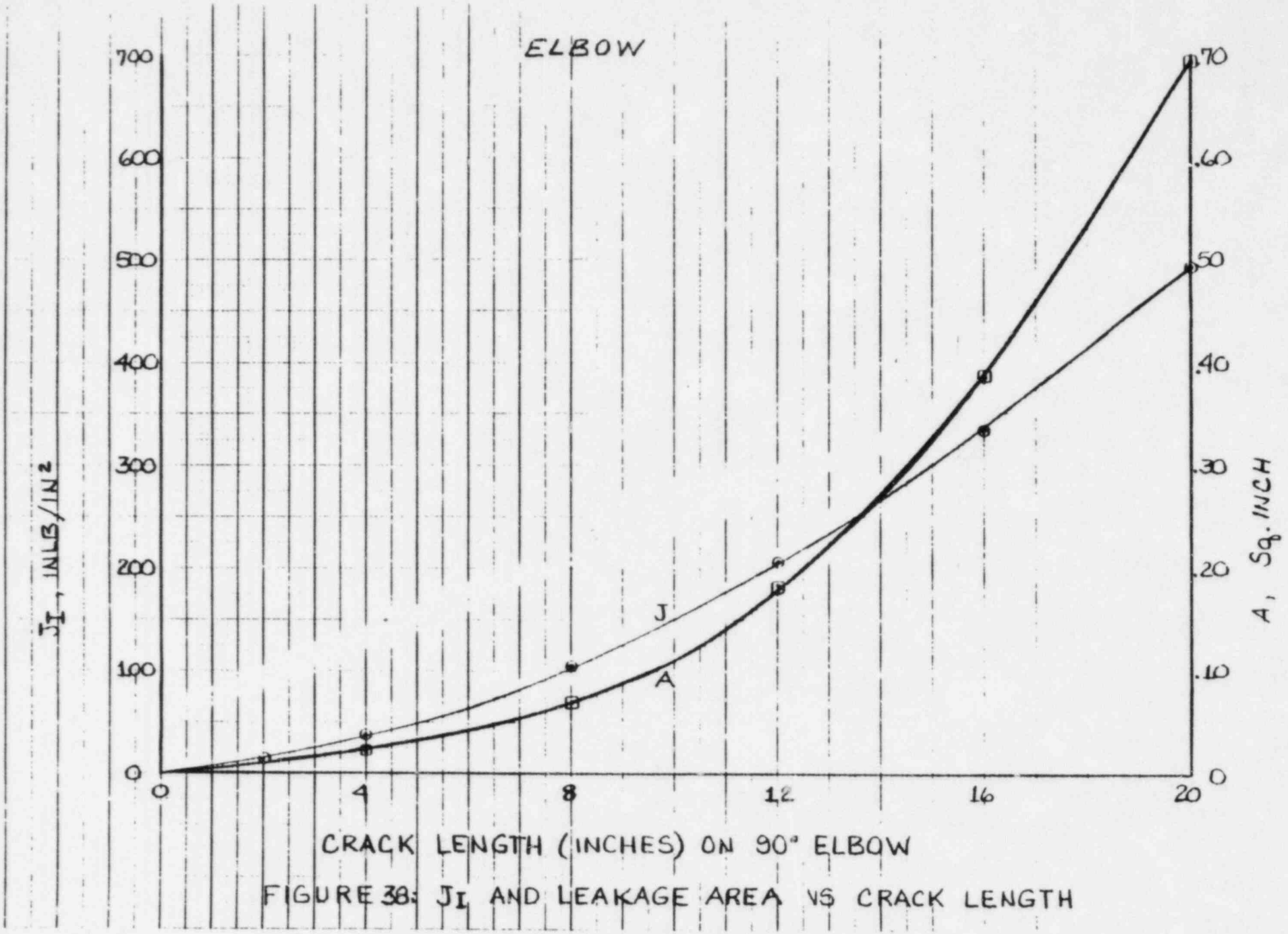

CRACK LENGTH (INCHES) ON 90° ELBOW

FIGURE 38: J_I AND LEAKAGE AREA VS CRACK LENGTH

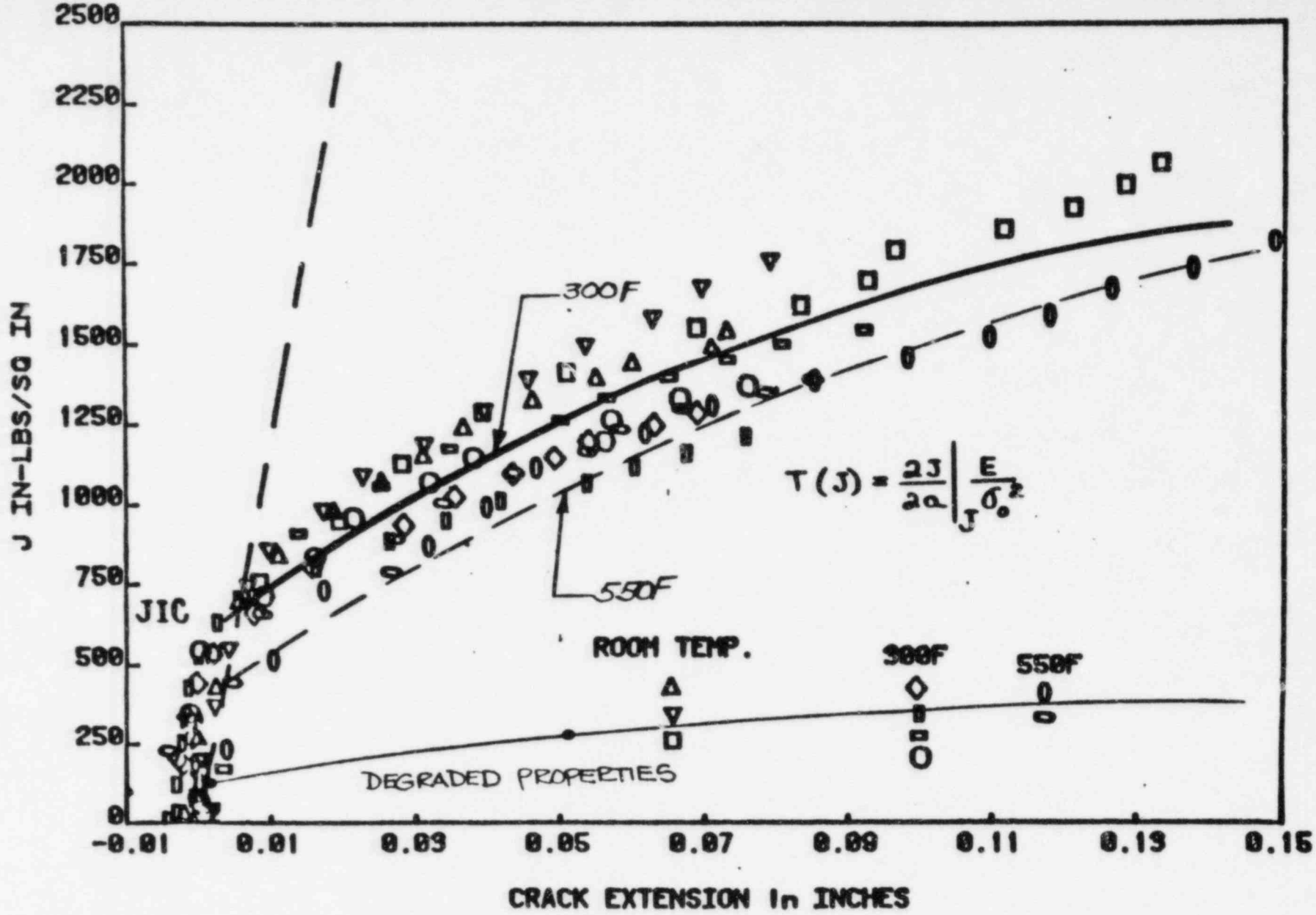

Fig.39: J vs CRACK EXTENSION, A516 (20% SIDE GROOVES)

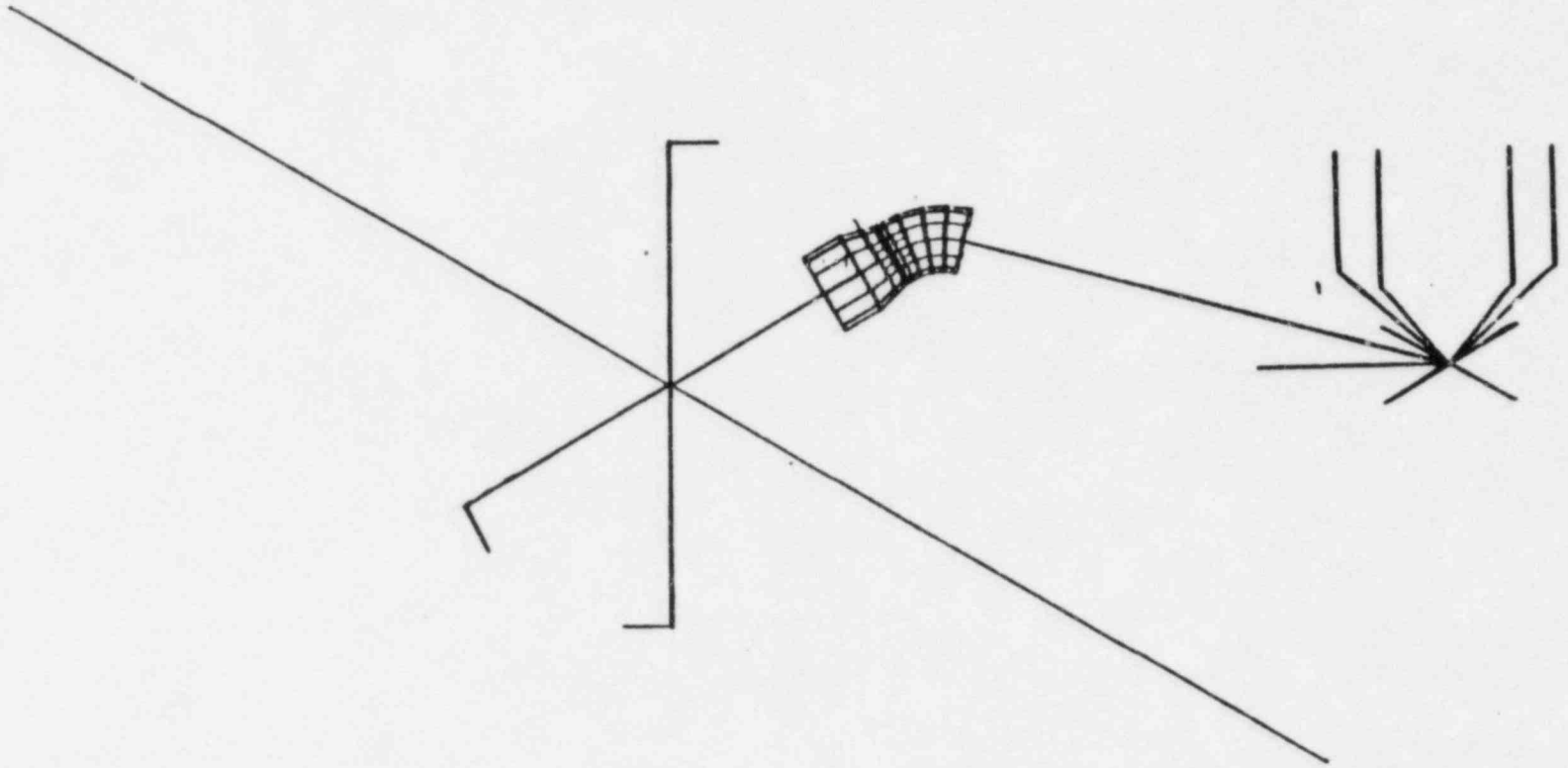

Fig. 40: FINITE ELEMENT MODEL FOR SYSTEM 80 SEISMIC LOADING ANALYSIS

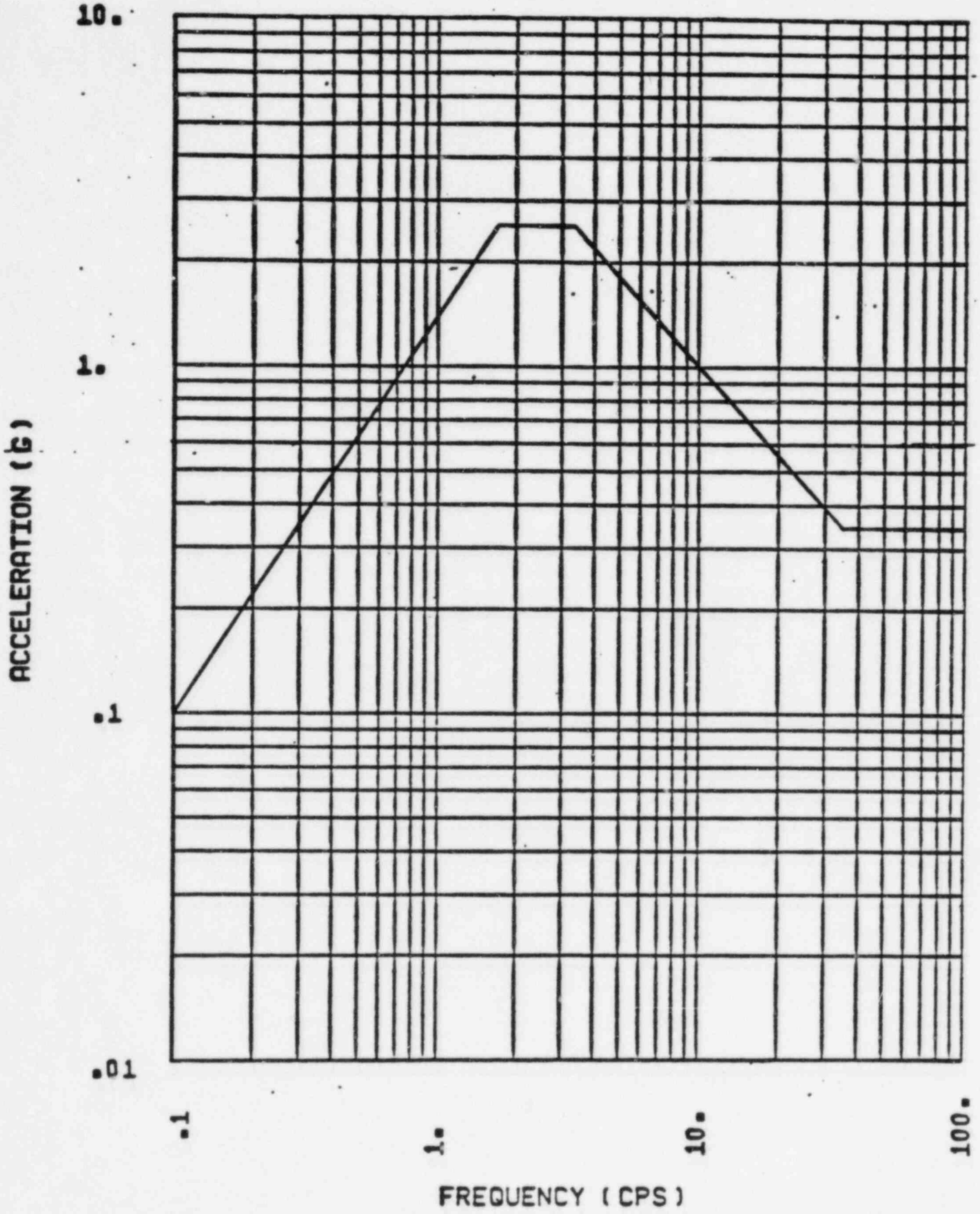

Fig. 41: SEISMIC SPECTRUM
ENVELOPE OF RV AND RCP SUPPORTS: SSE 2% DAMPING

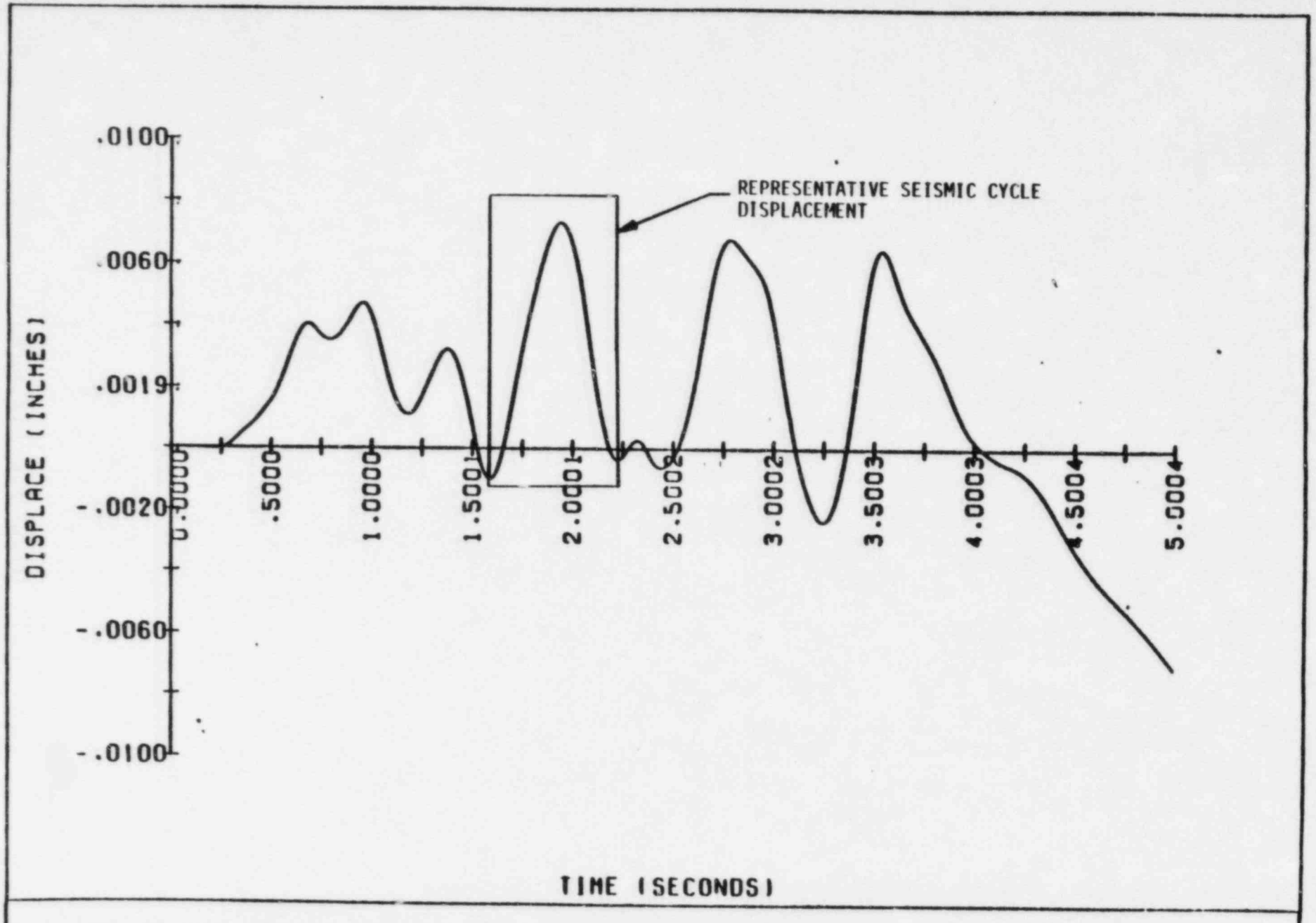

Fig. 42: SYSTEM 80 SSE ANALYSIS - DOUBLE INTEGRATION OF ARTIF ACCEL. TIME HISTORY

SYSTEM 80 SSE SPECTRUM ANALYSIS - ARTIF DISP. TH

FIGURE 13

J vs time for representative seismic cycle
30° circumferential (8 inch long) crack

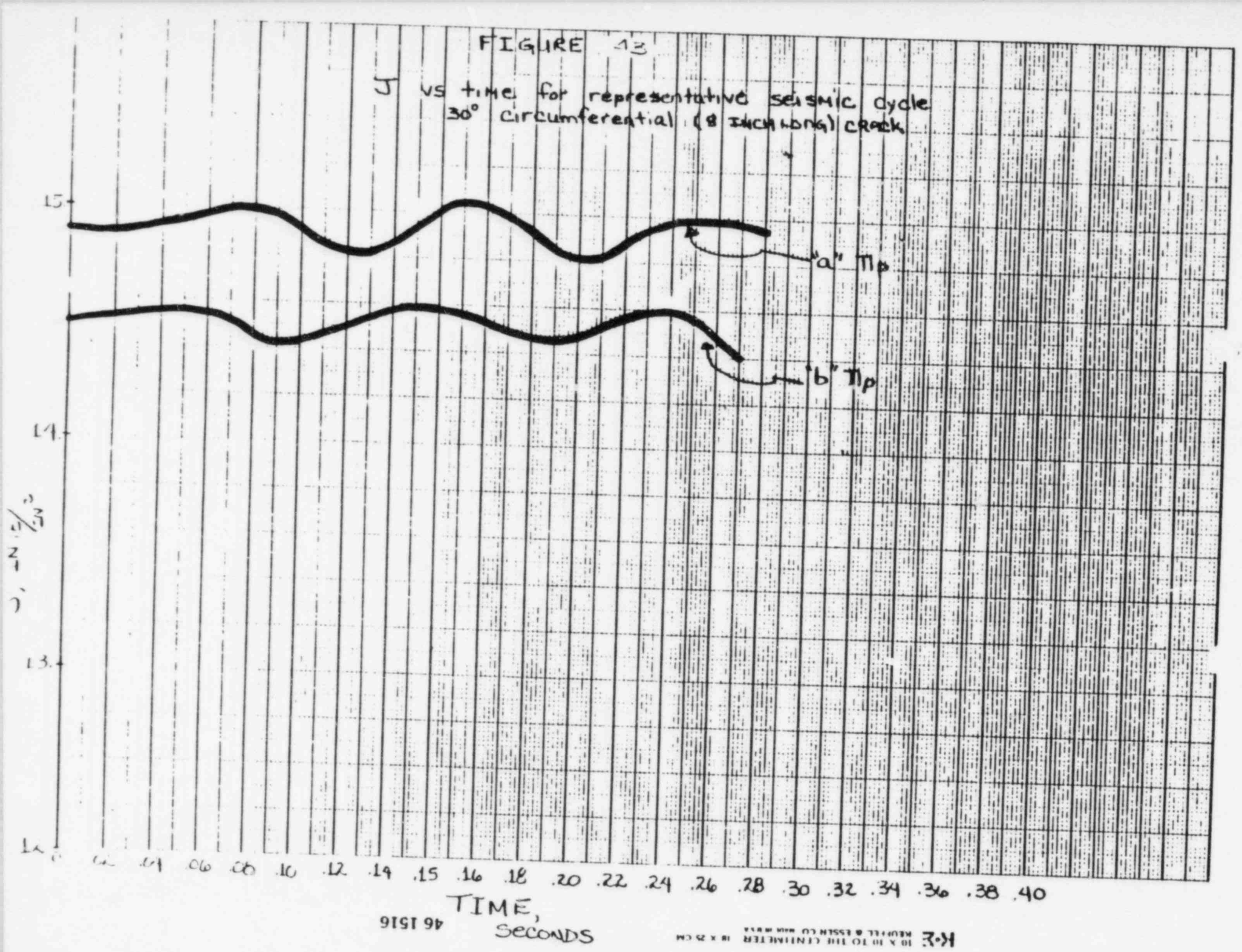

46 1516

10 X 10 TO THE CENTIMETER 18 X 25 CM
KEUFFEL & ESSER CO. MADE IN U.S.A.

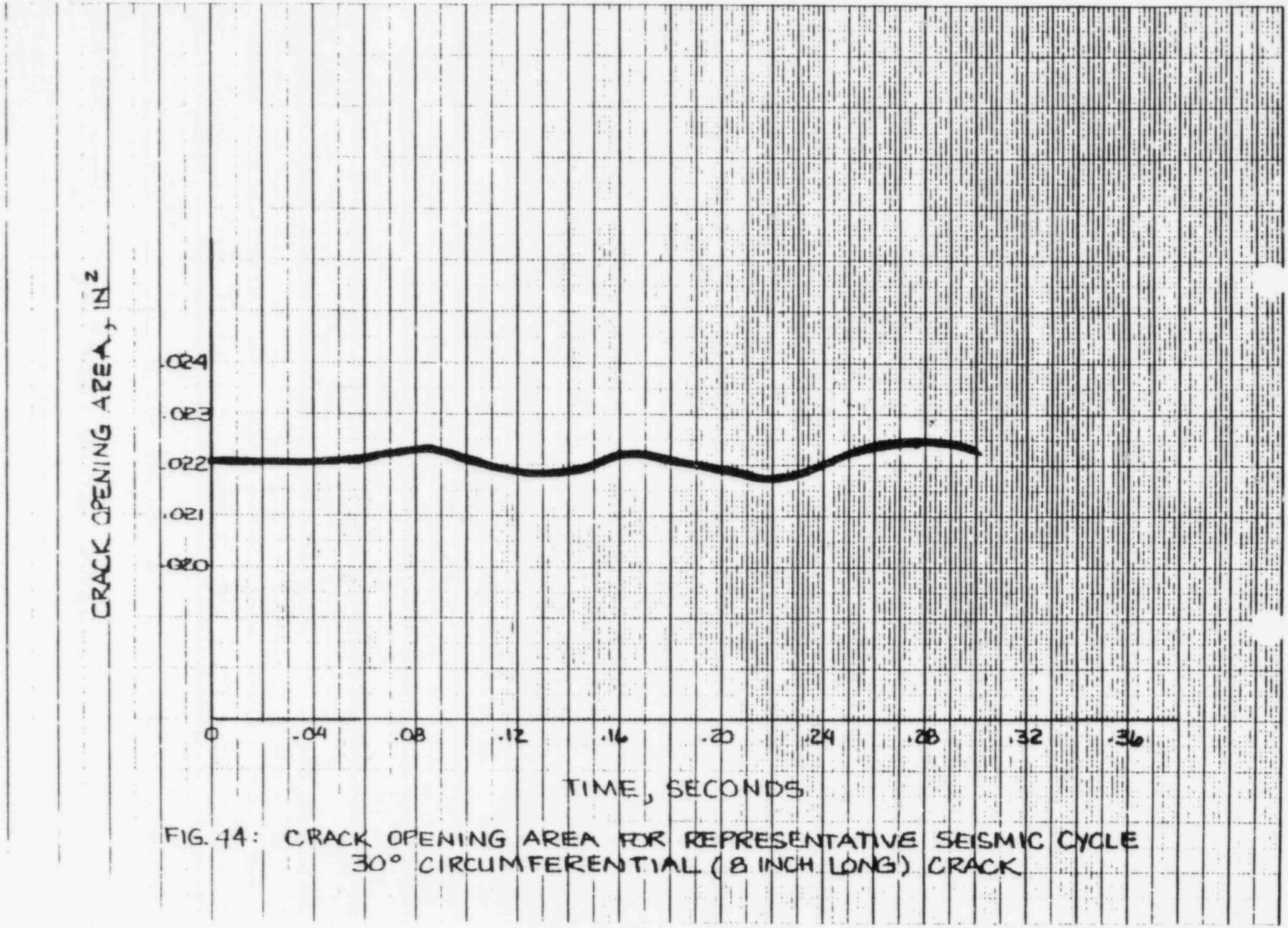

FIG. 44: CRACK OPENING AREA FOR REPRESENTATIVE SEISMIC CYCLE 30° CIRCUMFERENTIAL (8 INCH LONG) CRACK

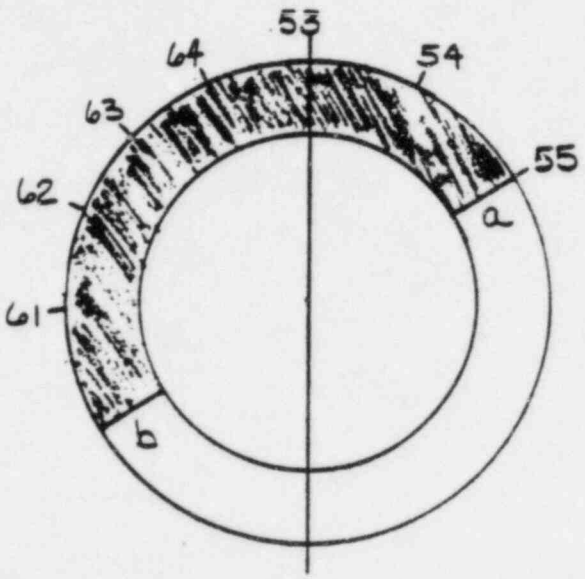

180° CRACK LOOKING TOWARD RV

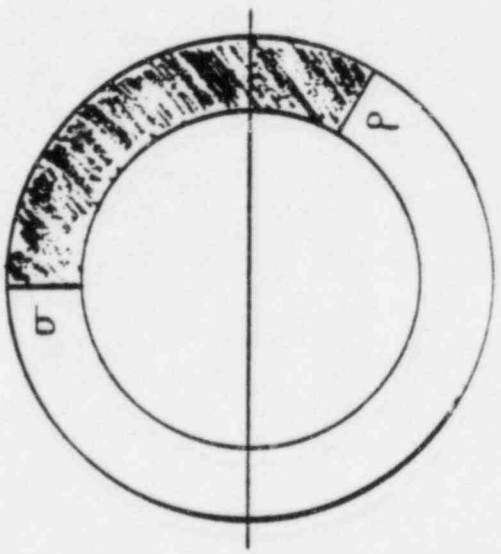

120° CRACK

Fig. 45: ASSUMED CRACK SIZE FOR DETERMINATION OF MAXIMUM STABLE CRACK SIZE

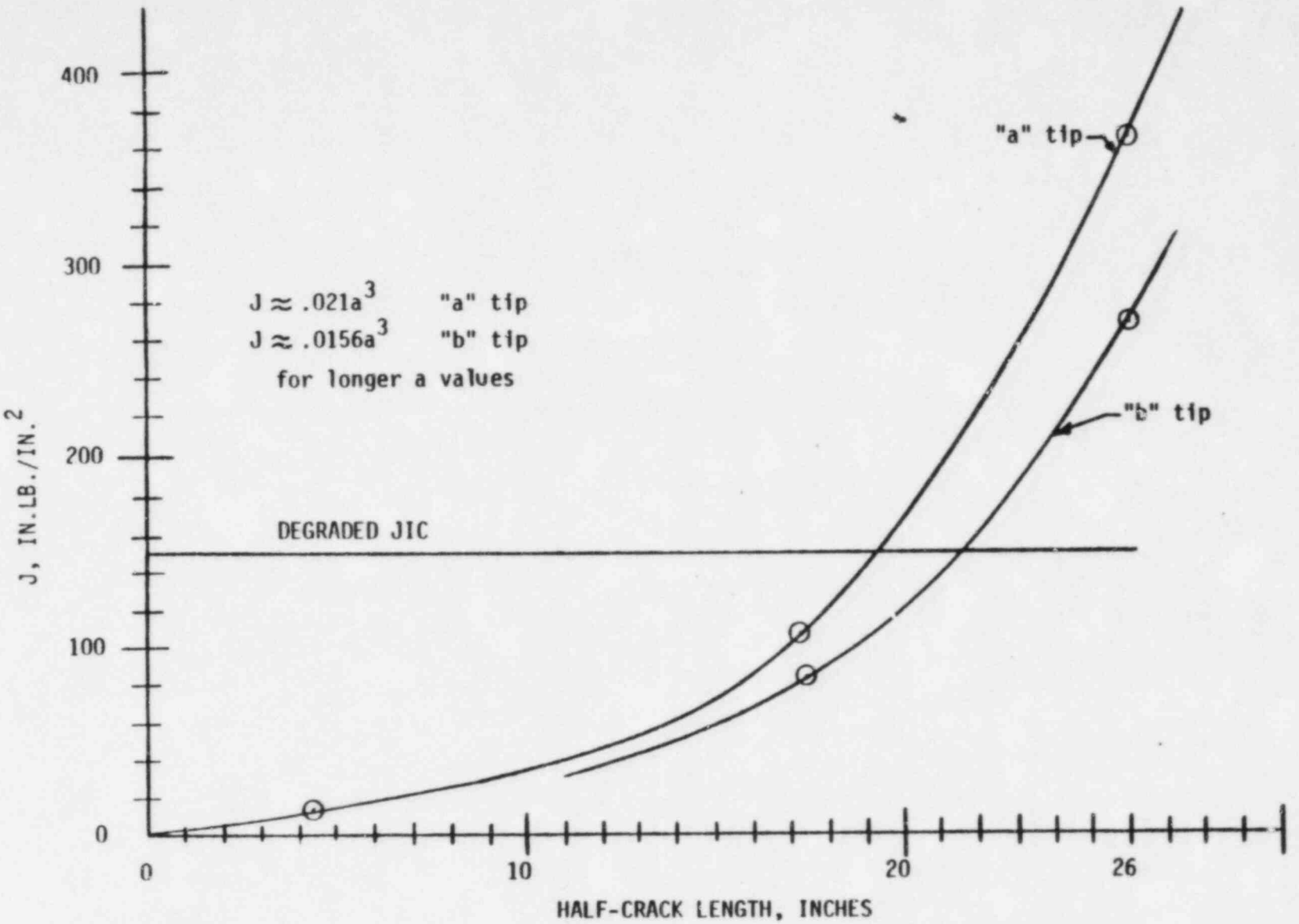

Fig. 46: J VS. CRACK SIZE FOR NORMAL OPERATING LOADS

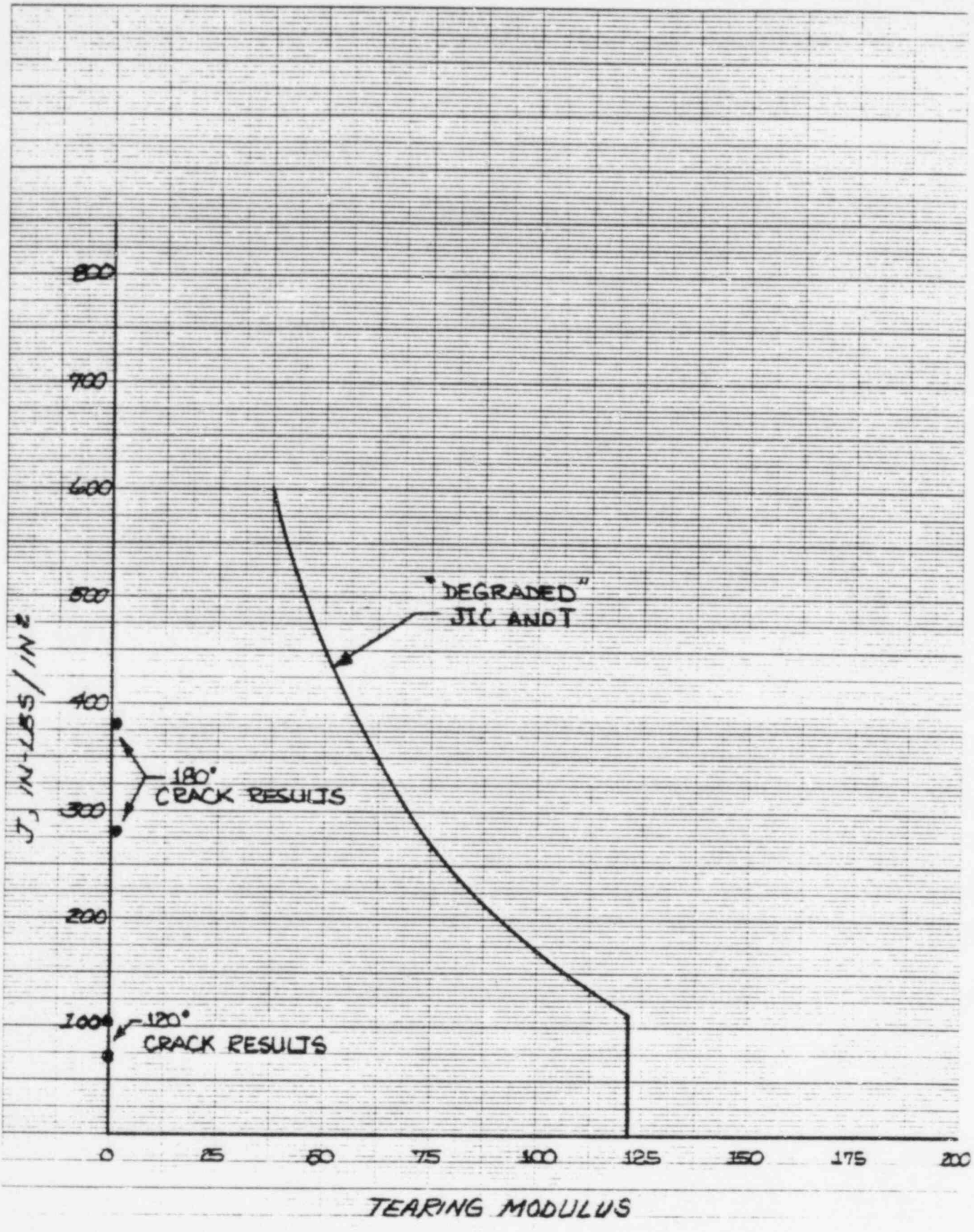

FIG. 47: INSTABILITY DIAGRAM FOR 180° AND 120° CRACKS

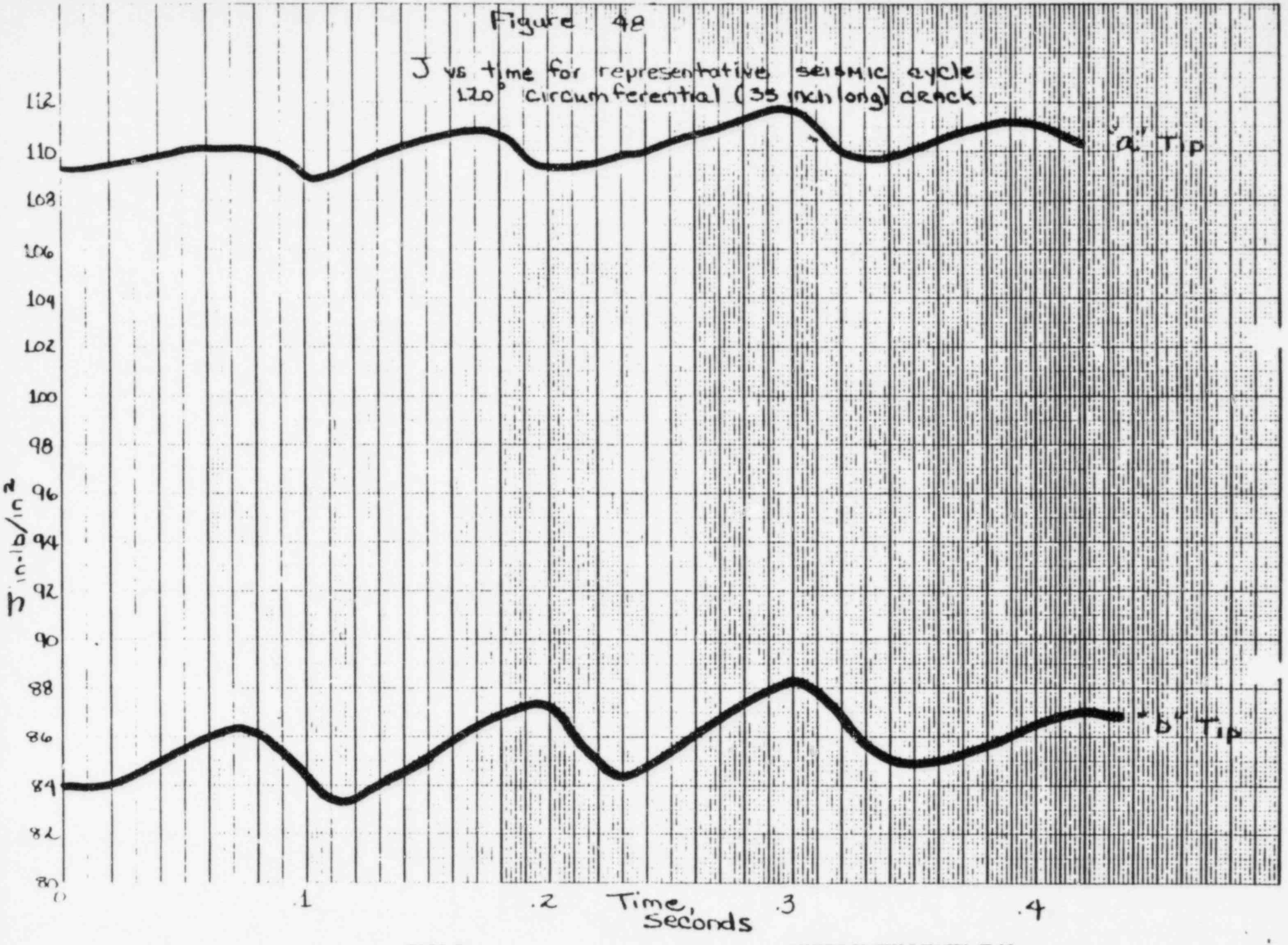

FIGURE 49 a

J vs time for representative seismic cycle
180° circumferential (52 in. long) crack
"a" Tip

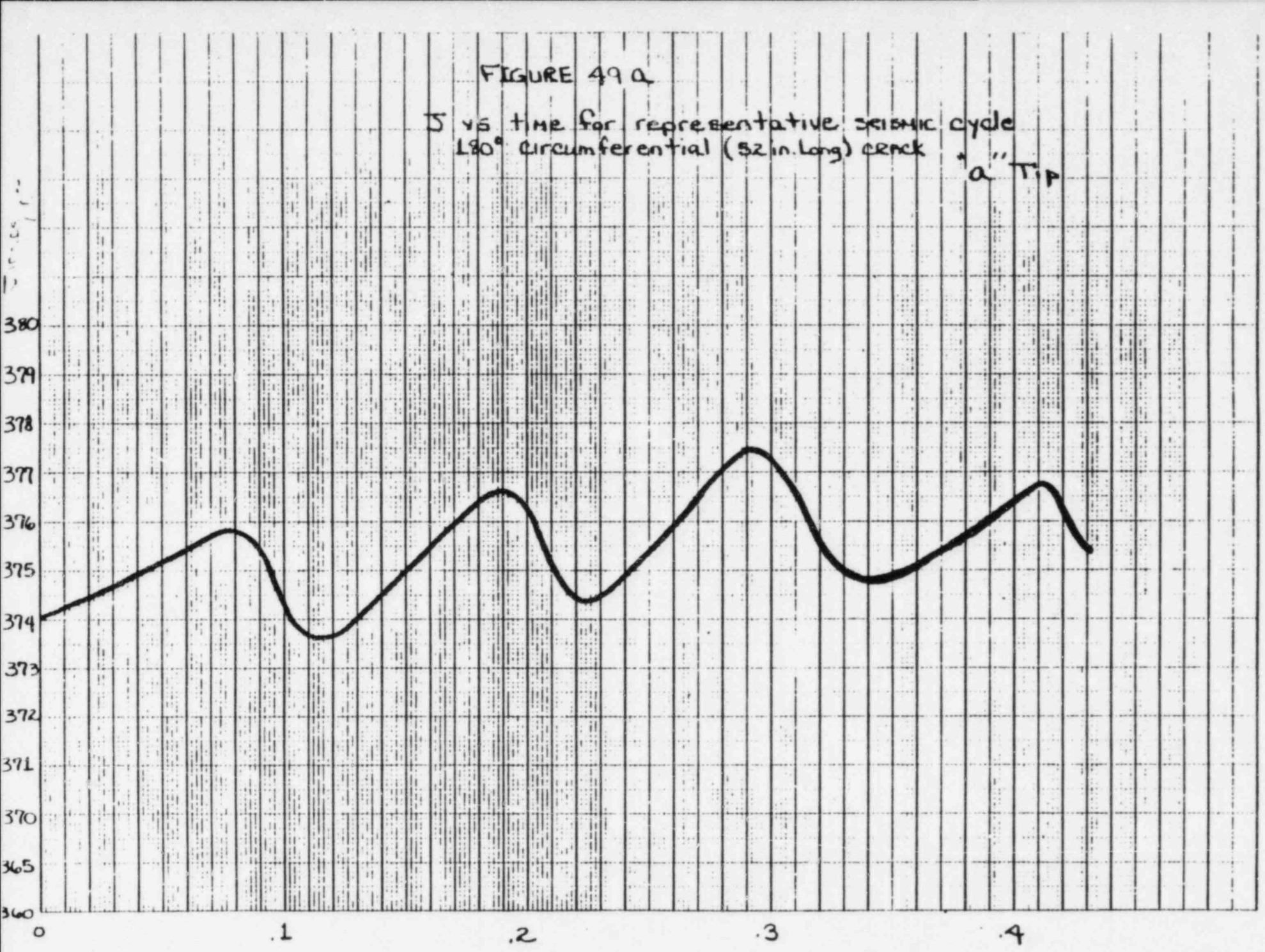

46 1516

KEUFFEL & ESSER CO. MADE IN U.S.A. 10 X 10 TO THE CENTIMETER 18 X 25 CM

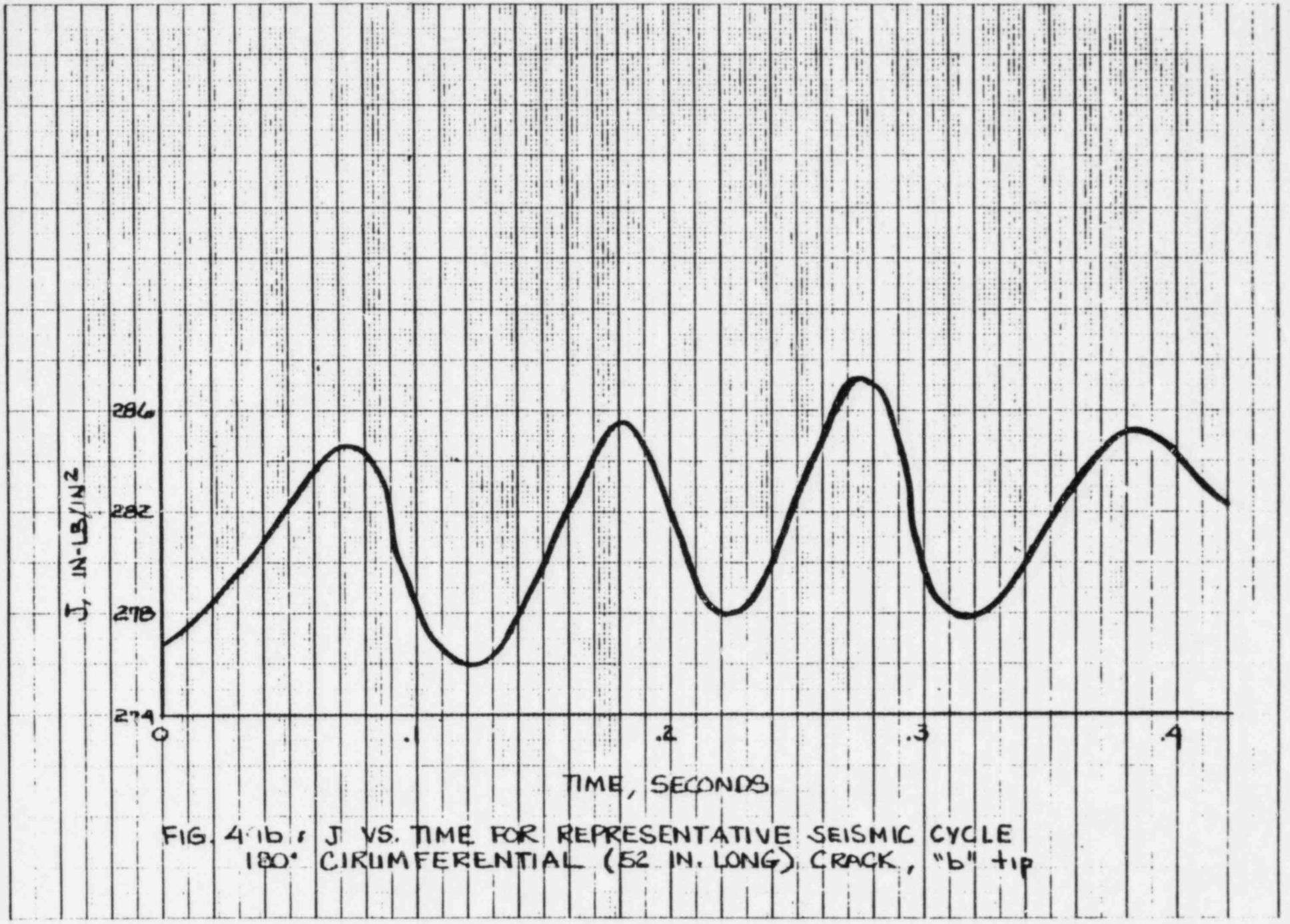

FIG. 4.16, J VS. TIME FOR REPRESENTATIVE SEISMIC CYCLE
180° CIRUMFERENTIAL (52 IN. LONG) CRACK, "b" tip

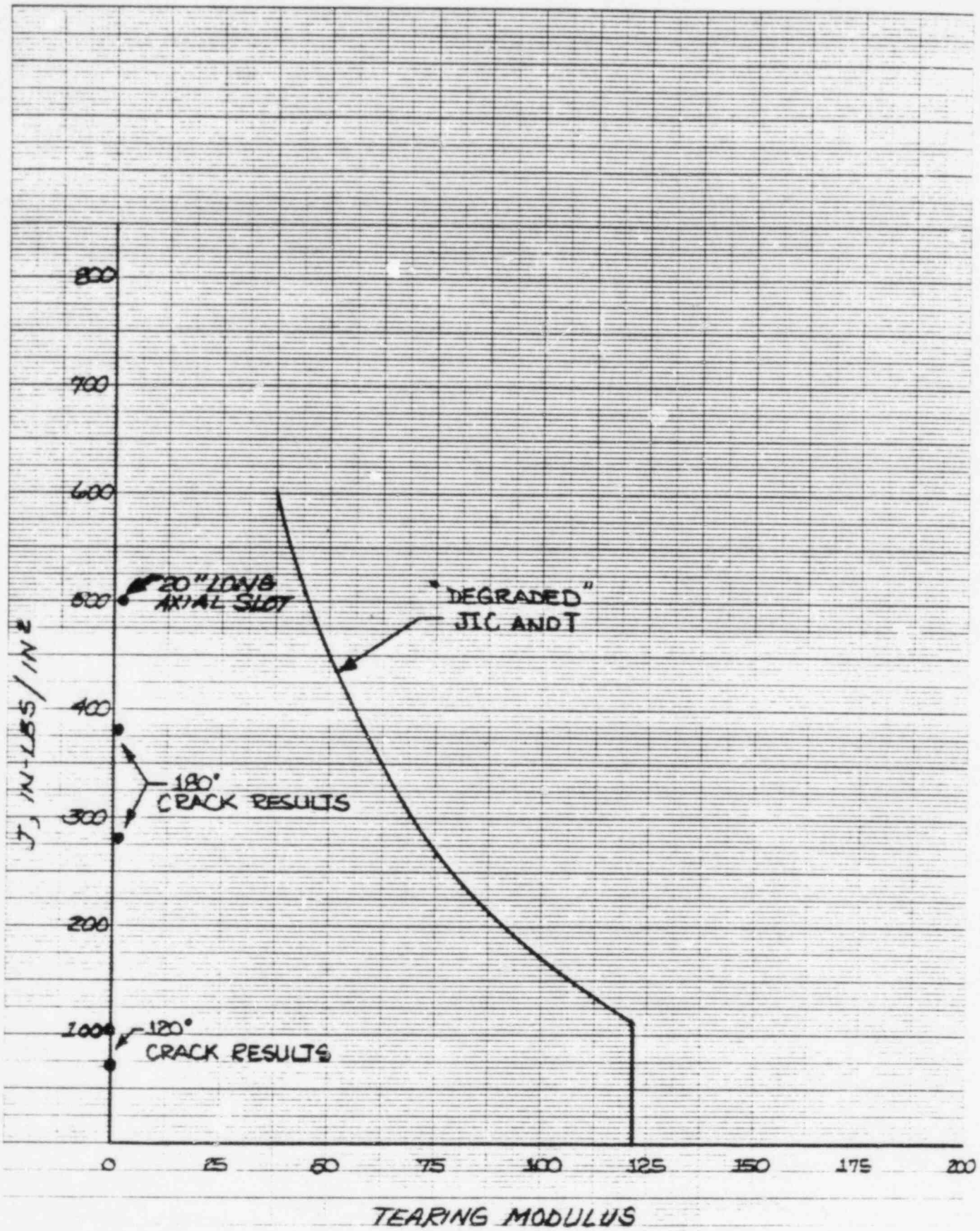

FIG. 50: INSTABILITY DIAGRAM FOR AXIAL SLOT IN ELBOW

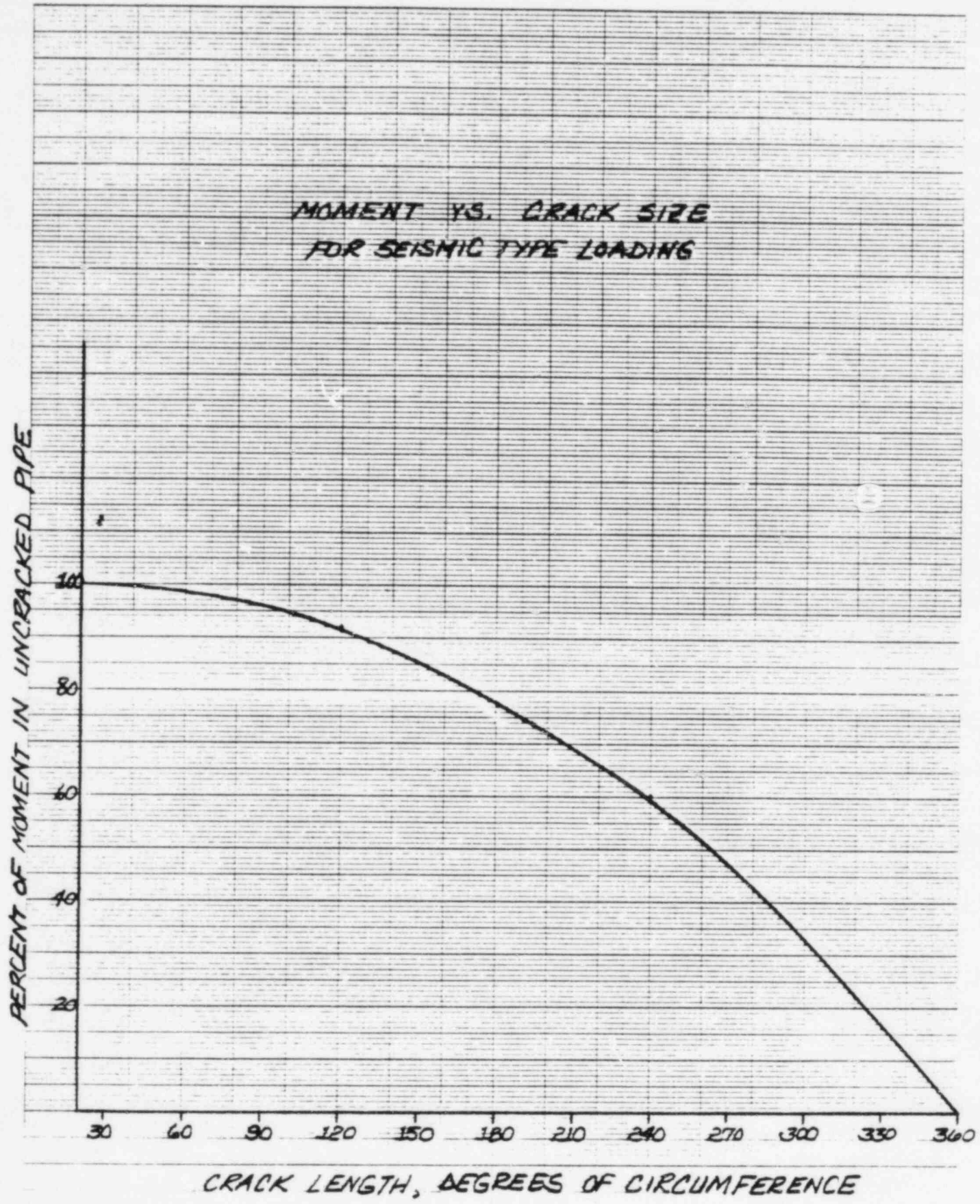
MOMENT VS. CRACK SIZE
FOR SEISMIC TYPE LOADING
PERCENT OF MOMENT IN UNCRACKED PIPE
100
80
60
40
20
30
60
90
120
150
180
210
240
270
300
330
360
CRACK LENGTH, DEGREES OF CIRCUMFERENCE

FIGURE 51

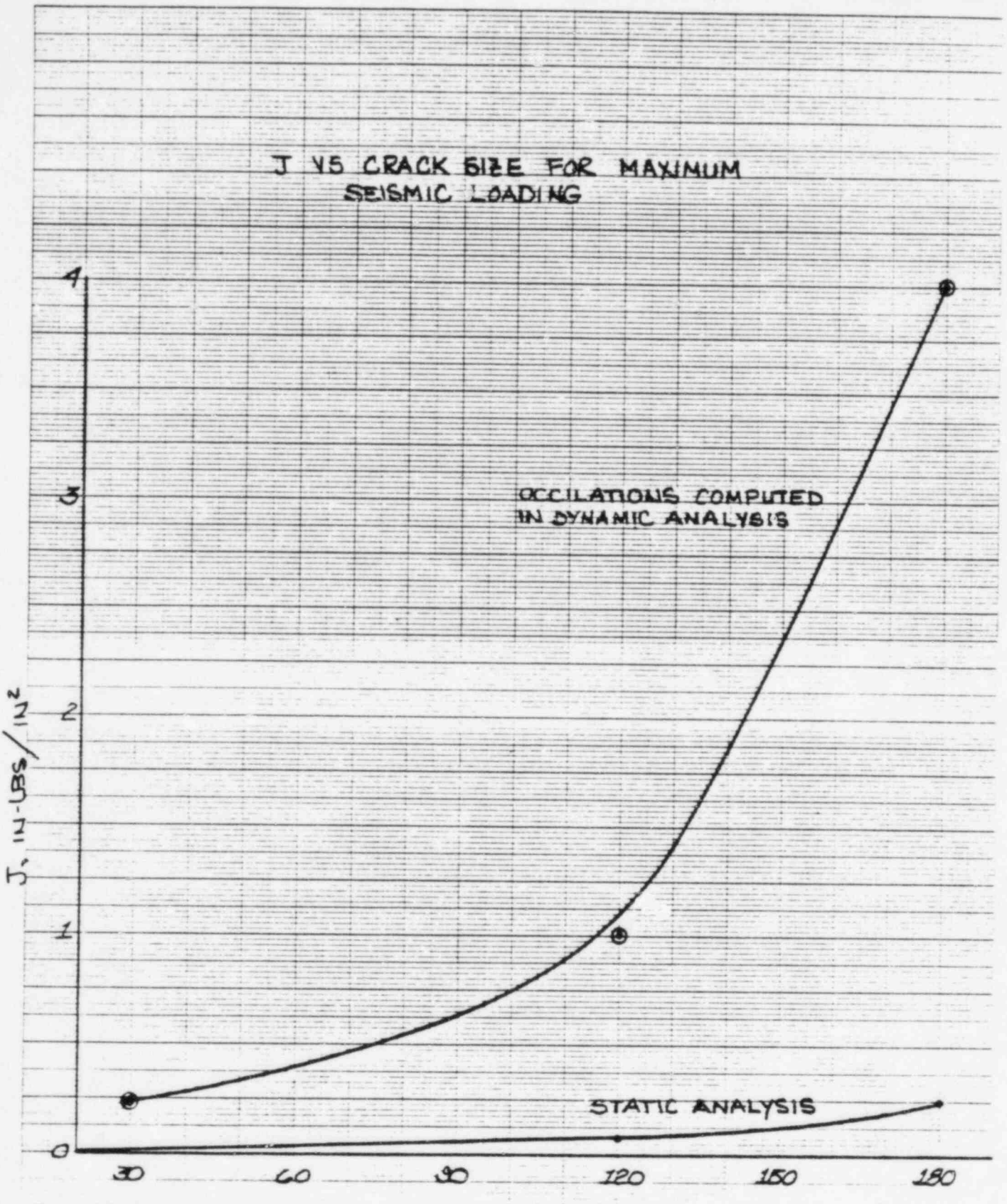
J VS CRACK SIZE FOR MAXIMUM SEISMIC LOADING
OCCILATIONS COMPUTED IN DYNAMIC ANALYSIS
STATIC ANALYSIS
J, IN-LBS/IN²
0
1
2
3
4
30
60
90
120
150
180
CRACK LENGTH, DEGREES OF CIRCUMFERENCE

FIGURE 52

DETERMINATION OF RESIDUAL
ELASTIC STIFFNESS

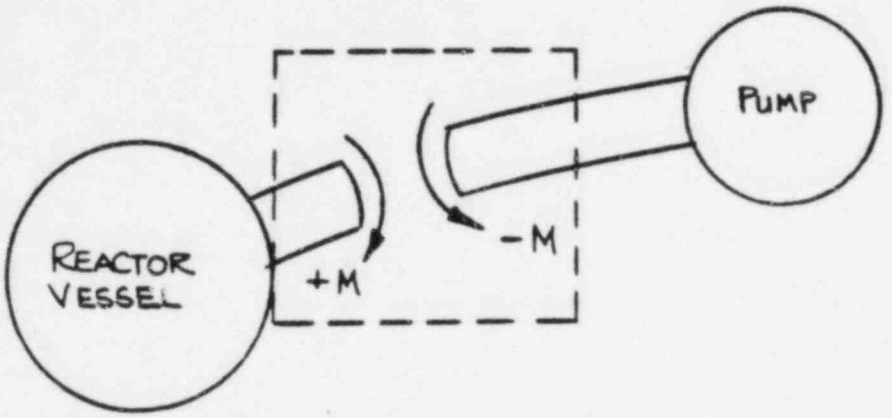

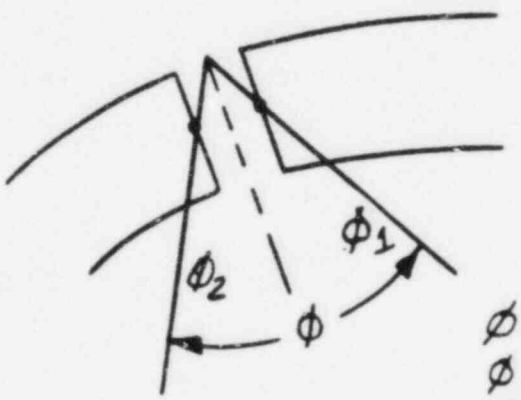

$\phi_1 = -1.745 \times 10^{-4}$
$\phi_2 = 5.107 \times 10^{-5}$
$\phi = 2.256 \times 10^{-4}$

FIGURE 53

Table 1

LOADING TRANSIENTS ANALYZED AND LIFE OCCURENCES

Loading transients	Life Occurances
a. Plant heatup, 100°F/hr	500
b. Plant cooldown, 100°F/hr	500
c. Plant loading, 5%/min.	15,000
d. Plant unloading, 5%/min.	15,000
e. 10% step load increase	2,000
f. 10% step load decrease	2,000
g. Normal plant variation ($\pm$ 100 psi, $\pm$ 10°F)	10^6
h. Reactor Trip	400
i. Leak test, 2250 psia, 100°F-400°F	200
j. Hydrostatic test, 3125 psia, 100°F-400°F	10
k. Loss of Reactor Coolant Flow (*)	40
l. Loss of Turbine Generator Load (*)	40
m. Loss of Secondary Pressure (*)	5
n. Operating Basis Earthquake (*)	200

* Abnormal Transient Conditions

Table 2

LOADS AND ELASTIC MATERIAL PROPERTIES USED FOR CRACK OPENING AREA STRUCTURAL ANALYSES

		COMBINED NORMAL OPERATING LOADS FOR THERMAL EXPANSION, WEIGHT, AND 2250 PSIA INTERNAL PRESSURE					
		F_X LBS	F_Y LBS	F_Z LBS	M_X FT-LBS	M_Y FT-LBS	M_Z FT-LBS
DLTE	ELBOW	-8.570×10^4	1.204×10^6	1.157×10^6	-2.619×10^5	-1.719×10^5	2.518×10^5
	NOZZLE	-1.202×10^6	-9.167×10^4	-1.533×10^6	9.103×10^5	-1.976×10^6	-3.414×10^5
HLTE	PIPE	-7.509×10^5	0.0	3.071×10^6	0.0	-6.406×10^6	0.0

YOUNG'S MODULUS = 2.900×10^7 PSI

POISSON'S RATIO = 0.293

TABLE 3

SEISMIC MOMENTS FOR PALO VERDE AT THE REACTOR VESSEL INLET NOZZLE

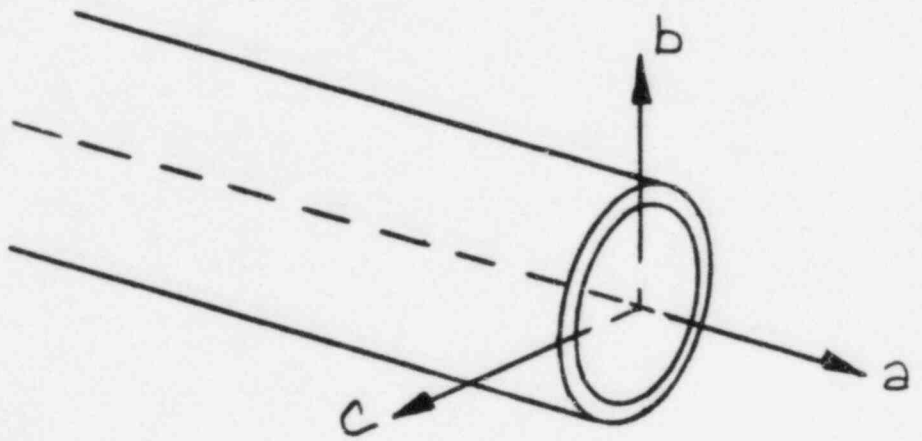

Ma = 840 IN-KIPS

Mb = 2140 IN-KIPS

Mc = 870 IN-KIPS

TABLE 4

T_{APPL} FOR VARIOUS CRACK SIZES

ASSUMMING FULLY PLASTIC MOMENT AT DISCHARGE LEG TERMINAL END

$$T_{APPL} = \frac{2h^2 \pm E}{K\phi}$$

WHERE $h = R(\cos\theta + \sin\frac{\theta}{2})$

$\theta = \frac{\text{CRACK LENGTH}}{2}$	h, INCHES	T_{APPL}
30°	18.56	13.5
60°	16.5	10.7
90°	11.7	5.3

APPENDIX A

Forces and Moments in the System 80 Main Loop Piping Due to Normal and Upset Loadings

Forces and moments computed in the System 80 main loop are presented in Table A. The location of the joints listed and the coordinate system used are given in Figure A-1. The loads and moments given envelope all System 80.

Loadings for a specific plant may be significantly less than the values given in Table A.

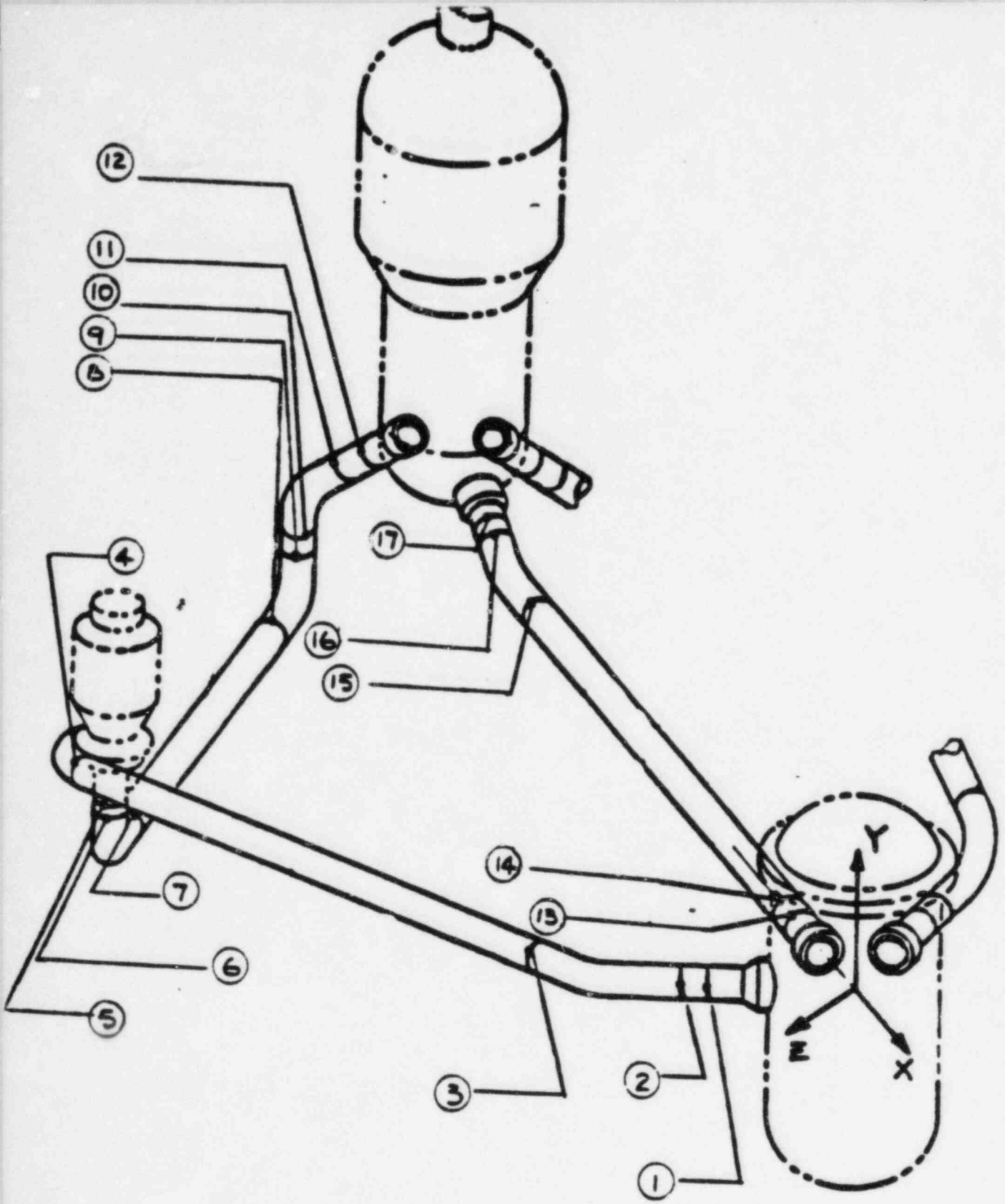

C - E COMBUSTION ENGINEERING, INC.	LOCATION OF PIPE JOINTS LISTED IN TABLE A	Figure A-1

Notes to the following listings 1 through 17

1. MX, MY & MZ denote global coordinates X, Y & Z moments due to thermal expansion.

2. $^{th}S_p$ denotes thermal stress calculated based on EQ (12) of the ASME Code Section III or

$$^{th}S_p = \frac{K_3}{2(1-\nu)} E\alpha |\Delta T1| + K_3 C_3 E_{AB} |\alpha_A TA - \alpha_B TB| + \frac{E\alpha}{1-\nu} |\Delta T2|$$

3. Abbreviations for the transients:

No t	-	Room temperature
N op	-	Normal Operation
PL HU	-	Plant Heatup
PL CD	-	Plant Cooldown
PL L	-	Plant Loading
PL UL	-	Plant Unloading
ST I1	-	Step Load Increase 1
ST I2	-	Step Load Increase 2
ST D1	-	Step Load Decrease 1
ST D2	-	Step Load Decrease 2
RE T1	-	Reactor Trip 1
RE T2	-	Reactor Trip 2
PL TH	-	Plant Leak Test Heatup
PL TC	-	Plant Leak Test Cooldown
HY T	-	Hydro Static Test
D WT	-	Due to Dead Weight Along
I	-	Load Set 1
L	-	Load Set 2
NI	-	Cycles for Load Set 1
NL	-	Cycles for Lead Set 2
NU	-	Cycles for the Smaller of Load Set 1 or Load Set 2
NA	-	ASME Code Section III Allowable Cycles

4. Listing values shown for the plant variations conditions, load set 7 through 10, were calculated based on a pressure variation of ± 50 psi and a temperature variation of $\pm 6^{o}F$, which are lower than the currently specified values of ±100 psi and $\pm 10^{o}F$. However, the effect of these deviations is negligible since load set 7 through load set 10 are not the controlling loading case and stresses induced from the total range of pressure and temperature variations contribute only a small portion of the resulting usage factor.

1. Inlet Nozzle at Nozzle End: Joint No. (1)

	Load Set	Cycles	Pressure Psi	MX FT-LB	MY FT-LB	MZ FT-LB	ΔT1 °F	TA °F	ΔT2 °F	TB °F	th^{S_p}
1.	No T	500	0	0	0	0	0	0	0	0	0
2.	N OP	10^6	2250	-628512	620331	-1438727	0	0	0	0	0
3.	PL HU	500	2250	-343248	25670	-519187	8.0	35.0	4.5	0	18514
4.	PL CD	500	0	-568770	368877	-1380816	-9.0	-38.5	-4.5	0	20297
5.	PL L	15000	2290	-628512	620331	-1438727	2.0	3.0	1.0	0	2065
6.	PL UL	15000	2210	-628512	620331	-1438727	-2.0	-3.0	-1.0	0	2065
7.	ST I1	4000	2250	-628512	620331	-1438727	-3.0	-1.0	-3.0	0	1946
8.	ST I2	4000	2280	-628512	620331	-1438727	2.5	1.0	2.0	0	1565
9.	ST D1	4000	2230	-628512	620331	-1438727	3.0	1.0	2.5	0	1816
10.	ST D2	4000	2186	-628512	620331	-1438727	-2.5	-1.0	-1.5	0	1435
11.	RE T1	480	1680	-628512	620331	-1438727	-14.0	-4.5	-11.0	0	8228
12.	RE T2	960	2250	-628512	620331	-1438727	4.0	1.0	7.0	0	3226
13.	PL TH	200	2250	0	0	0	7.5	33.0	4.5	0	17512
14.	PL TC	200	400	0	0	0	-8.0	-36.0	-4.5	0	18954
15.	HY T	10	3125	0	0	0	0	0	0	0	0
16.	D WT	-	-	29349	1540	67254	-	-	-	-	-

2. Discharge Side Elbow: Joint No.(2)

	Load Set	Cycles	Pressure Psi	MX FT-LB	MY FT-LB	MZ FT-LB	ΔT1 °F	TA °F	ΔT2 °F	TB °F	th^S_p
1.	No T	500	0	0	0	0	0	0	0	0	0
2.	N OP	10^6	2250	-530339	551837	-1382065	0	0	0	0	0
3.	PL HU	500	2250	-304960	36910	-497089	7.5	0	3.5	0	2084
4.	PL CD	500	0	-476011	346437	-1327276	-8.5	0	-4.0	0	2370
5.	PL L	15000	2290	-530339	551837	-1382065	2.5	0	1.0	0	651
6.	PL UL	15000	2210	-530339	551837	-1382065	-2.0	0	-1.0	0	651
7.	ST I1	4000	2250	-530339	551837	-1382065	-3.5	0	-3.0	0	1327
8.	ST I2	4000	2280	-530339	551837	-1382065	2.5	0	2.0	0	911
9.	ST D1	4000	2230	-530339	551837	-1382065	3.5	0	2.5	0	1197
10.	ST D2	4000	2186	-530339	551837	-1382065	-2.5	0	-1.5	0	781
11.	RE T1	480	1680	-530339	551837	-1382065	-15.0	0	-10.5	0	5075
12.	RE T2	960	2250	-530339	551837	-1382065	4.5	0	7.0	0	2521
13.	PL TH	200	2250	0	0	0	7.0	0	3.5	0	2005
14.	PL TC	200	400	0	0	0	-7.5	0	-3.5	0	2084
15.	HY T	10	3125	0	0	0	0	0	0	0	0
16.	D WT	-	-	28768	1201	66928	-	-	-	-	-

3. Discharge Side Elbow: Joint No. (3)

	Load Set	Cycles	Pressure Psi	MX FT-LB	MY FT-LB	MZ FT-LB	ΔT1 °F	TA °F	ΔT2 °F	TB °F	S_{th_p}
1.	No T	500	0	0	0	0	0	0	0	0	0
2.	N OP	10^6	2250	-220387	332634	-1047558	0	0	0	0	0
3.	PL HU	500	2250	-184078	48882	-366631	7.5	0	3.5	0	2084
4.	PL CD	500	0	-183150	254080	-1011216	-8.5	0	-4.0	0	2370
5.	PL L	15000	2290	-220387	332684	-1047558	2.5	0	1.0	0	651
6.	PL UL	15000	2210	-220387	332684	-1047558	-2.0	0	-1.0	0	651
7.	ST I1	4000	2250	-220387	332684	-1047558	-3.5	0	-3.0	0	1327
8.	ST I2	4000	2280	-220387	332684	-1047558	2.5	0	2.0	0	911
9.	ST D1	4000	2230	-220387	332684	-1047558	3.5	0	2.5	0	1197
10.	ST D2	4000	2186	-220387	332684	-1047558	-2.5	0	-1.5	0	781
11.	RE T1	480	1680	-220387	332684	-1047558	-15.0	0	-10.5	0	5075
12.	RE T2	960	2250	-220387	332684	-1047558	4.5	0	7.0	0	2521
13.	PL TH	200	2250	0	0	0	7.0	0	3.5	0	2005
14.	PL TC	200	400	0	0	0	-7.5	0	-3.5	0	2084
15.	HY T	10	3125	0	0	0	0	0	0	0	0
16.	D WT	-	-	24646	400	61921	-	-	-	-	-

4. Discharge Side Pipe: Joint No. (4)

	Load Set	Cycles	Pressure Psi	MX FT-LB	MY FT-LB	MZ FT-LB	ΔT1 °F	TA °F	ΔT2 °F	TB °F	th^{S_p}
1.	No T	500	0	0	0	0	0	0	0	0	0
2.	N OP	10^6	2250	1014769	-563805	1527743	0	0	0	0	0
3.	PL HU	500	2250	297634	-65964	537741	7.5	0	3.5	0	2084
4.	PL CD	500	0	983898	-297510	1422079	-8.5	0	-4.0	0	2370
5.	PL L	15000	2290	1014769	-563805	1527743	2.5	0	1.0	0	651
6.	PL UL	15000	2210	1014769	-563805	1527743	-2.0	0	-1.0	0	651
7.	ST I1	4000	2250	1014769	-563805	1527743	-3.5	0	-3.0	0	1327
8.	ST I2	4000	2280	1014769	-563805	1527743	2.5	0	2.0	0	911
9.	ST D1	4000	2230	1014769	-563805	1527743	3.5	0	2.5	0	1197
10.	ST D2	4000	2186	1014769	-563805	1527743	-2.5	0	-1.5	0	781
11.	RE T1	480	1680	1014769	-563805	1527743	-15.0	0	-10.5	0	5075
12.	RE T2	960	2250	1014769	-563805	1527743	4.5	0	7.0	0	2521
13.	PL TH	200	2250	0	0	0	7.0	0	3.5	0	2005
14.	PL TC	200	400	0	0	0	-7.5	0	-3.5	0	2084
15.	HY T	10	3125	0	0	0	0	0	0	0	0
16.	D WT	-	-	-65960	-612	-127009	-	-	-	-	-

5. Suction Side Pipe: Joint No. (5)

	Load Set	Cycles	Pressure Psi	MX FT-LB	MY FT-LB	MZ FT-LB	ΔT1 °F	TA °F	ΔT2 °F	TB °F	S_p th
1.	No T	500	0	0	0	0	0	0	0	0	0
2.	N OP	10^6	2250	-532880	-539857	742414	0	0	0	0	0
3.	PL HU	500	2250	217739	-21390	-254994	6.5	-2.0	3.0	0	2237
4.	PL CD	500	0	-124349	-356807	210700	-7.5	2.0	-3.5	0	2523
5.	PL L	15000	2290	-532880	-539857	742414	2.0	-1.0	1.0	0	793
6.	PL UL	15000	2210	-532880	-539857	742414	-2.0	1.0	-1.0	0	793
7.	ST I1	4000	2250	-532880	-539857	742414	-3.5	1.0	-2.5	0	1417
8.	ST I2	4000	2280	-532880	-539857	742414	2.5	-1.0	2.0	0	1130
9.	ST D1	4000	2230	-532880	-539857	742414	3.5	-1.0	2.5	0	1417
10.	ST D2	4000	2186	-532880	-539857	742414	-2.5	1.0	-1.5	0	1001
11.	RE T1	480	1680	-532880	-539857	742414	-15.0	2.0	-10.0	0	5385
12.	RE T2	960	2250	-532880	-539857	742414	5.0	-1.0	7.0	0	2819
13.	PL TH	200	2250	0	0	0	6.0	-2.0	3.0	0	2185
14.	PL TC	200	400	0	0	0	-6.5	2.0	-3.0	0	2237
15.	HY T	10	3125	0	0	0	0	0	0	0	0
16.	D WT	-	-	7978	8782	-25408	-	-	-	-	-

6. Suction Side Elbow: Joint No. (6)

	Load Set	Cycles	Pressure Psi	MX FT-LB	MY FT-LB	MZ FT-LB	ΔT1 °F	TA °F	ΔT2 °F	TB °F	th^{S_p}
1.	No T	500	0	0	0	0	0	0	0	0	0
2.	N OP	10^6	2250	-507634	-539867	574591	0	0	0	0	0
3.	PL HU	500	2250	192884	-21390	-223525	6,5	-2.0	3.0	0	2237
4.	PL CD	500	0	-142345	-395807	210051	-7,5	2,0	-3.5	0	2523
5.	PL L	15000	2290	-507634	-539857	674591	2,0	-1.0	1.0	0	793
6.	PL UL	15000	2210	-507634	-539857	674591	-2.0	1.0	-1,0	0	793
7.	ST I1	4000	2250	-507634	-539857	674591	-3.5	1,0	-2.5	0	1417
8.	ST I2	4000	2280	-507634	-539857	674591	2.5	-1,0	2,0	0	1130
9.	ST D1	4000	2230	-507634	-539857	674591	3,5	-1.0	2,5	0	1417
10.	ST D2	4000	2186	-507634	-539857	674591	-2.5	1,0	-1.5	0	1001
11.	RE T1	480	1680	-507634	-539857	674591	-15.0	2.0	-10.0	0	5385
12.	RE T2	960	2250	-507634	-539857	674591	5,0	-1,0	7,0	0	2819
13.	PL TH	200	2250	0	0	0	6.0	-2,0	3.0	0	2185
14.	PL TC	200	400	0	0	0	-6,5	2,0	-3.0	0	2237
15.	HY T	10	3125	0	0	0	C	0	0	0	0
16.	D WT	-	-	8538	8782	-25552	-	-	-	-	-

7. Suction Side Elbow: Joint No. (7)

	Load Set	Cycles	Pressure Psi	MX FT-LB	MY FT-LB	MZ FT-LB	ΔT1 °F	TA °F	ΔT2 °F	TB °F	$th S_p$
1.	No T	500	0	0	0	0	0	0	0	0	0
2.	N OP	10^6	2250	-138875	-351708	-155765	0	0	0	0	0
3.	PL HU	500	2250	-65112	-5010	104972	6.5	-2.0	3.0	0	2237
4.	PL CD	500	0	-252079	-251102	113158	-7.5	2.0	-3.5	0	2523
5.	PL L	15000	2290	-138875	-351708	-155765	2.0	-1.0	1.0	0	793
6.	PL UL	15000	2210	-138875	-351708	-155765	-2.0	1.0	-1.0	0	793
7.	ST I1	4000	2250	-138875	-351708	-155765	-3.5	1.0	-2.5	0	1417
8.	ST I2	4000	2280	-138875	-351708	-155765	2.5	-1.0	2.0	0	1130
9.	ST D1	4000	2230	-138875	-351708	-155765	3.5	-1.0	2.5	0	1417
10.	ST D2	4000	2186	-138875	-351708	-155765	-2.5	1.0	-1.5	0	1001
11.	RE T1	480	1680	-138875	-351708	-155765	-15.0	2.0	-10.0	0	5385
12.	RE T2	960	2250	-138875	-351708	-155765	5.0	-1.0	7.0	0	2819
13.	PL TH	200	2250	0	0	0	6.0	-2.0	3.0	0	2185
14.	PL TC	200	400	0	0	0	-6.5	2.0	-3.0	0	2237
15.	HY T	10	3125	0	0	0	0	0	0	0	0
16.	D WT	-	-	-7535	5188	2784	-	-	-	-	-

8. Suction Side Elbow: Joint No. (8)

	Load Set	Cycles	Pressure Psi	MX FT-LB	MY FT-LB	MZ FT-LB	ΔT1 °F	TA °F	ΔT2 °F	TB °F	$th S_p$
1.	No T	500	0	0	0	0	0	0	0	0	0
2.	N OP	10^6	2250	146610	85927	-549813	0	0	0	0	0
3.	PL HU	500	2250	-102077	32631	155993	6.5	-2.0	3.0	0	2237
4.	PL CD	500	0	-99746	87156	-97099	-7.5	2.0	-3.5	0	2523
5.	PL L	15000	2290	146610	85927	-549813	2.0	-1.0	1.0	0	793
6.	PL UL	15000	2210	146610	85927	-549813	-2.0	1.0	-1.0	0	793
7.	ST I1	4000	2250	146610	85927	-549813	-3.5	1.0	-2.5	0	1417
8.	ST I2	4000	2280	146610	85927	-549813	2.5	-1.0	2.0	0	1130
9.	ST D1	4000	2230	146610	85927	-549813	3.5	-1.0	2.5	0	1417
10.	ST D2	4000	2186	146610	85927	-549813	-2.5	1.0	-1.5	0	1001
11.	RE T1	480	1680	146610	85927	-549813	-15.0	2.0	-10.0	0	5385
12.	RE T2	960	2250	146610	85927	-549813	5.0	-1.0	7.0	0	2819
13.	PL TH	200	2250	0	0	0	6.0	-2.0	3.0	0	2185
14.	PL TC	200	400	0	0	0	-6.5	2.0	-3.0	0	2237
15.	HY T	10	3125	0	0	0	0	0	0	0	0
16.	D WT	-	-	-13411	-3153	10892	-	-	-	-	-

9. Suction Side Elbow: Joint No. (9)

	Load Set	Cycles	Pressure Psi	MX FT-LB	MY FT-LB	MZ FT-LB	ΔT1 °F	TA °F	ΔT2 °F	TB °F	th^{S_p}
1.	No T	500	0	0	0	0	0	0	0	0	0
2.	N OP	10^6	2250	23634	274318	-98893	0	0	0	0	0
3.	PL HU	500	2250	124096	48878	-128554	6.5	-2.0	3.0	0	2237
4.	PL CD	500	0	141132	232827	-181324	-7.5	2.0	-3.5	0	2523
5.	PL L	15000	2290	23634	274318	-58893	2.0	-1.0	1.0	0	793
6.	PL UL	15000	2210	23634	274318	-58893	-2.0	1.0	-1.0	0	793
7.	ST I1	4000	2250	23634	274318	-58893	-3.5	1.0	-2.5	0	1417
8.	ST I2	4000	2280	23634	274318	-58893	2.5	-1.0	2.0	0	1130
9.	ST D1	4000	2230	23634	274318	-58893	3.5	-1.0	2.5	0	1417
10.	ST D2	4000	2186	23634	274318	-58893	-2.5	1.0	-1.5	0	1001
11.	RE T1	480	1680	23634	274318	-58893	-15.0	2.0	-10.0	0	5385
12.	RE T2	960	2250	23634	274318	-58893	5.0	-1.0	7.0	0	2819
13.	PL TH	200	2250	0	0	0	6.0	-2.0	3.0	0	2185
14.	PL TC	200	400	0	0	0	-6.5	2.0	-3.0	0	2237
15.	HY T	10	3125	0	0	0	0	0	0	0	0
16.	D WT	-	-	-2385	-5746	-10452	-	-	-	-	-

10. Suction Side Elbow: Joint No. (10)

	Load Set	Cycles	Pressure Psi	MX FT-LB	MY FT-LB	MZ FT-LB	ΔT1 °F	TA °F	ΔT2 °F	TB °F	S_p th^{S_p}
1.	No T	500	0	0	0	0	0	0	0	0	0
2.	N OP	10^6	2250	23570	274318	-58721	0	0	0	0	0
3.	PL HU	500	2250	124160	48878	-128634	6.5	-2.0	3.0	0	2237
4.	PL CD	500	0	141177	232827	-181322	-7.5	2.0	-3.5	0	2523
5.	PL L	15000	2290	23570	274318	-58721	2.0	-1.0	1.0	0	793
6.	PL UL	15000	2210	23570	274318	-58721	-2.0	1.0	-1.0	0	793
7.	ST I1	4000	2250	23570	274318	-58721	-3.5	1.0	-2.5	0	1417
8.	ST I2	4000	2280	23570	274318	-58721	2.5	-1.0	2.0	0	1130
9.	ST D1	4000	2230	23570	274318	-58721	3.5	-1.0	2.5	0	1417
10.	ST D2	4000	2186	23570	274318	-58721	-2.5	1.0	-1.5	0	1001
11.	RE T1	480	1680	23570	274318	-58721	-15.0	2.0	-10.0	0	5385
12.	RE T2	960	2250	23570	274318	-58721	5.0	-1.0	7.0	0	2819
13.	PL TH	200	2250	0	0	0	6.0	-2.0	3.0	0	2185
14.	PL TC	200	400	0	0	0	-6.5	2.0	-3.0	0	2237
15.	HY T	10	3125	0	0	0	0	0	0	0	0
16.	D WT	-	-	-2387	-6746	-10452	-	-	-	-	-

11. Suction Side Elbow: Joint No. (11)

	Load Set	Cycles	Pressure Psi	MX FT-LB	MY FT-LB	MZ FT-LB	ΔT1 °F	TA °F	ΔT2 °F	TB °F	th^{S_p}
1.	No T	500	0	0	0	0	0	0	0	0	0
2.	N OP	10^6	2250	-106808	461649	451192	0	0	0	0	0
3.	PL HU	500	2250	289557	-64456	-350753	6.5	-2.0	3.0	0	2237
4.	PL CD	500	0	288112	197944	-153773	-7.5	2.0	-3.5	0	2523
5.	PL L	15000	2290	-106608	461649	451182	2.0	-1.0	1.0	0	793
6.	PL UL	15000	2210	-106808	461649	451182	-2.0	1.0	-1.0	0	793
7.	ST I1	4000	2250	-106808	461649	451182	-3.5	1.0	-2.5	0	1417
8.	ST I2	4000	2280	-106808	461649	451182	2.5	-1.0	2.0	0	1130
9.	ST D1	4000	2230	-106808	461649	451182	3.5	-1.0	2.5	0	1417
10.	ST D2	4000	2186	-106808	461649	451182	-2.5	1.0	-1.5	0	1001
11.	RE T1	480	1680	-106808	461649	451182	-15.0	2.0	-10.0	0	5385
12.	RE T2	960	2250	-106808	461649	451182	5.0	-1.0	7.0	0	2819
13.	PL TH	200	2250	0	0	0	6.0	-2.0	3.0	0	2185
14.	PL TC	200	400	0	0	0	-6.5	2.0	-3.0	0	2237
15.	HY T	10	3125	0	0	0	0	0	0	0	0
16.	D WT	-	-	6254	-5330	3015	-	-	-	-	-

12. Outlet Nozzle End: Joint No. (12)

	Load Set	Cycles	Pressure Psi	MX FT-LB	MY FT-LB	MZ FT-LB	ΔT1 °F	TA °F	ΔT2 °F	TB °F	th^S_p
1.	No T	500	0	0	0	0	0	0	0	0	0
2.	N OP	10^6	2250	-124465	577699	597508	0	0	0	0	0
3.	PL HU	500	2250	329863	-134723	-409661	9.0	8.0	5.0	0	7000
4.	PL CD	500	0	334116	175279	-138295	-10.0	-9.0	-5.0	0	7683
5.	PL L	15000	2290	-124465	577699	597508	2.5	1.5	1.5	0	1655
6.	PL UL	15000	2210	-124465	577699	597508	-2.5	-1.5	-1.0	0	1526
7.	ST I1	4000	2250	-124465	577699	597508	-3.0	-1.0	-3.0	0	1946
8.	ST I2	4000	2280	-124465	577699	597508	2.5	1.0	2.0	0	1565
9.	ST D1	4000	2230	-124465	577699	597508	3.0	1.0	2.5	0	1816
10.	ST D2	4000	2186	-124465	577699	597508	-2.5	-1.0	-1.5	0	1435
11.	RE T1	480	1680	-124465	577699	597508	-14.0	-3.0	-11.0	0	7568
12.	RE T2	960	2250	-124465	577699	597508	4.0	1.0	7.0	0	3225
13.	PL TH	200	2250	0	0	0	8.5	7.5	5.0	0	6659
14.	PL TC	200	400	0	0	0	-9.0	-8.0	-5.0	0	7000
15.	HY T	10	3125	0	0	0	0	0	0	0	0
16.	D WT	-	-	13948	-4452	11967	-	-	-	-	-

13. Hot Leg Outlet Nozzle End: Joint No. (13)

	Load Set	Cycles	Pressure Psi	MX FT-LB	MY FT-LB	MZ FT-LB	ΔT1 °F	TA °F	ΔT2 °F	TB °F	S_p th
1.	No T	500	0	0	0	0	0	0	0	0	0
2.	N OP	10^6	2250	-443	3250	-5707294	0	0	0	0	0
3.	PL HU	500	2250	-227	-3542	-2072053	14.0	44.0	6.5	0	24494
4.	PL CD	500	0	-747	-12743	-5814303	-15.0	-48.0	-7.0	0	26631
5.	PL L	15000	2290	-443	3250	-5707294	22.0	23.0	10.0	0	18076
6.	PL UL	15000	2210	-443	3250	-5707294	-30.5	-18.0	-19.0	0	20265
7.	ST I1	4000	2250	-443	3250	-5707294	0	0	0	0	0
8.	ST I2	4000	2280	-443	3250	-5707294	6.0	3.5	4.0	0	4036
9.	ST D1	4000	2230	-443	3250	-5707294	0	0	0	0	0
10.	ST D2	4000	2186	-443	3250	-5707294	-5.5	-1.0	-3.5	0	2683
11.	RE T1	480	1680	-443	3250	-5707294	-50.0	-17.0	-35.0	0	28702
12.	RE T2	960	2250	-443	3250	-5707294	0	0	0	0	0
13.	PL TH	200	2250	0	0	0	13.0	41.5	6.5	0	23148
14.	PL TC	200	400	0	0	0	-14.0	-44.5	-7.0	0	24844
15.	HY T	10	3125	0	0	0	0	0	0	0	0
16.	D WT	-	-	-185	-1097	539111	-	-	-	-	-

14. Hot Leg Pipe: Joint No. (14)

	Load Set	Cycles	Pressure Psi	MX FT-LB	MY FT-LB	MZ FT-LB	ΔT1 °F	TA °F	ΔT2 °F	TB °F	S_{th_p}
1.	No T	500	0	0	0	0	0	0	0	0	0
2.	N OP	10^6	2250	-443	3320	-5546572	0	0	0	0	0
3.	PL HU	500	2250	-227	-3414	-2008336	14.0	27.0	6.5	0	9811
4.	PL CD	500	0	-747	-12301	-5640955	-15.0	-29.0	-7.0	0	10536
5.	PL L	15000	2290	-443	3320	-5546572	22.0	16.0	10.0	0	9557
6.	PL UL	15000	2210	-443	3320	-5546572	-30.5	-13.5	-19.0	0	12675
7.	ST I1	4000	2250	-443	3320	-5546572	0	0	0	0	0
8.	ST I2	4000	2280	-443	3320	-5546572	6.0	2.0	4.0	0	2417
9.	ST D1	4000	2230	-443	3320	-5546572	0	0	0	0	0
10.	ST D2	4000	2186	-443	3320	-5546572	-5.5	-1.5	-3.5	0	2100
11.	RE T1	480	1680	-443	3320	-5546572	-50.0	-13.0	-35.0	0	19773
12.	RE T2	960	2250	-443	3320	-5546572	0	0	0	0	0
13.	PL TH	200	2250	0	0	0	13.0	25.5	6.5	0	9324
14.	PL TC	200	400	0	0	0	-14.0	-27.5	-7.0	0	10050
15.	HY T	10	3125	0	0	0	0	0	0	0	0
16.	D WT	-	-	-185	-1035	525621	-	-	-	-	0

15. Hot Leg Elbow: Joint No. (15)

	Load Set	Cycles	Pressure Psi	MX FT-LB	MY FT-LB	MZ FT-LB	ΔT1 °F	TA °F	ΔT2 °F	TB °F	S_p th
1.	No T	500	0	0	0	0	0	0	0	0	0
2.	N OP	10^6	2250	-443	5770	62893	0	0	0	0	0
3.	PL HU	500	2250	-227	1036	215462	12.5	-1.0	5.5	0	3606
4.	PL CD	500	0	-747	3139	409155	-14.5	1.0	-6.0	0	4049
5.	PL L	15000	2290	-443	5770	62893	23.5	-3.0	10.0	0	6937
6.	PL UL	15000	2210	-443	5770	62893	-32.0	3.0	-18.5	0	10475
7.	ST I1	4000	2250	-443	5770	62893	0	0	0	0	0
8.	ST I2	4000	2280	-443	5770	62893	6.0	-1.0	4.0	0	2198
9.	ST D1	4000	2230	-443	5770	62893	0	0	0	0	0
10.	ST D2	4000	2186	-443	5770	62893	-6.0	1.0	-3.5	0	2068
11.	RE T1	480	1680	-443	5770	62893	-52.5	3.0	-35.0	0	17969
12.	RE T2	960	2250	-443	5770	62893	0	0	0	0	0
13.	PL TH	200	2250	0	0	0	12.0	-1.0	5.5	0	3528
14.	PL TC	200	400	0	0	0	-13.0	1.0	-5.5	0	3685
15.	HY T	10	3125	0	0	0	0	0	0	0	0
16.	D WT	-	-	-185	1128	-112515	-	-	-	-	0

16. Hot Leg Elbow: Joint No. (16)

	Load Set	Cycles	Pressure Psi	MX FT-LB	MY FT-LB	MZ FT-LB	ΔT1 °F	TA °F	ΔT2 °F	TB °F	S_{th_p}
1.	No T	500	0	0	0	0	0	0	0	0	0
2.	N OP	10^6	2250	-238	6421	1169507	0	0	0	0	0
3.	PL HU	500	2250	145	2218	490662	12.5	-1.0	5.5	0	3606
4.	PL CD	500	0	545	7240	2415350	-14.5	1.0	-6.0	0	4049
5.	PL L	15000	2290	-238	6421	1169507	23.5	-3.0	10.0	0	6937
6.	PL UL	15000	2210	-238	6421	1169507	-32.0	3.0	-18.5	0	10475
7.	ST I1	4000	2250	-238	6421	1169057	0	0	0	0	0
8.	ST I2	4000	2280	-238	6421	1169507	6.0	-1.0	4.0	0	2198
9.	ST D1	4000	2230	-238	6421	1169507	0	0	0	0	0
10.	ST D2	4000	2186	-238	6421	1169507	-6.0	1.0	-3.5	0	2068
11.	RE T1	480	1680	-238	6421	1169507	-52.5	3.0	-35.0	0	17969
12.	RE T2	960	2250	-238	6421	1169507	0	0	0	0	0
13.	PL TH	200	2250	0	0	0	12.0	-1.0	5.5	0	3528
14.	PL TC	200	400	0	0	0	-13.0	1.0	-5.5	0	3685
15.	HY T	10	3125	0	0	0	0	0	0	0	0
16.	D WT	-	-	-3	1703	-326136	-	-	-	-	0

17. Hot Leg Nozzle End; Joint No. (17)

	Load Set	Cycles	Pressure Psi	MX FT-LB	MY FT-LB	MZ FT-LB	ΔT1 °F	TA °F	ΔT2 °F	TB °F	$th S_p$
1.	No T	500	0	0	0	0	0	0	0	0	0
2.	N OP	10^6	2250	-195	6480	1227509	0	0	0	0	0
3.	PL HU	500	2250	220	2325	480791	16.0	9.5	8.0	0	10120
4.	PL CD	500	0	805	7612	2641255	-18.5	-11.0	-8.5	0	11514
5.	PL L	15000	2290	-196	6480	1227509	26.5	9.0	13.0	0	13744
6.	PL UL	15000	2210	-196	6480	1227509	-32.5	-8.0	-21.5	0	16964
7.	ST I1	4000	2250	-196	6430	1227509	0	0	0	0	0
8.	ST I2	4000	2280	-196	6480	1227509	6.0	1.0	4.5	0	3060
9.	ST D1	4000	2230	-196	6480	1227509	0	0	.0	0	0
10.	ST D2	4000	2186	-196	6480	1227509	-5.5	-1.0	-4.0	0	2810
11.	RE T1	480	1680	-196	6480	1227509	-50.0	-8.5	-30.0	0	23631
12.	RE T2	960	2250	-196	6480	1227509	0	0	0	0	0
13.	PL TH	200	2250	0	0	0	15.0	9.0	8.0	0	9658
14.	PL TC	40	400	0	0	0	-16.5	-10.0	-8.0	0	10461
15.	HY T	10	3125	0	0	0	0	0	0	0	0
16.	D WT	-	-	32	1755	-345277	-	-	-	-	0

Seismic and Pump Vibration Loads

Location	Fx,(K)	Fy,(K)	Fz,(K)	Mx,(in-K)	My,(in-K)	Mz,(in-K)
Joint No. (2):						
SSE	145	33	157	2499	3693	2679
Pump Vibration	2.14	2.85	3.32	25.72	19.33	25.55
Joint No. (4):						
SSE	198	34	75	2308	977	4937
Pump Vibration	4.53	.39	1.71	26.88	43.98	62.89
Joint No. (5):						
SSE	29	13	23	1373	1834	1353
Pump Vibration	.74	.22	.84	55.41	27.21	47.35
Joint No. (11):						
SSE	56	45	56	3131	2318	3131
Pump Vibration	.84	.35	.84	44	49	44
Joint No. (14):						
SSE	510	125	89	2918	6574	10599
Pump Vibration	.78	.33	.15	.58	31.29	35
Joint No. (16):						
SSE	533	467	82	6752	6576	6247
Pump Vibration	.78	.82	.14	7.49	7.19	25.87

Notes:
1. All loads are in global coordinate system
2. Each of the six load components are maximums over all time. Maximums for all components do not necessarily occur simultaneously.
3. Loads for the remainder joints can be obtained from the given loads of the nearby joint by transposition.